INFLUENCE OF SONOPHORESIS AND CHEMICAL PENETRATION ENHANCER ON SKIN PERMEATION OF SODIUM FLUORESCEIN-LOADED LIPID NANOCARRIERS

By
MissWorranan Rangsimawong

A Thesis Submitted in Partial Fulfillment of the Requirements for the Degree
Doctor of Philosophy Program in Pharmaceutical Technology
Graduate School, Silpakorn University
Academic Year 2016

INFLUENCE OF SONOPHORESIS AND CHEMICAL PENETRATION ENHANCER ON SKIN PERMEATION OF SODIUM FLUORESCEIN-LOADED LIPID NANOCARRIERS

By
MissWorranan Rangsimawong

A Thesis Submitted in Partial Fulfillment of the Requirements for the Degree
Doctor of Philosophy Program in Pharmaceutical Technology
Graduate School, Silpakorn University
Academic Year 2016

อิทธิพลของโซโนโฟเรซิสและสารเคมีเพิ่มการซึมผ่านต่อการซึมผ่านผิวหนังของตัวพาไขมันขนาดนาโนที่บรรจุโซเดียมฟลูออเรสซีน

โดย

นางสาววรนันท์ รังสิมาวงศ์

วิทยานิพนธ์นี้เป็นส่วนหนึ่งของการศึกษาตามหลักสูตรปริญญาเภสัชศาสตรดุษฎีบัณฑิต

สาขาวิชาเทคโนโลยีเภสัชกรรม

บัณฑิตวิทยาลัย มหาวิทยาลัยศิลปากร

ปีการศึกษา 2559

The Graduate School, Silpakorn University has approved and accredited the thesis title of “Influence of sonophoresis and chemical penetration enhancer on skin permeation of sodium fluorescein-loaded lipid nanocarriers” submitted by Miss Worranan Rangsimawong as a partial fulfillment of the requirements for the degree of Doctor of Philosophy in Pharmaceutical Technology.

…….....

(Associate Professor Panjai Tantatsanawong, Ph.D.)

Dean of Graduate School

...../...../.....

The Thesis Advisors

1. Associate Professor Tanasait Ngawhirunpat, Ph.D.
2. Associate Professor Praneet Opanasopit, Ph.D.

The Thesis Examination Committee

…….. Chairman
(Associate Professor Suwannee Panomsuk, Ph.D.)
...../...../.....

…….. Member
(Professor Kozo Takayama, Ph.D.)
...../...../.....

…….. Member
(Associate Professor Tanasait Ngawhirunpat, Ph.D.)
...../...../.....

…….. Member
(Associate Professor Praneet Opanasopit, Ph.D.)
...../...../.....

55354803 : MAJOR : PHARMACEUTICAL TECHNOLOGY
KEY WORDS : SONOPHORESIS / LIPID NANOCARRIERS / CHEMICAL PENETRATION ENHANCER / HYDROPHILIC COMPOUND / SKIN PENETRATION MECHANISM
WORRANAN RANGSIMAWONG : INFLUENCE OF SONOPHORESIS AND CHEMICAL PENETRATION ENHANCER ON SKIN PERMEATION OF SODIUM FLUORESCEIN-LOADED LIPID NANOCARRIERS. THESIS ADVISORS : ASSOC. PROF. TANASAIT NGAWHIRUNPAT, Ph.D. AND ASSOC. PROF. PRANEET OPANASOPIT, Ph.D. 169 pp.

The aim of this study was to investigate the influence of sonophoresis (SN) and chemical penetration enhancer on skin permeation of hydrophilic compound-loaded lipid nanocarriers. Three types of lipid nanocarriers (liposomes (CL), niosomes (NI), and solid lipid nanoparticles (SLN)) were formulated for entrapped sodium fluorescein (NaFl). The effect of PEG2000-DSPE and terpene (d-limonene, LI) in nanocarriers were evaluated in term of the physicochemical properties, morphology, and membrane fluidity of liposome vesicles. For the influence of using SN with lipid nanocarrier formulations on transdermal delivery of NaFl, *in vitro* skin permeation and deposition studies were determined by using Franz diffusion cells through porcine skin. The possible penetration mechanism was also clarified by using confocal laser scanning microscopy (CLSM), scanning electron microscopy (SEM), selectively block hair follicle technique, fourier transform infrared spectroscopy (FTIR), and differential scanning calorimetry (DSC). All nanocarrier formulations showed small particle size in nanometer scale (between 31 to 202 nm), spherical shape, and negative surface charge (-9 to -35 mV). The entrapped NaFl into SLN was higher than NI and CL, respectively. Liposome formulations with PEGylation had a significantly smaller size with higher entrapment efficiency and loading efficiency than non-PEGyted liposomes. As LI was added into the formulations, the particle size of nanocarriers decreased, but the NaFl entrapment efficiency increased. The membrane fluidity of carriers with LI was higher than those without LI. For the influence of using SN and nanocarrier formulations on the skin, SN significantly increased the NaFl flux of NaFl solution (51.1-fold enhancement), but it decreased the NaFl flux of almost lipid nanocarrier formulations. Although PEGylated liposomes with d-limonene (PL-LI) had the highest NaFl penetrated into and through the skin (92.8-fold enhancement), the NaFl penetration of the combination of SN with PL-LI was lower than NaFl solution and PL-LI without SN, respectively. SN also decreased the amount of NaFl in stratum corneum of all formulations. CLSM images showed the brightest fluorescence intensity of NaFl and Rh-PE-probed PL-LI in the skin especially in hair follicles, suggesting that the high fluidity vesicles and entrapped NaFl co-transported into and through the skin. Applying SN decreased the distribution of both NaFl and nanocarriers into the skin. For SEM images of skin surface, SN treated skin exhibited the lifted up of corneocytes, which the combination of the lipid nanocarriers with SN showed small corneocytes lifting. Moreover, FTIR and DSC results revealed the greatest enhancing mechanism of PL-LI on the modifying stratum corneum barrier, indicating that LI significantly increased lipid organization change. While FTIR spectrum of stratum corneum treated with SN showed no effect on the stratum corneum lipid ordering. Therefore, PL-LI enhanced NaFl transport via transfollicular and intercellular pathway due to the physicochemical properties of these vesicles and the effect of chemical penetration enhancer on the disruption of intercellular lipid in the stratum corneum. After applying SN, both skin structure and lipid nanocarriers were affected. The sonicated skin was repaired by disrupted lipid nanocarriers, leading to decrease of NaFl permeated through skin. These results show the better understanding of the skin penetration mechanism of the combination of SN and different types of lipid nanocarrier system. The useful fundamental information can be utilized to develop the treatment condition for improving skin delivery of hydrophilic drug.

Program of Pharmaceutical Technology Graduate School, Silpakorn University
Student's signature..... Academic Year 2016
Thesis Advisors' signature 1..... 2.....

55354803 : สาขาวิชาเทคโนโลยีเภสัชกรรม
คำสำคัญ : โซโนโฟเรซิส / ตัวพาไขมันขนาดนาโน / สารเคมีเพิ่มการซึมผ่าน / สารที่ชอบน้ำ / กลไกการซึมผ่านผิวหนัง

วรนันท์ รังสิมาวงศ์ : อิทธิพลของโซโนโฟเรซิสและสารเคมีเพิ่มการซึมผ่านต่อการซึมผ่านผิวหนังของตัวพาไขมันขนาดนาโนที่บรรจุโซเดียมฟลูออเรสซีน อาจารย์ที่ปรึกษาวิทยานิพนธ์ : ภก.รศ.ดร. ธนะเศรษฐ์ ง้าวหิรัญพัฒน์ และ ภญ.รศ.ดร.ปราณีต โอปณะโสภิต 169 หน้า.

การวิจัยนี้มีวัตถุประสงค์เพื่อศึกษาอิทธิพลของโซโนโฟเรซิสและสารเคมีเพิ่มการซึมผ่านต่อการซึมผ่านผิวหนังของสารที่ชอบน้ำที่บรรจุในตัวพาไขมันขนาดนาโน ซึ่งเตรียมตัวพาไขมันขนาดนาโน 3 รูปแบบ คือ ลิโพโซม นีโอโซม และอนุภาคนาโนชนิดไขมันแข็ง (เอสแอลเอ็น) เพื่อกักเก็บโซเดียมฟลูออเรสซีน (NaFI) โดยประเมินผลของ PEG2000-DSPE และเทอร์พีน (ดี-ลิโมนีน) ในตัวพาไขมันขนาดนาโนต่อสมบัติทางเคมีฟิสิกส์ สัณฐานวิทยา และความเหลวของผนังอนุภาคลิโพโซม สำหรับอิทธิพลของการใช้โซโนโฟเรซิสร่วมกับสูตรตำรับตัวพาไขมันขนาดนาโนต่อการนำส่ง NaFI ผ่านผิวหนังนั้นจะประเมินการซึมผ่านผิวหนังและการสะสมของยาในผิวหนังแบบภายนอกร่างกายโดยใช้ฟรานซ์ดิฟฟิวชันเซลล์ในการศึกษาผ่านหนังลูกหมู ศึกษากลไกการซึมผ่านที่น่าจะเป็นไปได้โดยการใช้กล้องจุลทรรศน์แบบคอนโฟคอลชนิดที่ใช้เลเซอร์ในการสแกน (ซีแอลเอสเอ็ม) กล้องจุลทรรศน์อิเล็กตรอนแบบส่องกราด (เอสอีเอ็ม) เทคนิคการปิดกั้นรูขุมขนแบบจำเพาะ ฟูเรียร์ทรานสฟอร์มอินฟราเรดสเปกโทรสโกปี (เอฟทีไออาร์) และดิฟเฟอเรนเชียลสแกนนิงแคลอริมิเตอร์ (ดีเอสซี) สูตรตำรับตัวพาขนาดนาโนทั้งหมดแสดงขนาดอนุภาคเล็กในระดับนาโนเมตร (ระหว่าง 31 ถึง 202 นาโนเมตร) ทรงกลม และประจุที่ผิวเป็นลบ (-9 ถึง -35 มิลลิโวลต์) โดย NaFI ถูกกักเก็บในตำรับเอสแอลเอ็นสูงกว่าตำรับนีโอโซมและตำรับลิโพโซม ตามลำดับ สูตรตำรับเพ็กลิโพโซม จะมีขนาดอนุภาคเล็กกว่า และมีความสามารถในการกักเก็บและการบรรจุยาสูงกว่าลิโพโซมอย่างมีนัยสำคัญ การเติมดี-ลิโมนีนในสูตรตำรับมีผลต่อการลดขนาดอนุภาคของตัวพาขนาดนาโน และเพิ่มความสามารถในการกักเก็บ NaFI ในสูตรตำรับ ความเหลวของผนังอนุภาคของตัวพาที่เติมดี-ลิโมนีนมีค่าสูงกว่าสูตรตำรับที่ไม่เติมดี-ลิโมนีน สำหรับอิทธิพลของการใช้โซโนโฟเรซิสร่วมกับสูตรตำรับตัวพาขนาดนาโน พบว่า โซโนโฟเรซิสมีผลต่อการเพิ่มอัตราการซึมผ่านผิวหนังของ NaFI ในรูปแบบสารละลายอย่างมีนัยสำคัญ (เพิ่มขึ้น 51.1 เท่า) แต่มีผลลดอัตราการซึมผ่านผิวหนังของ NaFI ในเกือบทุกสูตรตำรับตัวพาไขมันขนาดนาโน ถึงแม้ว่าเพ็กลิโพโซมที่มีดี-ลิโมนีน จะมีค่าการซึมผ่านของ NaFI เข้าสู่และผ่านผิวหนังสูงที่สุด (เพิ่มขึ้น 92.8 เท่า) อย่างไรก็ตามการซึมผ่านของ NaFI ของการใช้โซโนโฟเรซิสร่วมกับเพ็กลิโพโซมที่มีดี-ลิโมนีน พบว่า อัตราการซึมผ่านผิวหนังมีค่าน้อยกว่า NaFI ในรูปสารละลาย และ NaFI ในตำรับเพ็กลิโพโซมที่มีดี-ลิโมนีนที่ไม่ให้โซโนโฟเรซิสตามลำดับ นอกจากนี้การใช้โซโนโฟเรซิสยังส่งผลลดปริมาณของ NaFI ในชั้นสตราตัมคอร์เนียมของทุกสูตรตำรับ โดยยืนยันผลจากภาพถ่ายที่ได้จากเครื่องซีแอลเอสเอ็ม พบความเข้มของสารเรืองแสงสีเขียวของ NaFI และสีแดงของโรดามีน-พีอีที่ติดอยู่กับเพ็กลิโพโซมที่มีดี-ลิโมนีนในชั้นผิวหนัง โดยเฉพาะบริเวณรูขุมขน ซึ่งบอกเป็นนัยว่าอนุภาคที่มีความเหลวสูงอย่างเพ็กลิโพโซมที่มีดี-ลิโมนีนสามารถนำส่ง NaFI เข้าไปในผิวหนังโดยผ่านทางรูขุมขน ในขณะที่การใช้โซโนโฟเรซิสจะไปลดการกระจายของทั้ง NaFI และตัวพาเข้าสู่ผิวหนัง ภาพถ่ายจากเครื่องเอสอีเอ็มของผิวหนังด้านบนที่ได้รับโซโนโฟเรซิสแสดงการยกตัวขึ้นของเซลล์คอร์นีโอไซต์ ส่วนภาพถ่ายผิวหนังด้านบนที่ได้รับตัวพาร่วมกับโซโนโฟเรซิสแสดงการยกตัวของเซลล์คอร์นีโอไซต์เพียงเล็กน้อย เทอร์โมแกรมที่ได้จากการวิเคราะห์ด้วยเอฟทีไออาร์และดีเอสซีแสดงให้เห็นถึงกลไกการเพิ่มการซึมผ่านของเพ็กลิโพโซมที่มีดี-ลิโมนีนต่อการดัดแปลงตัวกั้นของชั้นสตราตัมคอร์เนียม และการเติมดี-ลิโมนีนเพิ่มการเปลี่ยนแปลงการจัดเรียงโครงสร้างของไขมันได้อย่างมีนัยสำคัญ ในขณะที่สเปคตรัมจากเอฟทีไออาร์ของสตราตัมคอร์เนียมที่ได้รับโซโนโฟเรซิสไม่พบผลกระทบต่อการจัดเรียงตัวของไขมันในชั้นสตราตัมคอร์เนียม ดังนั้น กลไกของเพ็กลิโพโซมที่มีดี-ลิโมนีนที่ช่วยเพิ่มการนำส่ง NaFI ผ่านผิวผนัง คือ ผ่านทางรูขุมขนและผ่านช่องว่างระหว่างเซลล์ เนื่องจากสมบัติทางเคมีฟิสิกส์ของอนุภาคและสารเคมีเพิ่มการซึมผ่านมีผลต่อการทำลายไขมันที่อยู่ระหว่างเซลล์ของชั้นสตราตัมคอร์เนียม เมื่อให้โซโนโฟเรซิสร่วมด้วยทั้งโครงสร้างของผิวหนังและตัวพาจะได้รับผลกระทบ โดยผิวหนังที่ให้โซโนโฟเรซิสร่วมด้วยนั้นจะเกิดการซ่อมแซมโดยตัวพาที่แตกจากโซโนโฟเรซิส จึงส่งผลลดการซึมผ่านของ NaFI ผลที่ได้จากการศึกษานี้ทำให้เข้าใจถึงกลไกการซึมผ่านผิวหนังของการใช้โซโนโฟเรซิสร่วมกับระบบตัวพาไขมันขนาดนาโนชนิดต่าง ๆ ซึ่งข้อมูลพื้นฐานเหล่านี้สามารถนำไปใช้ให้เกิดประโยชน์สูงสุดต่อการพัฒนาการนำส่งสารที่ชอบน้ำผ่านผิวหนัง

สาขาวิชาเทคโนโลยีเภสัชกรรม บัณฑิตวิทยาลัย มหาวิทยาลัยศิลปากร
ลายมือชื่อนักศึกษา..... ปีการศึกษา 2559
ลายมือชื่ออาจารย์ที่ปรึกษาวิทยานิพนธ์ 1.....2.....

ACKNOWLEDGEMENTS

I would like to express sincere appreciation to every people who contributed in diverse ways to the completion of this research. First of all, I would like to express the deepest appreciation to my dissertation advisor, Assoc. Prof. Dr. Tanasait Ngawhirunpat and my dissertation co-advisor, Assoc. Prof. Dr. Praneet Opanasopit for their professional and excellent guidance, encouragement, and providing me with an excellent atmosphere for conducting a research.

My next gratitude goes to Prof. Dr. Kozo Takayama for giving me a great opportunity to work at his laboratory, Department of Pharmaceutics, Hoshi University, Tokyo, Japan and supporting me in my research works and also in my living in Japan. I also would like to acknowledge Assoc. Prof. Dr. Yasuko Obata for her precious suggestions and helpful support. I also would like to thank all friends in Hoshi University for their warm welcoming and help.

I gratefully acknowledge the Commission of Higher Education (Thailand), the Thailand Research Funds through the Royal Golden Jubilee Ph.D Program (Grant No. PHD/0091/2554), Faculty of Pharmacy, the Graduate School of Silpakorn University for the financial support, and the Silpakorn University Research and Development Institute for facility support.

I would like to sincere thanks to all teachers and staffs especially Assoc. Prof. Dr. Suwanee Panomsuk and Assoc. Prof. Dr. Theerasak Rojanarata for the knowledge and generous support. I also would like to thank to all members of the Pharmaceutical Development of Green Innovation group (PDGIG), especially Dr. Sureewan Duangjit, Dr. Thirapit Subongkot, Dr. Ponwanit Charoenputtakum, and Miss. Areerut Sripatthanaporn for their helpful support, friendship, caring, and encouragement.

Finally, I would like to pass my special thanks to my beloved family who is always beside me. Thank you so much for their all support, caring, love, encouragement, understanding, and belief in me.

TABLE OF CONTENTS

LIST OF TABLES

LIST OF FIGURES

LIST OF ABBREVIATIONS

®	registered trademark
% EE	percent entrapment efficiency
%LE	percent loading efficiency
% w/v	percent weight by volume
$^{\circ}$C	degree celsius
µg	microgram(s)
µL	microliter(s)
µm	micrometer(s)
AFM	atomic force microscope
Chol	cholesterol
C	the concentration of NaFI in the formulation
C_i	the initial concentration of NaFI added into the formulation
C_d	donor concentration
CL	conventional liposomes
cm^{-1}	wavenumbers
cm^2	square centimeter(s)
Conc.	concentration
CP	cetyl palmitate
CLSM	confocal laser scanning microscopy
DPH	1,6-diphenyl-1,3,5-hexatriene
DSC	differential scanning calorimetry
DLS	dynamic light scattering
OH	hydroxide
e.g.	exempli gratia (latin); for example
ER	enhancement ratio
et al.	and others
etc.	et cetera (latin); and other things/ and so forth
J	Flux

FTIR	fourier transform infrared spectroscopy
g	gram(s)
G	the correction factor given by the ratio of the vertically to the horizontally polarized light
GI	gastrointestinal
h	hour(s)
HCl	hydrochloride
i.e.	id est (latin); that is
kDa	kilodalton(s)
kg	kilogram(s)
kHz	kilohertz
K_p	permeability coefficients
kV	kilovolt (s)
L	liter(s)
log P	log octanol-water partition coefficient
LI	d-limonene
mg	milligram(s)
min	minute(s)
mL	milliliter(s)
mm	millimeter(s)
mm^2	square meter(s)
mM, mmol	millimolar(s)
mV	millivolt(s)
MW	molecular weight
NaFI	sodium fluorescein
ng	nanogram(s)
NLC	nanostructured lipid carriers
nm	nanometer(s)
NI	niosomes
NIP	PEGylated niosomes
NIP-LI	PEGylated niosomes with d-limonene

PBS	phosphate buffer saline
PC	phosphatidylcholine
PDI	polydispersity index
PEG2000-DSPE	Na-salt n-(carbonyl-methoxypolyethylene glycol-2000)-1,2-distearoyl-sn-glycero-3-phosphoethanolamine
pH	potentia hydrogenii (latin); power of hydrogen
pI	isoelectric point
pK_a	-log 10ka
PL	PEGylated liposomes
PL-LI	PEGylated liposomes with d-limonene
I_{vv}	emission intensities perpendicular to the horizontally polarized light (90°, 0°)
I_{vh}	emission intensities parallel to the horizontally polarized light (90°, 90°)
Rh-PE	rhodamine B 1,2-dihexadecanoyl-sn-glycero-3-phosphoethanolamine triethylammonium salt
r	anisotropy value
rpm	round per minute
s	second
SC	stratum corneum
S.D.	standard deviation
SEM	scanning electron microscopy
SLN	solid lipid nanoparticles
SLNP	PEGylated solid lipid nanoparticles
SLNP-LI	PEGylated solid lipid nanoparticles with d-limonene
SN	sonophoresis
TEM	transition electron microscopy
T_m	transition midpoint temperature
v/v	volume by volume
W	watt(s)

CHAPTER 1
INTRODUCTION

1.1 Statement and significance of the research problem

Transdermal drug delivery system has been an important transportation of various drug into body and represents an attractive alternative to oral delivery of drugs, because it can avoid the hepatic first pass metabolism by gastrointestinal enzymetic system that is a problem of oral drug delivery. Transdermal delivery also has advantages over hypodermic injections, which are painful, generate dangerous medical waste, and pose the risk of disease transmission by needle re-use. While transdermal delivery is non-invasive and can be self-administered to improve patient acceptance and compliance (Prausnitz and Langer, 2009). Besides the need for transdermal administration of drugs as an alternative route for the oral route and parenteral route, targeting to the skin is also an important issue, especially when considering skin diseases (Bouwstra et al., 2003). However, the major limitation of transdermal drug delivery is the permeability barrier of the skin. The skin's barrier selectively and effectively inhibits chemical penetration (Menon, Lee, and Robert, 1998).

The outermost layer of skin, stratum corneum, acts as a rate limiting barrier, which contains flattened dead epidermal cells (corneocytes) embedded in hydrophobic lipid domains (brick and mortar) (Walters, 2002). Thus, the percutaneous absorption of compounds and water loss is controlled by stratum corneum layer. Two possible penetration pathways of drug through skin barrier have been reported: the intercellular penetration pathway through the lipid layers surrounding the corneocytes and the transcellular penetration pathway directly passing through both the phospholipid membranes and the cytoplasm of the dead keratinocytes. Moreover, human skin and other animal model skin also include hair follicles, sweat ducts, and blood vessels. Although the follicular openings have only ~0.1% of the total skin surface area, the follicular penetration pathway may have a

greater role than previously believed (Bouwstra et al., 2003, Lademann et al., 2008). For passive transport, small, potent and moderately lipophilic drugs occur mostly through lipid bilayers of the stratum corneum, while the transdermal transport of hydrophilic drugs can occur through hair follicles and sweat ducts but do not permit the stratum corneum layer (Kalluri and Banga, 2011, Ibrahim and Li, 2010).

To overcome the limitation of skin barrier, several enhancement techniques have been investigated, such as chemical enhancers (Karande and Mitragotri, 2009, Ibrahim and Li, 2010, Polat et al., 2012), iontophoresis (Fang et al., 2002), microneedles (Guo et al., 2013, Petchsangsai, Opanasopit, and Ngawhirunpat, 2014, Loizidou et al., 2015), sonophoresis (Alvarez-Román et al., 2003, Herwadkar et al., 2012, Aldwaikat and Alarjah, 2015), electroporation (Wong et al., 2006, Tokudome and Sugibayashi, 2004), nanoparticles (Lopez et al., 2011) and liposomes (Elsayed et al., 2006, Sinico et al., 2005). Although these techniques can improve skin permeability, the penetration mechanisms of each technique are different.

Liposomes have been used for dermal and transdermal drug delivery. These lipid vesicles contain phospholipids arranged in one or more concentric bilayers enclosing an equal number of aqueous compartments, which can entrap hydrophilic agents within the inner aqueous sphere and lipophilic agents intercalated into the lipid bilayer (Pierre and Santos Miranda Costa, 2011). However, conventional liposomes are of little or no value for transdermal drug delivery because they do not deeply penetrate skin, remaining confined to the upper layers of the stratum corneum (Touitou et al., 2000). Cevc et al. have reported that deformable liposomes (Transfersomes®), which an edge activator was added into phospholipids bilayer of the vesicles to destabilize the lipid bilayer and to increase deformability, can increase skin permeability when applied under non-occluded conditions (Cevc and Blume, 1992).

Niosomes and liposomes are functionally the same with similar physicochemical properties depending on the composition of bilayer and the preparation methods, but differ chemically in their structure units. Niosomes are made of hydrated non-ionic surfactants and cholesterol that provide greater stability and lack many of the disadvantages associated with liposomes, i.e., high cost, low availability, and the variable purity problems associated with phospholipids. Vesicular nanocarriers of

niosomes have been used as potential transdermal drug delivery systems due to properties such as enhanced drug penetration, local depot for sustained drug release, and a rate-limiting membrane for modulation of systemic absorption of drugs via the skin (Muzzalupo and Tavano, 2015).

The modification of the vesicles with polyethylene glycol (PEG) was developed to improve the colloidal stability by changing the physicochemical properties of particles via the polymer coating and to enhance the blood circulation time by reducing systemic uptake of mononuclear phagocytes (Immordino, Dosio, and Cattel, , 2006). A few reports are available on dermal application of PEGylated liposomes (PL). Jain et al. reported that the topical application of PEGylated surfactant-containing liposomes can increase the skin permeation of zidovudine by binding to water molecules and increasing the hydration of stratum corneum barrier (Jain, Tiwary, and Jain, 2008). In addition, Knudsen et al. (2012) reported that calcipotriol-loaded liposomes with 1 mol% PEG significantly increased the accumulation of calcipotriol in the skin and hair follicles compared to non-PEGylated liposomes. The size of liposomes affected the penetration of calcipotriol into the stratum corneum. Small unilamellar vesicles enhanced calcipotriol penetration more than large ones. Liposomes with long circulation times containing skin penetration enhancers may yield a transdermal drug delivery system that can affect the blood circulation time of liposomes. Therefore, the use of PL as carriers for transdermal drug delivery still requires further study.

Solid lipid nanoparticles (SLN) have been reported to be an alternative system to emulsions, liposomes, microparticles and their polymeric counterparts for various application route due to various advantages such as feasibility of incorporation of lipophilic and hydrophilic drugs, improved physical stability, low cost compared to liposomes, and easy to scale-up and manufacturing (Mehnert and Mader, 2001, Uner and Yener, 2007). SLN are colloidal nanocarrier systems composed of a high melting point lipid/s (including high melting point glycerides or waxs) as a solid core coated by surfactants (Mandawgade and Patravale, 2008). The small particle sizes of SLN are in close contact with the stratum corneum, thus promoting the amount of the encapsulated agent which penetrates into the skin (Mei et al., 2003).

Terpenes have been widely used as skin penetration enhancers for both hydrophilic and hydrophobic drugs. D-limonene ($C_{10}H_{16}$) is a monocyclic monoterpenes, small molecular sizes, and high log P value (log P= 4.57) that can remain in the lipid portion of the stratum corneum and enhance the transport of drugs through skin by fluidizing or perturbing the integrity of the stratum corneum barrier (Lu et al., 2014). Moreover, the combination of terpene and other formulation has been reported to enhanced skin penetration of various drugs by a synergistic effect of penetration enhancer. Terpenes containing ultra-deformable liposomes have also been reported to increase skin penetration of sodium fluorescein mainly via a transfollicular pathway and slightly via intercellular and transcellular pathways (Subongkot et al., 2012, Subongkot et al., 2013).

Sonophoresis (SN) is a non-invasive technique to increase skin permeability of hydrophilic and large molecular weight compounds, such as caffeine (Boucaud et al., 2001, Sarheed and Abdul Rasool, 2011), hydrocortisone (Sarheed and Frum, 2012), calcein, and FITC-labeled dextrans. The transdermal delivery of hydrophilic solutes under influence low-frequency ultrasound is likely to be non-specifically transported across the stratum corneum (Morimoto et al., 2005). Cavitation effects caused by collapse and oscillation of cavitation bubbles in the ultrasound field have been the main possible mechanisms to create aqueous pathways across the stratum corneum by the distortion of lipid bilayer, which can lead to enhancing the hydrophilic drugs transported across the skin (Mitragotri, Blankschtein, and Langer, 1996). Low-frequency SN can easily be coupled with other transdermal delivery techniques to produce the synergistic effect on drug delivery through an intracellular pathway such as tape stripping (Escobar-Chávez et al., 2008), microneedle, electroporation (Petchsangsai, Opanasopit, and Ngawhirunpat, 2014), iontophoresis (Fang et al., 2002), and chemical enhancers (Mutalik et al., 2009).

The combination of SN and liposomes in skin permeation has been rarely studied, and it is still controversial in the synergistic effect of these methods. Vyas et al. showed that the application of ultrasound and ointment-containing liposomes enhanced diclofenac-entrapped liposome permeated across the skin that the diffusion is probably due to the breaking of lamellae on sonication (Vyas, Singh, and Asati, 1995). However, liposomes application to sonicated skin before applied bovine serum

albumin (BSA) solution can reduce BSA penetration and transepidermal water loss, because liposomes repaired the sonication-induced skin disruption (Dahlan, Alpar, and Murdan, 2009). The penetration mechanism may depend on various factors, including formulation, type of lipid nanocarriers, or method of SN and lipid carriers application. Moreover, the mechanistic study for lipid nanocarriers penetrated into skin combined with SN has not reported, especially in liposome as a transfollicular drug delivery system.

Sodium fluorescein (NaFI) is a low molecular hydrophilic compound (MW 376 Da, log P = -1.52) and a fluorescence compound that uses as a diagnostic tool in topical application (Michinori et al., 1997). Hydrophilic compounds are less permeate through the skin because of their physicochemical limitations (Chen, Liu, and Fahr, 2011). Enhancement strategies are necessary to improve the transdermal delivery of hydrophilic drugs applied to the skin, such as liposomal carrier for delivery of hydrophilic drug through the skin or physical methods to improve the skin permeability (Pierre and Santos Miranda Costa, 2011). Therefore, the aim of the present study was to develop lipid nanocarriers (liposomes, niosomes, SLN, and PEGylated nanocarriers) as skin delivery carriers for enhancing skin permeation of hydrophilic drug, NaFI, and to investigate the physicochemical characteristic of nanocarriers (particle size, shape, zeta potential, entrapment efficiency, loading efficiency, and bilayer membrane fluidity) and *in vitro* skin penetration. In addition, the effect of nanocarriers combined with SN on the skin penetration was investigated. Finally, to investigate possible mechanisms of skin penetration pathways by which nanocarriers and SN, tape stripping technique, confocal laser scanning microscopy (CLSM), scanning electron microscopy (SEM), selectively block hair follicle, fourier transform infrared spectroscopy (FTIR), and differential scanning calorimetry (DSC) were performed.

1.2 Objective of this research

1.2.1 To develop lipid nanocarriers (liposomes, niosomes, SLN, and PEGylated nanocarriers) for enhancing skin penetration of hydrophilic drug (NaFI).

1.2.2 To investigate the influence of formulations on the physicochemical properties (i.e. particle size, charge, morphology, entrapment efficiency, and membrane fluidity) and *in vitro* skin penetration of NaFI

1.2.3 To determine the effect of nanocarriers combined with SN on the skin penetration of NaFI.

1.2.4 To examine the penetration mechanism of nanocarriers combined with SN on skin penetration of NaFI.

1.3 The research of hypothesis

1.3.1 Different physicochemical properties of lipid nanocarriers, i.e. particle size, size distribution, surface charge, morphology, entrapment efficiency, and membrane fluidity influence the *in vitro* skin penetration of hydrophilic compound.

1.3.2 Penetration enhancement methods, i.e. lipid nanocarriers, penetration enhancer, or SN, can be potentially used as a skin delivery carrier for enhancing skin penetration of hydrophilic compound. The combination enhancement techniques can change the penetration mechanism.

CHAPTER 2
LITERATURE REVIEWS

2.1 Transdermal delivery

2.1.1 Skin structure and functions

The skin is the largest organ in the body (more than 10% of the body mass) that consists of four functional layers: the stratum corneum (nonviable epidermis), the remaining layers of the epidermis (viable epidermis), the dermis, and the subcutaneous tissue. There are also several associated appendages: hair follicles, sweat dusts, apocrine glands, and nails (Figure 2.1). Many functions of the skin can be classified as protective, maintaining homeostasis, or sensing. For instance, the barrier properties of stratum corneum involve a chemical entity resistance to entry into the body. After the proportion of entity bypassing the stratum corneum, metabolism process is performed in viable epidermis, which sensing of and attention to the damage caused by an entity induces the releasing of inflammatory mediator in the epidermis, with involvement of the dermis. Finally, the removal of entity from site can process by dermal blood supply and distribution into those body organs, specifically responsible for elimination of the entity by metabolism (liver) and excretion (kidney) (Walters, 2002).

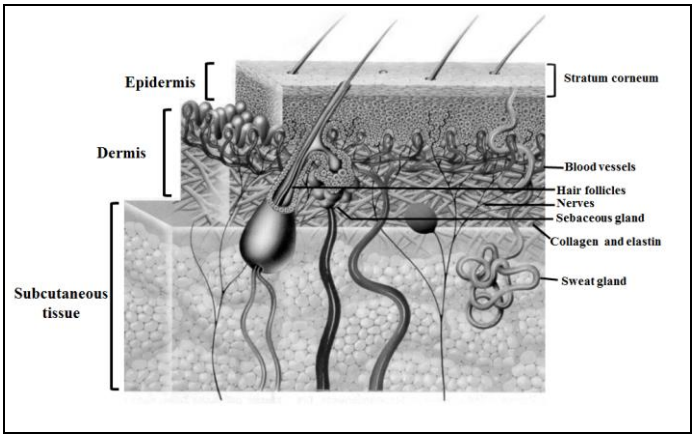

Figure 2.1 Skin structure includes the stratum corneum, the viable epidermis, the dermis and the subcutaneous tissue. Local skin structures are blood vessels, hair follicles, nerves, sebaceous glands, and the sweat glands.

Source: Grams, Y.Y. **Influence of molecular properties and delivery system design on the transfollicular transport across the skin**. Division of

Drug Delivery Technology of the Leiden/Amsterdam Center for Drug Research: Leiden University.

Stratum corneum

The superficial layer of the epidermis, stratum corneum, is approximately 10–20 μm thick, which represents 15-20 flattened, stacked, hexagonal, and dead epidermal cells (corneocytes) embedded in hydrophobic lipid domains ("brick and mortar" model). Each stratum corneum cell contains insoluble bundled keratins (~70 %) and lipids (~20 %) encased in a cell envelope, accounting for about 5% of the stratum corneum weight. The corneocytes are mainly packed with keratin filaments, surrounded by a cell envelope of cross-linked proteins and a covalently bound lipid envelope. In the part of intercellular region, a complex mixture of non-polar compounds such as ceramides, free fatty acid, cholesterol, and cholesterol sulphate is summarized in Table 2.1. Interconnecting between each corneocyte are protein structures, referred to as desmosomes. The barrier function is further facilitated by the continuous desquamation of this horny layer with a total turnover occurring once every 2-3 weeks. The stratum corneum barrier properties may be partly related to its very high density (1.4 g/cm^3 in the dry state), its low hydration by 15-20 %, compared with the usual 70 % of the body, and its low surface area for solute transport (less than 0.1 μm-wide intercellular regions of the stratum corneum). Therefore, the stratum corneum function is a barrier to control the percutaneous absorption of compounds and prevents the loss of internal body components (e.g. water loss) and the external environment (Walters, 2002, Bouwstra et al., 2003).

Table 2.1 Lipid components of the stratum corneum intercellular space

Lipid components	**% w/w**	**mol %**
Cholesterol esters	10.0	7.5[a]
Cholesterol	26.9	33.4
Cholesterol sulfate	1.9	2.0
Total cholesterol derivatives	38.8	42.9
Ceramide 1	3.2	1.6
Ceramide 2	8.9	6.6

Ceramide 3	4.9	3.5
Ceramide 4	6.1	4.2
Ceramide 5	5.7	5.0
Ceramide 6	12.3	8.6
Total ceramides	41.1	29.5
Fatty acids	9.1	17.0[a]
Others	11.1	10.6[b]

[a] Based on C16 alkyl chain. [b] Based on MW of 500

Source: Walters, K.A. "Dermatological and Transdermal Formulation." The structure and Function of Skin, Walters, K.A. and Robert, M.S.(Eds). New York: Marcel Dakker.

Epidermis

Underlying the stratum corneum is the viable epidermis (50–100 mm thick), which is responsible for the generation of stratum corneum. The viable epidermis is a stratified epithelium consisting of basal, spinous, and granular cell layers. Each layer is defined by position, shape, morphology, and state of differentiation of keratinocytes. This layer is a dynamically self-renewing tissue, so a loss of the cells from the stratum corneum surface (desquamation) is balanced by cell growth in lower epidermis. The origins of epidermis cells lie in the basal lamina near the dermis layer, which consists of melanocytes, Langerhans cells, Merkel cells, and two major keratinic cell types: the first functioning as stem cells having the capacity to divide and produce new cells; and the second serving to anchor the epidermis and the basement membrane.

After leaving the basal layer, the keratinocytes start to differentiate and migrate through the stratum spinosum and stratum granulosum, undergoing a number of changes in both structure and composition. The keratinocytes synthesize and express numerous different structural proteins and lipids during their maturation. The last sequences of keratinocyte differentiation represent the transformation into chemically and physically resistant cornified squames of the stratum corneum, called corneocytes (Bouwstra et al., 2003).

Dermis

Directly adjacent to the epidermis, the dermis (approximately 0.1-0.5 cm thick) provides the mechanical support such as nutritive, immune, and other support systems for the epidermis through a thin papillary layer. Moreover, the dermis plays a role in temperature, pressure, and pain regulation. The main structural components of dermis consist of collagenous fibers (70 %), providing a scaffold of support and cushioning, and elastic connective tissue, providing elasticity, in a semigel matrix of mucopolysaccharides. The fibroblasts are presented as the main cells to produce the connective tissues (i.e. collagen, laminin, fibronectin, and mast cells), which are involved in the immune and inflammatory response. Moreover, melanocytes also involve in the production of the pigment melanin.

The dermis layer have the network of vascular to facilitate the skin nutrition and immune responses. The flow rate of blood in the skin is about 0.05 ml. min^{-1}, providing a vascular exchange area equivalent to that of the skin surface area. Skin blood vessels were derived from the subcutaneous tissue, with an arterial network supplying the papillary layer, the hair follicles, the sweat and apocrine glands, the subcutaneous area, and the dermis itself. Another an important component in the dermis is lymphatic system that provides regulation of interstitial pressure, mobilization of defense mechanisms, and waste removal.

Subcutaneous tissue

The deepest layer of skin, subcutaneous tissue or hypodermis, contains a network of fat cells arranged in lobules and links to the dermis by interconnecting collagen and elastin fibers. The fat cells in this layer are possibly 50% of the body's fat. Therefore, hypodermis acts as a heat insulator, a shock absorber, and an energy storage region. Another main cell in the epidermis is the fibroblasts and macrophages, so the major roles of this layer are to carry the vascular and neural systems for skin and anchor the skin to underlying muscle (Szuba and Rockson, 1997).

Skin appendages

Hair follicles and their associated sebaceous glands, eccrine sweat glands, apocrine sweat glands, and nails are distributed across the entire skin surface with the

exception of the soles of the feet, the palms of the hand, and the lips. A sebaceous gland is associated with each follicle in various diameter sizes from 200 to 2,000 μm. The sebum consisting of triglycerides, free fatty acids, and waxes is secreted for protecting and lubricating the skin as well as maintaining a pH~5. This fraction area is slightly more than 1 per 1,000 of the total skin surface. The eccrine sweat glands are epidermal structures that are simple, coiled tubes arising from a coiled ball in approximately 100 μm-diameter, and located in the lower dermis. A dilute salt solution with pH~5 is secreted by stimulating of temperature-controlling determinants, such as exercise, high environmental temperature, and emotional street through the autonomic nervous system. Another sweat gland, the apocrine glands are also coil tubes in the specific body regions. The nail plate is flattened keratinized cells fused into a dense layer. In the keratinization process, the cell undergoes shape and other changes similar to the epidermal cells forming the stratum corneum (Cameli et al. 1994), but the keratinized layer is very tight. The chemical compositions of the nail plate are many similarities to the hair that the major components are highly folded keratin proteins (containing many disulfide linkages) with small amount of lipids (0.1 to1.0 %) (Walters, 2002).

2.1.2 Routes of permeation

The molecules have to overcome the horizontal structure of multilayer stratum corneum and the vertical structure of hair follicles in order to penetrate through the skin. Therefore, drug transport routes through skin barrier have three possible penetration pathway: I. the intercellular penetration pathway through the lipid layers surrounding the corneocytes, II. the transcellular penetration pathway directly passing through both the phospholipid membranes and the cytoplasm of the dead keratinocytes (Figure 2.2), and III. the follicular penetration pathway into the hair follicles (Blume-Peytavi et al., 2010). The lipophilic drugs occur mostly through lipid bilayers of the stratum corneum, while the transdermal transport of hydrophilic drugs can occur through hair follicles and sweat ducts (Ibrahim and Li, 2010).

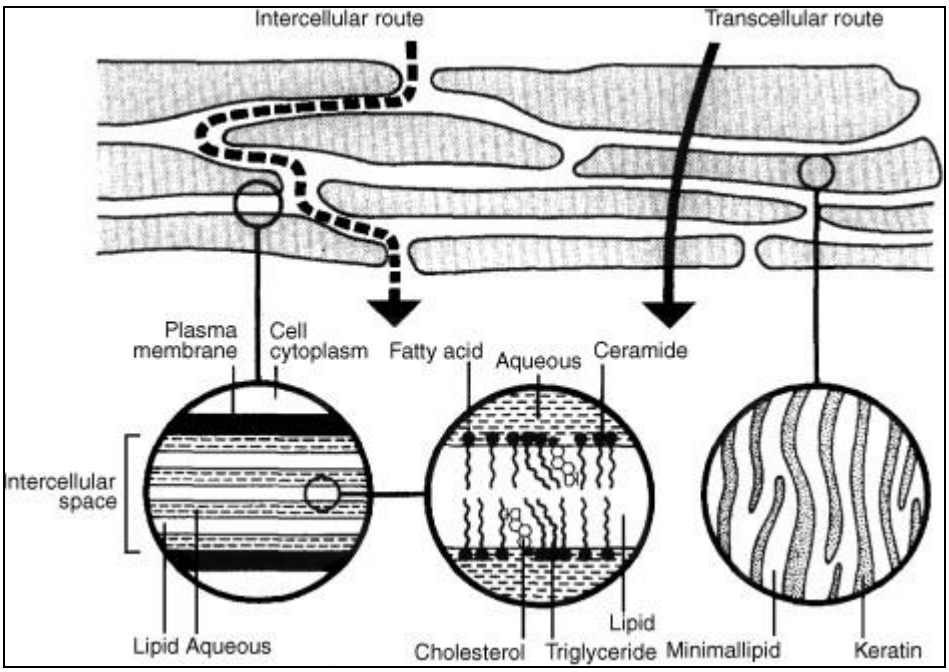

Figure 2.2 Simplified diagram of stratum corneum and two routes of drug penetration: intercellular route and transcellular route.

Source: El Maghraby, G. M., Barry, B. W., and Williams, A. C. "Liposomes and skin: From drug delivery to model membranes." **European Journal of Pharmaceutical Sciences** 34, 4 – 5: 203 - 222.

Intercellular pathway

Drugs crossing the skin by intercellular route must pass through the small spaces of the continuous lipid matrix. Although the thickness of the stratum corneum is only ~10-20 μm, the phospholipid membranes and the cytoplasm of the dead keratinocytes in the stratum corneum make this route more tortuous and the actual diffusional path crossing the skin around 400 μm. Therefore, this pathway is the most common path to penetrate the skin of small uncharged molecules by partitioning into and diffusing through repeated aqueous and lipid domains.

Transcellular pathway

Drugs crossing the skin by directly passing through the smallest spaces of the corneocytes cells are called as a transcellular pathway. Because the passage of molecules through the stratum corneum depends on partitioning of molecules

between lipophilic and hydrophilic compartments, including the almost impenetrable corneocyte intracellular matrix of keratin and keratohyaline, few drugs have the properties to cross via this pathway. The polar solute is diffused by a high-energy pathway involving immobilized water near the outer surface of keratin filaments. Therefore, the highly hydrate keratin provides an aqueous environment for hydrophilic drug, while the nonpolar solute diffuses through a nonpolar lipid pathway (Roberts, 2002; Yadav, 2012).

Follicular pathway

Human skin and other animal model skin have hair follicles, sweat ducts, and blood vessels. Although the follicular openings have approximately 0.1 % of the total skin surface area, the follicular penetration pathway exhibits a great role to delivery hydrophilic and high molecular weight molecules, as well as particle-based drug delivery systems. Due to extend deep into the dermis, the actual surface area available for penetration significantly increased. A rich perifollicular vascularization and the differentiation pattern along the follicular duct and the follicle possesses also play an important role on the skin penetration. Many studies suggest that the follicular penetration route may be especially relevant for systemic drug delivery system (Bouwstra et al., 2003, Lademann et al., 2008, Knorr, 2009).

2.1.3 The physicochemical properties of drug for effective transdermal delivery

The skin's barrier selectively and effectively inhibits chemical penetration (Menon, Lee, and Robert, 1998). The outermost layer of skin, the stratum corneum, acts as a rate limiting barrier. Only very few drug candidates have been approved for transdermal delivery, which molecules should have appropriate physicochemical properties, such as low melting point (<150 $^{\circ}$C), low molecular weight (<500 D), intermediate lipophilicity (log P = 1-3), and high potency (total daily dose < 10 mg) for passively partitioning across the lipophilic layer of stratum corneum into the deeper layers of skin. The barrier properties do not permit to permeate passively for large molecular weight and hydrophilic molecules (Kalluri and Banga, 2011). Consequently, several approaches by using both the chemical and physical

enhancement strategies have been established in an attempt to overcome the barrier properties and deliver drug molecules through the skin (Smith, 2007).

2.1.4 Fick's law of diffusion

The inhomogeneous of skin layered structure and the presence of appendages interrupting the intact stratum corneum makes a very complexation of the diffusion processes in human skin. For the processes of diffusion, drugs have been calculated by Fick's first law (Equation 1). In this case, the skin membrane is a homogeneous and the acceptor phase must be a sink condition for the penetrant. The proportion of transported mass; d_m (g) per time; d_t (h) is directly correlated to the diffusion coefficient; D (cm^2/s), the size of the defined area; A (cm^2), and the concentration gradient (g/cm^3). However, it is reverse proportional to the distance; dx (cm) of the transported mass. The diffusion coefficient depends on physicochemical characteristics of the medium and the penetrant. In a steady state situation, a constant gradient is presented in the membrane (Grams, 2005).

$$\frac{dm}{dt} = -DA\frac{dc}{dx} \tag{1}$$

However, human skin has a very complex structure. Fick's second law has been derived from the equation 1 for assuming the undirectional diffusion of molecules from outer surface into the tissue (Equation 2). The rate of change in concentration with time at appoint within a diffusional area is proportional to the rate of change in the concentration gradient at that point.

$$\frac{\partial c}{\partial t} = D\frac{\partial^2 c}{\partial x^2} \tag{2}$$

Plotting the cumulative amount of penetrated drug against time, a linear dependency is presented in steady state conditions. The flux (J) can be determined directly from the slope. The lag time is obtained by extrapolating the linear portion of the penetration profile to the abscissa (Figure 2.3). The skin permeation of model drug is analyzed using a mathematical model based on Fick's law of diffusion (Equation 3):

$$K_p = \frac{J}{C_d} \tag{3}$$

where K_p is the permeability coefficient, J is the steady-state flux, and C_d is the donor concentration of the formulations (Williams, 2003).

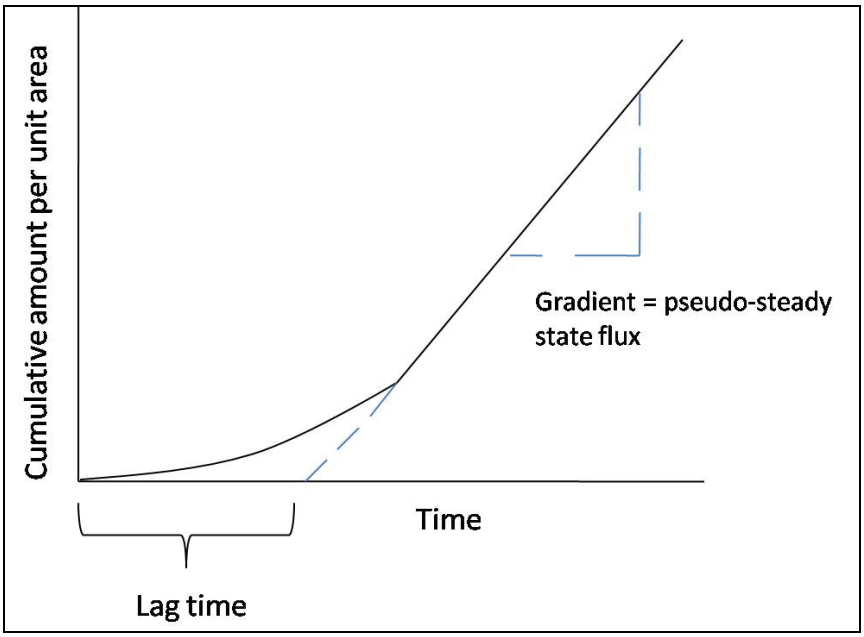

Figure 2.3 Typical permeation profile for an infinite dose application of skin membranes

Source: Williams, A.C. **Transdermal and topical drug delivery; from Theory to clinical Practice**. London: Pharmaceutical Press.

2.2 Methods for enhancing drug transport through the skin

To overcome the limitation of the skin barrier, several enhancement techniques have been investigated for improving skin permeability as shown in Figure 2.4 (Barry, 2001). The combination of two or more techniques may provide a synergistic effect to enhance drug delivery into the skin, such as sonophoresis combination with chemical enhancer (Herwadkar et al., 2012), microneedle combination with electrophoresis and sonophoresis (Petchsangsai et al., 2014), microneedle combination with liposomes (Guo et al., 2013). However, some interactions may provide an inhibitory effect to reduce drug permeated through the skin.

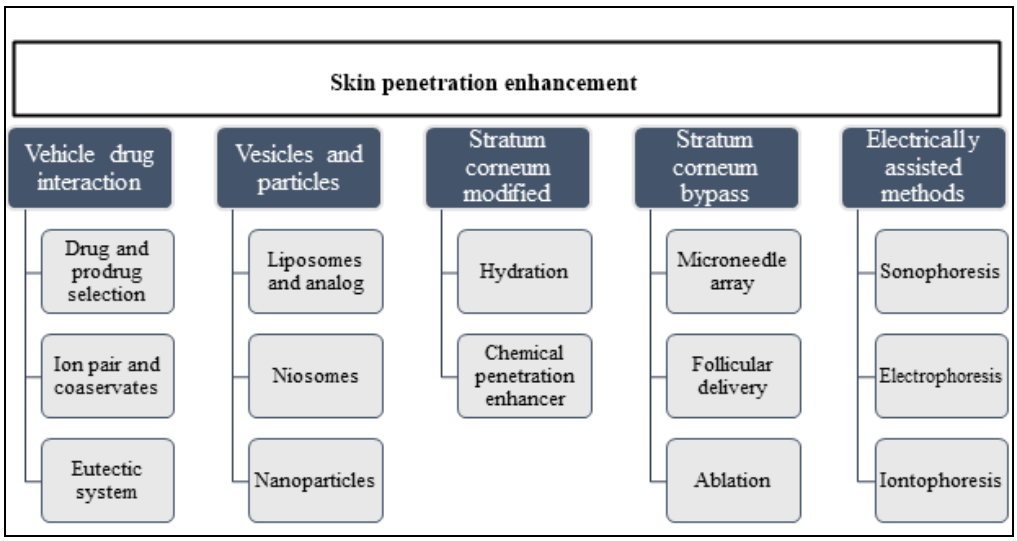

Figure 2.4 Skin penetration enhancement techniques

Source: Barry, B. W. "Novel mechanisms and devices to enable successful transdermal drug delivery." **European Journal of Pharmaceutical Sciences** 14, 2: 101 - 114.

2.2.1 Vehicle drug interaction

The prodrugs have been interested in term of enhancing the skin permeation, improving chemical and enzymatic stability, and reducing skin irritation potential. For the parent drug that is relatively hydrophilic, increasing its lipophilicity can result in improved percutaneous flux through the lipid domain of the diffusional stratum corneum barrier. By contrast, it has also been possible to improve the flux of extremely hydrophobic compounds by creating more hydrophilic prodrugs to overcome the controlled diffusion viable tissue (Paudel et al., 2010). Therefore, the reason that increasing both lipid and aqueous solubility of the drug is important to increase the permeation of drug through the intercellular compartment of stratum corneum. For improving transdermal drug delivery, many reports have been successfully developed such as the delivery of ketorolac piperazinylalkyl prodrugs (Qandil et al., 2008), and PEGylation on acetaminophen (Thomas et al., 2009).

An ion pair or eutectic system has also been used to modify the interaction between drug and vehicle. In case of charged drug molecules, it cannot readily permeate through human skin. The lipophilic ion pair formulation has been

formulated by adding an oppositely charged to the charged drug, leading to form an ion-pair and then neutralize the surface charge. This complex can be partitioned into and can permeate through the stratum corneum (Benson, 2005). For eutectic system, the low melting point of drugs leads to increasing solubility and enhancing the skin penetration. A mixture of two components can inhibit the crystalline process of each other, because the melting point of a mixed component is less than that of each component alone. According to previous reports, ibuprofen has been successfully formed topical eutectic mixtures with terpenes (Stott et al., 1998), menthol (Yong at al., 2004), and methyl nicotinate (Wolloch and Kost, 2010). Moreover, propranolol with fatty acids and lignocaine with menthol have also been investigated (Kang et al., 2000, Stott et al., 2001).

2.2.2 Vesicles and particles

2.2.2.1 Liposomes and analogs

Liposomes have been used for dermal and transdermal drug delivery. This lipid vesicle is made from phospholipids arranged in one or more concentric bilayers enclosing an equal number of aqueous compartments (Figure 2.5), which the ability of phospholipids to form bilayers depends on their amphipathic nature, the presence of a hydrophilic or polar region in the head (attracts water), and a non-polar region or lipophilic tail (repels water). Thus, it can entrap both hydrophilic agents within the inner aqueous sphere and lipophilic agents intercalated into the lipid bilayer (de Leeuw et al., 2009, Pierre and Costa, 2011). Various amphipathic molecules, natural or synthetic, have been used to form liposomes. Lecithin is the natural phospholipid and the major component of most biological membranes, which have commonly encountered to prepare liposome vesicles. For improving bilayer characteristics of liposomes, cholesterol was used to increase the microviscosity of the bilayers resulting in reduced the permeability of water soluble molecules through the membrane bilayer and increased the incorporation efficiency. This also resulted in the stabilization of the membrane and the rigidity of the bilayer in the presence of biological fluids such as blood/plasma (Yatvin and Lelkesm, 1982, Lee et al., 2005).

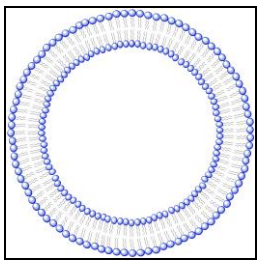

Figure 2.5 Liposomal structure built from phospholipid molecule

Three types of liposome vesicles have been investigated by various lipid compositions, methods of preparation, and the properties of the encapsulated agents. The unilamellar lipid vesicle is a single bilayer enclosing an aqueous compartment, according to size, these are known as the small unilamellar vesicle (SUV;~25 to 100 nm) or the large unilamellar vesicle (LUV;~100 to 400 nm). While more bilayers are presented in the large vesicles referring as the multilamellar vesicle (MLV;~0.2 to 10 μm) (Vemuri and Rhodes, 1995).

For the first introduction, the potential value of liposomes for topical therapy was investigated by Mezei and Gulasekharam (1980). They found that liposomal lotion increased four to five fold concentrations of triamcinolone acetonide in the epidermis and dermis compared to a conventional formulation (Mezei and Gulasekharam, 1980). For improving dermal or transdermal drug delivery, liposome formulations have been developed depending on characteristics such as size, surface charge, and chemical composition (El Maghraby, Campbell, and Finnin, 2005, Dubey, Mishra, and Jain, 2007, Mura et al., 2007, Cevc and Vierl, 2010, Pierre and Costa, 2011).

Mechanism of liposomes for transdermal drug delivery has been clarified into 5 routes as shown in Figure 2.6:

i. In the free drug mechanism, the drug permeates through the skin after exiting from the vesicles (Ganesan et al., 1984). El Maghraby, Williams, and Barry. (1999) reported that estradiol-loaded in liposomes exhibited the peak of transepidermal flux and drug release from vesicles at the same time.

ii. In the penetration enhancing mechanism, the vesicles can change the ultrastructure of the intercellular lipids (Kato, Ishibashi, and Miyake, 1987). Zellmer, Pfeil, and Lasch (1995) reported that the composition of vesicles affected on the

stratum corneum lipids, which dimyristoylphosphatidylcholine liposomes changed the enthalpy of the lipid-related transitions of the stratum corneum. Kirjavainen et al. (1996) revealed that the conical shape of phospholipid molecules, dioleoylphosphatidylethanolamine (DOPE) or lyso-phosphatidylcholine (lyso-PC), provided the greatest effect on the skin (Kirjavainen et al., 1996). This indicated that phospholipid acted directly on the permeability barrier of the stratum corneum (Yokomizo and Sagitani, 1996). However, only non-rigid phospholipid vesicles provided a possible accelerant effect on the interaction of liposomes with stratum corneum (El Maghraby, Williams, and Barry, 1999). Moreover, the importance of liposome structure has been investigated by El Maghraby et al. (2000), who reported that phospholipid molecules permeated into the stratum corneum and promoted the transepidermal flux of oestradiol more than solution form (El Maghraby, Williams, and Barry, 2000). Discrepancies in the literature reports of the penetration enhancing effects by using different formulations can be attributed to the use of different lipid components in the vesicles, which non-rigid lipids tend to produce the greatest enhancing effects (El Maghraby, Barry, and Williams, 2008).

iii. In the adsorption and/or fusion of vesicles with the stratum corneum mechanism, the vesicles may adsorb to the stratum corneum surface with subsequent directly transfer of drug from vesicles to the skin. Vesicles may also fuse and mix with the stratum corneum lipid matrix, referring to increase the partition of drug into the skin. However, lipid vesicles cannot penetrate through intact healthy stratum corneum, instead, they dissolve and form a unit membrane structure (Schaller and Korting, 1996, Kirjavainen et al., 1996). Moreover, the major component of liposomes, phospholipid, increased the continuity of the lipid matrix in the skin, resulting in facilitated the movement of lipophilic molecules (Keith and Snipes, 1982).

iv. In intact vesicular skin penetration mechanism, traditional liposomes with intact vesicles cannot penetrate the healthy skin. Large lipid vesicles of traditional liposomes can penetrate diseased skin with its damaged stratum corneum (as in eczema) but cannot invade densely packed stratum corneum with hyperkeratosis as in psoriasis (El Maghraby, Barry, and Williams, 2008). Subsequently,

fluoromicrographic studies showed that intact SUVs penetrated no deeper than the stratum corneum (Lasch et al., 1992). However, the intact vesicles of ultradeformable liposomes have been reported to invade the skin and go deep enough to be absorbed by the systemic circulation. The transdermal hydration gradient can produce a force sufficient to drive ultradeformable vesicles through the stratum corneum and into the epidermis. Phospholipid hydrophilicity leads to xerophobia (tendency to avoid dry surrounding). Accordingly, the vesicles on the skin surface try to follow the local hydration gradient for remaining maximally swollen, and moving into deeper skin strata (Cevc and Blume, 1992, Cevc, Schätzlein, and Blume, 1995). In addition, the deformation of SUVs was as effective as large MLVs. The reduction of vesicle size improved the drug deposition into deeper strata and penetration through the skin, while large structures improved the drug deposition only (Valenta and Janisch, 2003, Verma et al., 2003).

v. In the transappendageal penetration route, hair follicles and sweat ducts plays a minor role in transdermal delivery of liposomes. The vesicle size up to 600 nm of diameter can penetrate through the skin but those of 1,000 nm or more remain in the stratum corneum. However, the transfollicular delivery from liposomes was enhanced only after it was combined with iontophoresis technique (Han, Kim, and Kim 2004, El Maghraby, 2006).

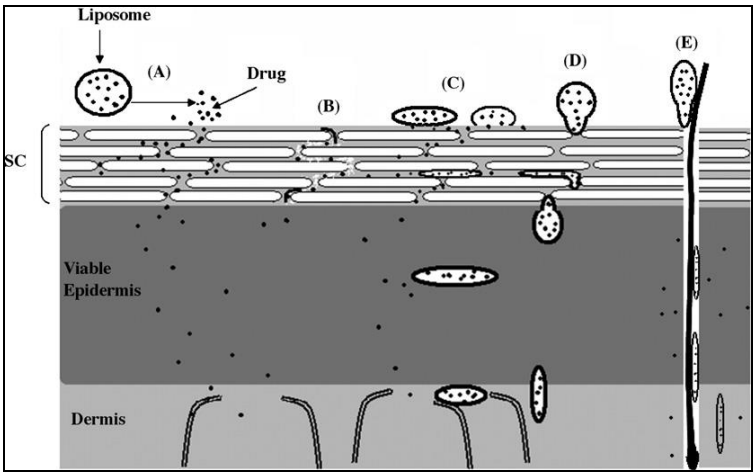

Figure 2.6 Possible mechanisms of action of liposomes as skin drug delivery systems: (A) the free drug mechanism, (B) the penetration enhancing process of liposome components, (C) vesicle adsorption to and /or fusion with the

stratum corneum, (D) intact vesicle penetration into and through the intact skin, and (E) the transappendageal route.

Source: El Maghraby, G.M., Williams, A.C., Barry, B.W. "Can drug-bearing liposomes penetrate intact skin?." **Journal of Pharmacy and Pharmacology** 58, 4: 415 - 429.

Therefore, some advantages of liposome on transdermal drug delivery are: (i) similar to biological membranes, interacting of liposomes with the similar skin lipids leads to enhanced local drug concentrations (Pierre et al., 2001); (ii) liposomes may serve as a local depots (reservoir effect) for the sustained release of dermatological active compounds including antibiotics, corticosteroids and retinoic acid due to the penetration capacity of individual phospholipid molecules into the lipid layers of the stratum corneum and epidermis. Liposomes can also decrease systemic absorption and minimize collateral symptoms due to a reservoir effect (Schreier and Bouwstra, 1994, Kim et al., 1997); (iii) phospholipid-containing liposomal formulations may act as penetration enhancers by destabilizing, fusing or mixing with the lipid matrix of stratum corneum, and subsequently loosening the lipid structure of the stratum corneum. The impaired barrier function of these layers increases the partitioning of the drug in the skin (Kirjavainen et al., 1999). However, conventional liposomes are of little or no value for transdermal drug delivery because they do not deeply penetrate skin, remaining confined to the upper layers of the stratum corneum (Touitou et al., 2000). Moreover, the large size of the liposomes was not able to enter the capillary circulation, resulting in provided a reservoir effect at the site of action (El Maghraby, Barry, and Williams, 2008).

Deformable liposomes

Cevc and Blume (1992) reported that deformable liposomes (Transfersomes®) is the first generation of elastic vesicles. These vesicles were formulated by adding an edge activator into phospholipids bilayer, leading to destabilization of the lipid bilayer and increase in the deformability of vesicles. Due to the high elasticity of vesicles, it can increase skin permeability when applied under non-occluded conditions. A single chain surfactant such as sodium cholate, sodium

deoxycholate, span 60, span 65, span 80, tween 20, tween 60, tween 80 or dipotassium glycyrrhizinate was used as the edge activators for providing ultradeformability of the transferosomes. Deformable liposomes can penetrate through the stratum corneum by two mechanisms. Firstly, vesicles can act as drug carrier systems, whereby intact vesicles enter the stratum corneum carrying vesicles bound drug molecules into the skin by using the driving force from "transdermal gradient". This force is the difference in water content between the relatively dehydrated skin surface (approximately 20 % water) and the aqueous viable epidermis (close to 100 %) that can affect the permeation of molecules through skin. Secondly vesicles can act as penetration enhancers, whereby vesicle bilayers enter the stratum corneum by squeezing themselves through the channels in the stratum corneum (less than one-tenth the diameter of the transferosome) and subsequently modify the intercellular lipid lamellae. This can also facilitate free drug molecules into and across the stratum corneum (Honeywell-Nguyen Arenja, and Bouwstra, 2003, Benson, 2005, Karande and Mitragotri, 2009).

Ethosomes

Ethosomes are novel lipid carriers consisting of phospholipid, high concentration (20-45 %) of ethanol, and water. The interdigitating of ethanol with lipid bilayers affects the characteristic of ethosome vesicles. Therefore, the incorporation of high ethanol concentration exhibits a small vesicle size and negative surface charge. The size of ethosomal vesicles was reported to increase with decreasing ethanol concentration in the range of 20-45 %. Presence of ethanol allows for better solubility of many drugs, thus exhibiting high encapsulation efficiency for a wide range of molecules, including lipophilic drugs (Touitou et al., 2000, Elsayed et al., 2007, Prausnitz and Langer, 2008).

Ethosomes were reported to improve *in vivo* and *in vitro* skin delivery of various drugs such as minoxidil, testosterone (Touitou et al., 2000), acyclovir (Horwitz et al., 1999), cannabidiol (Lodzki et al., 2003), erythromycin (Godin and Touitou, 2005), ammonium glycyrrhizinate (Paolino et al., 2005), sotalol, sodium salicylate, propanolol (Kirjavainen et al, 1999), trihexyphenidyl (Dayan and Touitou, 2000), zidovudine (Jain et al., 2004) and azelaic acid (Esposito, Menegatti,

and Cortesi, 2004). The skin penetration mechanisms of ethosomes might be caused by two factors (Figure 2.7). Firstly, ethanol interacts with lipid molecules in the polar head group region, resulting in reduced the melting temperature (T_m) of the stratum corneum lipids and increased their fluidity. Moreover, the intercalation of ethanol into the polar head group can result in an increase in the membrane permeability, leading to providing soft and flexible vesicles. These vesicles exhibit more easily penetrate into deeper layers of the skin than conventional liposomes. Secondly, intact ethosome vesicles can penetrate through the disordered stratum corneum. The release of drug in the deeper layers of skin and its transdermal absorption could be the result of ethosomes fusion with skin lipids and drug release at various points along the penetration pathway (Elsayed et al., 2007). Therefore, the effect of ethanol on the stratum corneum lipids and the vesicle fluidity, as well as dynamic interaction between ethosome vesicles and the stratum corneum may contribute to the superior delivery properties (Prausnitz and Langer, 2008).

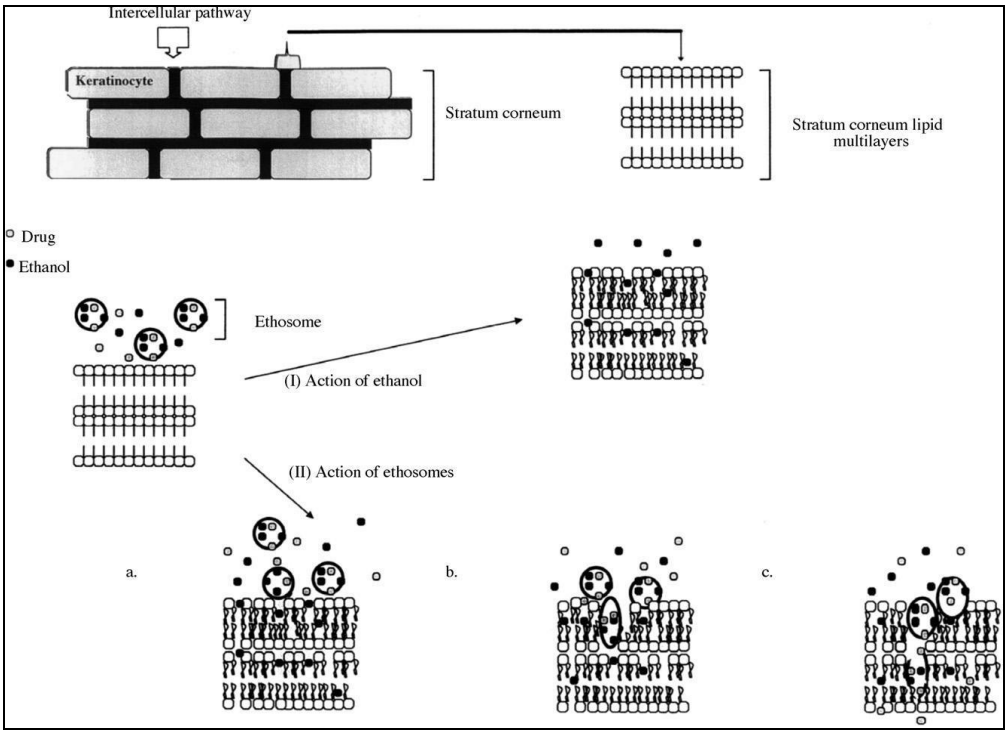

Figure 2.7 Mechanism of ethosomes as skin delivery systems

Source: Touitou, E., Dayan, N., Bergelson, L., Godin, B., Eliaz, M. "Ethosomes — novel vesicular carriers for enhanced delivery: characterization and skin penetration properties." **Journal of Controlled Release** 65, 3: 403 - 418.

Invasomes

Invasomes composed of phospholipids, ethanol and a mixture of terpenes as a penetration enhancer have been introduced by Verma (2002). Several lipophilic and hydrophilic penetration enhancers (i.e. labrasol, transcutol and cineole) were used to formulate penetration enhancer–containing vesicles that have been used as skin delivery carriers for minoxidil (Mura et al., 2009), diclofenac (Manconi et al., 2011), and temoporfin. For the mechanism of penetration enhancement of invasomes, terpenes are considered as a potential penetration enhancer to increase drug permeation by disrupting lipid packaging of stratum corneum and/or disturbing the stacking of the bilayers (Dragicevic-Curic et al., 2008).

PEGylated liposomes (PL)

Among the different polymers investigated in the attempt to improve the blood circulation time of liposomes, poly-(ethylene glycol) (PEG) has been widely used as a polymeric steric stabilizer. It can be incorporated on the liposomal surface in different ways, but the most widely used method is to anchor the polymer in the liposome membrane via a cross-linked lipid (i.e., PEG-distearoylphosphatidylethanolamine (DSPE)). Grafting PEG onto the liposome surface has demonstrated in several biological and technological advantages. The most significant properties of PEGylated vesicles are their strongly reduced mononuclear phagocyte system (MPS) uptake, leading to prolonged blood circulation, and improved the distribution of drug into tissues. Moreover, the PEG chains on the liposome surface avoid the vesicle aggregation, and then improve the stability of formulations. (Immordino, Dosio, and Cattel, 2006).

The behavior of PEGylated liposomes is depended on the characteristics and properties of the specific PEG linked to the surface. Figure 2.8 represents the regimens proposed of polymers attached to the liposome surface, depending on the graft density of the polymer (Gennes, 1980). The degree of surface

coverage and distance between the graft sites were determined by the molecular mass of polymer and the graft density. In most cases, the longer-chain PEG produced the greatest improvements of blood residence time. Allen et al (1991) reported that the blood level of liposomes with a longer molecular weight PEG (i.e., PEG 1900 and PEG 5000) was higher than liposomes with a shorter chain PEG (i.e., PEG 750 and PEG 120). The presence of PEG 2000 doubled the amount of lipid remaining in the plasma compared to formulations containing PEG 350 to 750. Moreover, Garbuzenko et al. (2005) reported the effect of various mole percentages of PEG2000–DSPE on the size and the lipid bilayer packing of LUV. Liposome size and specific turbidity were decreased by increasing temperature and PEG–DSPE mol%, except at 7 ± 2 mol%. When the grafted PEG is up to 4 mol% in LUV, the mushroom regime is found (Garbuzenko et al., 2005).

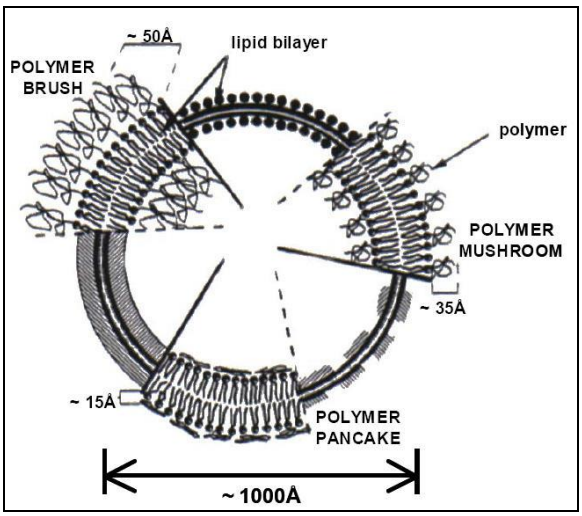

Figure 2.8 Schematic diagram of poly-(ethylene glycol) (PEG) configurations regimes (mushroom, brush and pancake) for polymer grafted to the surface of liposome bilayer

Source: Immordino, M.L., Dosio, F., Cattel, L. "Stealth liposomes: review of the basic science, rationale, and clinical applications, existing and potential." **International Journal of Nanomedicine** 1, 3: 297 - 315.

A few reports are available on the dermal application of PL. Jain, Tiwary reported that the topical application of PEGylated surfactant-containing

liposomes can increase the skin permeation of zidovudine by binding to water molecules and increasing the hydration of the stratum corneum barrier. In addition, calcipotriol-loaded liposomes with 1 mol% PEG significantly increased the accumulation of calcipotriol in the skin and hair follicles compared to non-PEGylated liposomes. The size of the liposomes also affected the penetration of calcipotriol into the stratum corneum: small vesicles enhanced calcipotriol penetration more than large ones (Knudsen et al., 2012). However, liposomes with long circulation times containing skin penetration enhancers may yield a transdermal drug delivery system and increase the blood circulation time of liposome vesicles.

2.2.2.2 Niosomes

Niosomes and liposomes are functionally the same with similar physicochemical properties depending on the composition of the bilayer and the preparation methods, but differ chemically in their structure units. Niosomes are made from a mixture of surfactants, such as sorbitan esters and analogs, sugar-based, polyoxyethylene-based, polyglycerol, or crown ether-based surfactants, and membrane additives, such as cholesterol or its derivatives. Nonionic surfactants have less potential to cause irritation, when compared with anionic and cationic surfactant, respectively (Moghassemi and Hadjizadeh, 2014). The greater stability and lack many of the disadvantages associated with liposomes, i.e., high cost, low availability, and the variable purity problems associated with phospholipid have been reported (Muzzalupo and Tavano, 2015).

Niosome vesicle is a potential nanocarrier for transdermal drug delivery due to the properties such as enhanced drug penetration, local depot for sustained drug release, and a rate-limiting membrane for modulation of systemic absorption of drugs via the skin. The enhanced skin permeability of compound by niosomes is caused from the alteration of the barrier function of stratum corneum. The reversible perturbation of lipid organization (Manconi et al., 2006), reduction of transepidermal water loss for increasing hydration of the stratum corneum and loosing its closely-packed cellular structure (Abdelkader et al., 2014), and adsorption and/or fusion of niosomes on the surface of the skin lead to increased thermodynamic activity gradient of drug at the interface, which is the driving force for drug

permeation (Mali et al., 2013). Therefore, niosomes have been used to enhance skin delivery of many drugs, such as minoxidil (Balakrishnan et al., 2009), nimesulide (Shahiwala and Misra, 2002), vinpocetine (El-Laithy et al., 2011), 17β-Estradiol (Fang et al., 2001), tenoxicam (Ammar et al., 2011) and ellagic acid (Junyaprasert et al., 2012).

Modification of vesicles have been developed for multipurpose, such as the improvement of wettability and the reduction of drug side effects by creating targeted niosomes. There are several types of modification methods that the grafting PEG onto niosome surface is one of the most important method. High hydrophilicity of PEG on niosome surface lead to forming a layer of H_2O molecules around themselves, and this layer prevents them from recognition and endocytosis by reticuloendothelial system to prolong blood circulation, which is a key factor for the successful application *in vivo* (Liu et al., 2007, Hong et al., 2009, Wang and Chen, 2011).

2.2.2.3 Nanoparticles

Nanoparticle structure exhibits a diameter size ranging from 1 to 100 nm. In case of using as transdermal carrier, nanoparticles are reported to be localized mainly in hair follicle openings and on the stratum corneum surface. Some studies reported the localization of quantum dots nanoparticles (4 to 5 nm-sized) in the deeper layers of the stratum corneum, the viable epidermis and deeper hair follicle parts (Smijs and Bouwstra, 2010). For polymer-based particles, the particle size between 40 and 130 nm can penetrate the skin, which the hair follicles might be an important pathway for skin invasion of particulate materials. On the other hand, polymer particles (up to 300 nm) seemed not to occur in human skin (Stracke et al., 2006).

Solid lipid nanoparticles (SLN), nanostructured lipid carriers (NLC) and lipid drug conjugates are types of carrier system based on solid lipid matrix. SLN is an alternative system to emulsions, liposomes, microparticles, and their polymeric counterparts for various application routes, which provides various advantages such as feasibility of incorporation of lipophilic and hydrophilic drugs, improved physical stability, low cost compared to liposomes, and easy to scale-up and manufacturing

(Mehnert and Mader, 2001, Uner and Yener, 2007). This particle is colloidal nanocarrier systems composed of a high melting point lipid/s (including high melting point glycerides or wax) as a solid core coated by surfactants (Mandawgade and Patravale, 2008) (Figure 2.9).

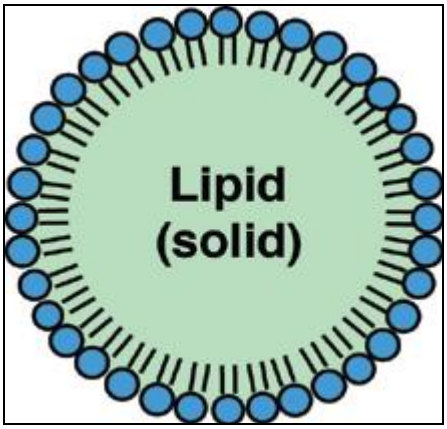

Figure 2.9 Structure of SLN

Source: Kakadia, P.G., Conway, B.R. "Solid Lipid Nanoparticles: A Potential Approach for Dermal Drug Delivery." **American Journal of Pharmacological Sciences.** 2, 5A: 1 - 7.

SLN is a very attractive colloidal carrier system for skin applications due to their various desirable effects on skin and well suited for use on damaged or inflamed skin. Moreover, these particles are based on non-irritant and non-toxic lipids (Wissing and Muller, 2003). Several claimed benefits of SLN feature for topical drug therapy include biocompatible ingredients, drug release modification, adhesion to the skin, and film formation with subsequent hydration of the superficial skin layers. However, the penetration into and across deeper skin layers is restricted due to the barrier function of the stratum corneum. The different kinds of nanoparticles provide the potential for penetration into hair follicles. SLN is also applicable drug delivery systems for transfollicular route in order to enhance the dermal and transdermal bioavailability of active pharmaceutical ingredients, which sebum-like lipid material and a size of less or equal 640 nm are appropriate specifications for particulate formulations (Lauterbach and Müller-Goymann, 2015). However, smaller particle sizes of SLNs are in close contact with the stratum

corneum, thus promoting the amount of the encapsulated agent penetrated into the skin (Mei et al., 2003).

The grafting of a hydrophilic substance like PEG onto colloidal particles can modify the surface hydrophobicity of particles and sterically stabilize them, leading to being a stealth SLN. PEG derivatives contain both hydrophilic and hydrophobic residues for giving them amphiphilic characteristics. In an aqueous PEG coated SLN dispersion, soluble hydrophilic residue of PEG turns to the water phase, and insoluble hydrophobic residue is oriented on the lipophilic part of SLN by formation of a shell around it (Figure 2.10). The protective layer prevents agglomeration during the production and/or storage, and subsequently, improves physical stability and dispersability of inner phase. Concentration of stealth agents strongly affects the rate of the phagocytic uptake (Heurtault et al., 2003, Uner and Yener, 2007). Bocca et al (1 9 9 8) studied the phagocytic uptake of PEG-coated dipalmitoylphosphatidylamine and stearic acid SLN by murine macrophages. They reported a significant increase in particle size related to the PEG concentration in the formulations and a decrease in murine uptake compared with non-stealth SLN. Optimum particle size for lymphatic uptake was reported between 1 0 and 1 0 0 nm (Swartz, 2001). In general, the coating nanoparticles with stabilizing hydrophilic molecules increases the particle size and leads to extended blood circulation of SLN. Many researchers also indicated that the colloidal carrier systems are required to possess smaller size, additionally hydrophobicity, and strong negative surface charge for effective penetration into the lymphatic interstitium (Porter, 1997, Harivardhan Reddy et al., 2005).

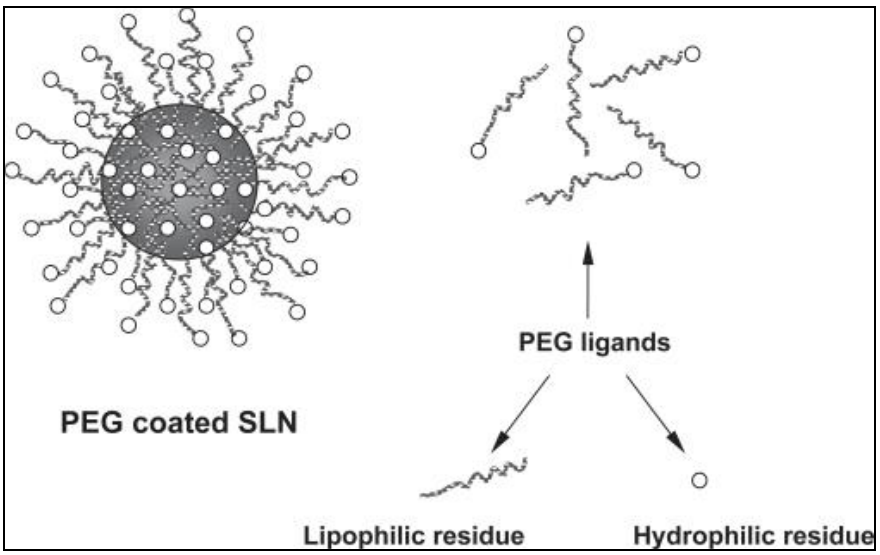

Figure 2.10 Schematic representation of SLN coated with PEG and molecular residues of PEG.

Source: Uner, M., and Yener, G. "Importance of solid lipid nanoparticles (SLN) in various administration routes and future perspectives." **International Journal of Nanomedicine** 2, 3: 289 - 300.

2.2.3 Stratum corneum modified

Numerous penetration enhancers were used to improve transdermal drug delivery by using various mechanism of action (Table 2.2). Many potential sites and modes of action have been identified as shown in Figure 2.11. Firstly, action at intercellular lipid by attacking and modifying the well-organized intercellular lipid domain of the stratum corneum leads to increase in the drug partition into the intracellular keratin domains or the tissue, Secondly, action at desmosomes and protein structures between corneocytes or altering metabolic activity within the skin was investigated. And thirdly, action within corneocytes by swelling, further keratin denaturation and vacuolation within individual horny layer cells was also investigated (Menon, 1998, Williams and Barry , 2004).

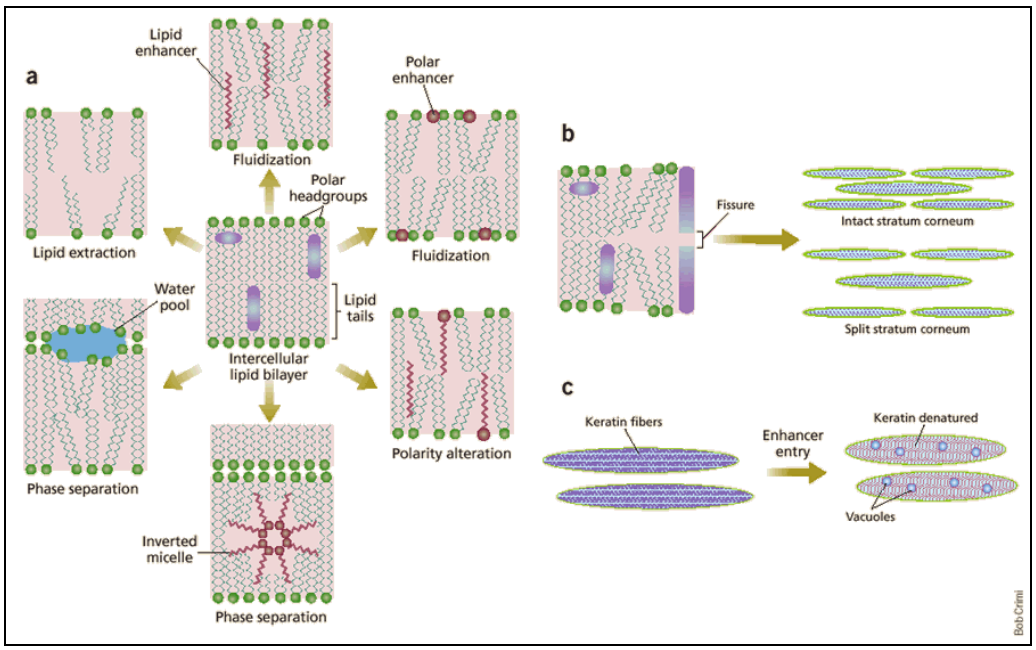

Figure 2.11 (a) Action at intercellular lipids. (b) Action at desmosomes and protein structures. (c) Action within corneocytes.

Source: Menon, G.K. Ultrastructural effects of some solvents and vehicles on the stratum corneum and other skin components: Evidence for an "extended mosaic partitioning model of the skin barrier". Dermal absorption and toxicity assessment. M. S. Roberts and K. A. Walters. New York, Marcel Dekker. 1: 727.

Table 2.2 The skin penetration enhancers

Type	Mechanism	References
Water	Hydrate the stratum corneum, increase fluidity of lipid bilayer	Potts and Francoeur, 1991
Sulphoxides Dimethylsulphoxide (DMSO)	- Denature proteins and change the intercellular keratin confirmation, from α helical to a β sheet in the stratum corneum. - DMSO is the "universal solvent" that can increase drug	Anigbogu et al., 1995, Williams and Barry, 2004

	partition from a formulation into skin membrane.	
Azone Laurocapram	Interacts with the lipid domains of the stratum corneum to disrupt their packing arrangement.	Hoogstraate et al., 1991, Pilgram et al., 2001
Fatty acids Lauric acid Oleic acid Polyunsaturated Linoleic Linolenic acids	- Interacts with and modifies the lipid domains of the stratum corneum - A long chain fatty is a separate phase (or as 'pools') within the bilayer lipids.	Ongpipattanakul et al., 1991, Santoyo and Ygartua, 2000, Funke et al., 2002
Alcohols, fatty alcohols and glycols Ethanol l-butanol, 1-octanol 1-propranolol PG	- The solvent effect can increase the solubility of the drug into the stratum corneum with a consequent improvement for drug partitioning into the membrane - Disrupts intercellular lipid packing within the stratum corneum bilayers	Friend et al., 1988, Megrab et al., 1995, Andega et al., 2001
Surfactants Sodium lauryl sulfate (SLS) Cetyltrimethyl ammonium bromide	- Solubilize lipids within the stratum corneum. - Swell the stratum corneum and interact with intercellular keratin	Tupker et al., 1990
Urea	Urea is a hydrating agent and has keratolysis property resulting in diffusion channel creation	Gloor et al., 2001
Terpenes and terpenoids Limonene	Fluidizing or perturbing the integrity of the stratum corneum barrier	Lu et al., 2014

Menthol 1,8-cineole		
Phospholipids	- Phospholipids in a non-vesicular form occlude the skin surface and thus can increase tissue hydration. - Fuse with stratum corneum lipids	Kato, Ishibashi, and Miyake, 1987

2.2.3.1 Terpenes and terpenoids

Terpenes are found in essential oils and can be classified by the number of isoprene units (Monoterpenes (C_{10}), Sesquiterpenes (C_{15}), Diterpenes (C_{20}), Sesterterpenes (C_{25}), Triterpenes (C_{30}), and Tetraterpenes (C_{40})) and the chemical groups (i.e. alcohols, esters, ketones, and so on) (Figure 2.12) (Chen et al., 2014). Terpenes have been widely used as skin penetration enhancers for both hydrophilic and hydrophobic drugs. The smaller molecule of terpenes tend to be more active permeation enhancers than the larger sequiterpenes. It also appears that hydrocarbon or non-polar group containing terpenes (such as limonene) provide better enhancement for lipophilic permeants than do the 'polar' terpenes. Conversely, the polar group containing terpenes (such as menthol, 1,8-cineole) provide better enhancement for hydrophilic permeants (Williams and Barry, 2004).

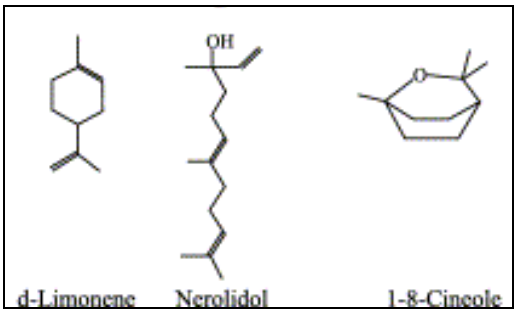

Figure 2.12 Example terpenes that promote skin penetration of a variety of drugs.

Source: Williams, A.C. and Barry, B.W. "Penetration enhancers." **Advanced Drug Delivery Reviews** 56, 5: 603 - 618.

The penetration mechanism of this agent is the modification of the stratum corneum, leading to improvement of the drug partition into the tissue. Many terpenes permeate human skin well (Cornwell and Barry, 1994), and large amounts of terpenes (up to 1.5 μg/cm^2) were found in the epidermis (Cal et al., 2001). During steady state permeation experiments using terpenes as penetration enhancers, the lag time for permeation is usually reduced. D-limonene ($C_{10}H_{16}$) is a monocyclic monoterpenes, small molecular sizes, and high log P value (log P= 4.57) that can remain in the lipid portion of the stratum corneum and enhance the transport of drugs through the skin by fluidizing or perturbing the integrity of the stratum corneum barrier (Lu et al., 2014). Moreover, the combination of terpene and other formulation provided a synergistic effect to enhance skin penetration of various drugs. Terpenes containing ultra-deformable liposomes have also been reported to increase skin penetration of sodium fluorescein (Subongkot et al., 2012) mainly via a transfollicular pathway and smaller contributions via intercellular and transcellular pathways (Subongkot et al., 2013).

2.2.4 Stratum corneum bypass

2.2.4.1 Microneedles

Microneedles are fabricated using a microelectromechanical system employing silicon, metals, polymers, or polysaccharides with an approximate length 50-900 μm and an external diameter of not more than 300 μm. Three types of microneedles such as solid coated, dissolvable/degradable, and hollow microneedles have been used to pierce the superficial skin layer followed by delivery of the macromolecular drug such as insulin, growth hormones, immunobiologicals, proteins and peptides (Bariya et al., 2012, Guo et al., 2013). The combination of microneedle with iontophoresis, sonophoresis and electrophoresis can be used to modify drug delivery (Petchsangsai et al., 2014, Donnelly et al., 2014).

2.2.4.2 Follicular delivery

Transfollicular pathway is an interesting route for delivery of the drug to target site, as hair follicles are closely surrounded by capillaries, antigen-presenting cells, sebaceous glands. Moreover, the bulge region of the hair follicle is

the host of stem cells. Hair follicles represent shunt pathways across the stratum corneum barrier, which may facilitate the absorption of large or hydrophilic molecules such as vaccine antigens (Patzelt and Lademann, 2013).

2.2.4.3 Ablation

To eliminate the barrier layer of stratum corneum, various techniques have been used such as thermal ablation by using high temperature (> 100 $^{\circ}$C) in short exposure (< 1 s) (Park et al., 2008), microdermabration (Fang et al., 2004), and photothermal ablation (Tang et al., 2013).

2.2.5 Electrically assisted methods

2.2.5.1 Sonophoresis (SN)

SN is a non-invasive technique for increasing the skin permeability of hydrophilic and large molecular weight compounds, such as caffeine (Boucaud et al., 2001, Sarheed and Abdul Rasool, 2011), hydrocortisone (Sarheed and Frum, 2012), calcein, and FITC-labeled dextrans (Morimoto et al., 2005). The ultrasound frequency in the range of 20 kHz to 16 MHz has been used. The application of low-frequency ultrasound (20–100 kHz) enhanced the skin permeability more effectively than high-frequency ultrasound (1–16 MHz). Tang et al. (2002) applied 20 kHz ultrasound (1.6–33.5 W/cm^2, 0.1:0.9 on/off duty cycle for 2 h) to full-thickness pig skin, and obtained an increase in electric skin conductivity corresponding to the possible collapse of transient cavitation on, or in the vicinity of, the skin surface. The transdermal delivery of hydrophilic solutes under the influence of low-frequency ultrasound are likely to be non-specifically transported across the stratum corneum (Morimoto et al., 2005).

The application of ultrasound to the skin by simultaneous treatment is performed by applying ultrasound energy through the drug-containing coupling medium. The enhancement of drug transport were clarified into two ways: i) by structural changes to the skin that increase skin permeability, and ii) through convection-related mechanisms that occur only when ultrasound is applied. Thus transdermal transport enhancement will decrease after ultrasound is turned off. However, the action of ultrasound on drugs or other active ingredients can cause the

molecules degradation or other chemical reactions, resulting in loss of activity or effectiveness of the therapeutic compound and caused undesired reactions (Riesz and Kondo, 1992). The application of ultrasound to the skin has the capacity to increase skin permeability through a variety of mechanisms including acoustic streaming (ter Haar, 2007, Azagury et al., 2014), rectified diffusion, cavitation (Ogura et al., 2008, Polat et al., 2011, Rich et al., 2014), the cellular-level effect (Krasovitskia et al., 2011) and thermal effect (Ita, 2015).

The role of cavitation as the primary mechanism of skin permeability enhancement during low frequency SN was reported that the cavitation outside the skin plays a more significant role than inside the skin (Tang et al., 2002). In addition, transient cavitation is the most significant enhancing mechanism of skin permeability during low frequency SN (Terahara et al., 2002). For the location of these transient cavitation events in the coupling medium, the required critical distance of a bubble from the skin surface to cause disruption of the surface is approximately the radius of bubble. However, no more than 150 μm at the operating frequency of 20 kHz was found (Tezel et al., 2003). Only one diameter of a bubble away from a solid surface is not likely to maintain symmetry during its oscillation. Moreover, the most likely reason for skin permeability enhancement of low frequency SN is microjet penetration into, or collapse near, the skin surface, resulting in enhanced the skin perturbation (Figure 2.13). Additionally, transient cavitation in the vicinity of membrane is only significant at frequencies in the low frequency SN and increased with decreasing ultrasound frequency, which scales directly with the membrane permeability (Ueda et al., 2009). Furthermore, a strong correlation between ultrasound frequency and the radius of skin pore, or the resonant bubble radius and ultrasound frequency showed the same result, suggesting that the direct action of cavitation bubbles collapsing onto the skin (Polat et al., 2011). Other recent studies have reported that cavitation bubble collapses on the skin surface as microjets play a dominant role in the skin permeability enhancement compared to other cavitation-related mechanisms, such as shock wave emission (Wolloch and Kost, 2010) that small pits can be observed on skin imaged from scanning electron micrograph (Watanabe et al., 2009).

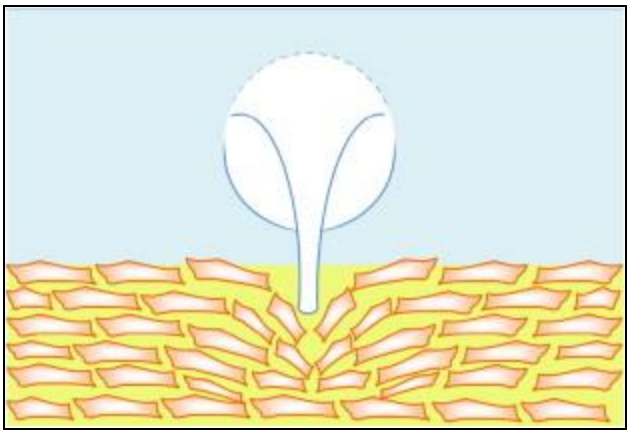

Figure 2.13 Illustration of a cavitation bubble asymmetrically collapsing into the stratum corneum as a microjet under low frequency SN. Legend: keratinocytes ( ), lipid bilayers ( ), and coupling medium ( ).

Source: Polat, B.E., et al. "Ultrasound-mediated transdermal drug delivery: Mechanisms, scope, and emerging trends." **Journal of Controlled Release** 152, 3: 330 - 348.

Cavitation effects caused by collapse and oscillation of cavitation bubbles in the ultrasound field are the main possible mechanisms to create aqueous pathways across the stratum corneum. The distortion of lipid bilayer leads to enhance the hydrophilic drugs transported across the skin (Mitragotri, Blankschtein, and Langer, 1996). Moreover, the combination of SN with chemical enhancers, such as surfactants (e.g. sodium lauryl sulfate (SLS)) (Herwadkar et al., 2012), ethanol and linoleic acid (Johnson et al., 1996), citral in 50% v/v aqueous ethanol (Mutalik et al., 2009), laurocapram (Azone) (Meidan et al., 1998), and d-limonene in ethanol (Tiwari, 2004), results in a synergistic effect in the enhancement of transdermal transport.

The effects of a surfactant present in the coupling medium during sonophoretic treatment can be broadly classified into two types: (i) the effect of the surfactant on ultrasound-related phenomena, and (ii) the effect of ultrasound on surfactant penetration, dispersion, and partitioning in the skin. Because surfactants can affect cavitation through several mechanisms such as their preferential adsorption

at interfaces and tending to reduce the surface tension of aqueous solutions that refer to its greatest effect on the oscillation of a cavitation bubble (Polat et al., 2011). Moreover, in addition to decreasing the surface tension, surfactants also play a role in stabilizing cavitation bubbles by inhibiting bubble coalescence and growth, especially in the case of charged surfactants (due to the electrostatic repulsions between charged bubbles). Therefore, the addition of surfactants to the coupling medium leads to a larger population of smaller cavitation bubbles. Lee et al. (2005) reported that the shielding and stabilization effect of SLS was a more significant role than surface tension effects, which leads to decrease transient cavitation activity.

Moreover, low-frequency sonophoresis can easily be coupled with other transdermal delivery techniques to produce the synergistic effect on drug delivery through an intracellular pathway, such as tape stripping (Escobar-Chavez et al., 2008), microneedle, electroporation (Petchsangsai, Opanasopit, and Ngawhirunpat, 2014), and iontophoresis (Fang et al., 2002). Lee et al. (2010) reported that the ultrastructural change on the stratum corneum surface shows the importance of the penetration pathway of lanthanum nitrate ($LaNO_3$) tracer in the viable epidermis after combined treatment with low frequency sonophoresis and tape stripping, which the tightly packed lipid bilayers were discrete elongated defects. However, the combination of sonophoresis and lipid nanocarrier in skin permeation has been rarely studied, and it is still controversial in the synergistic effect of these methods.

2.2.5.2 Electroporation

Electroporation is thought to increase skin permeation of drugs by creating new pores or pathways in the stratum corneum. This method has to apply a short (microsecond to millisecond) electric pulse of sufficient voltage to temporarily break down a permeability barrier of the skin surface. During the short time when the barrier function of the membrane or skin is compromised, molecules up to several kilodaltons can pass through the skin (Denet et al., 2004, Wong et al., 2006).

2.2.5.3 Iontophoresis

Iontophoresis is the method where the movements of ions across a membrane enhanced using an externally applied potential difference. Cationic drugs are driven into and through the skin by the anode (active electrode), which also extracts anion from the tissue underneath the skin into the anode. At the cathode (return electrode) anionic buffer ions are driven into the skin and cations from the tissues are extracted into the cathode. It is also possible to include an additional charged drug in the return electrode to be delivered simultaneously or to use a mixture of drugs in the active electrode to enhance the desired effect or to increase skin permeation (Rawat et al., 2008).

2.3 Technique for study the skin penetration mechanism

2.3.1 Modification of the stratum corneum lipid organization

2.3.1.1 Fourier-transform infrared (FTIR) spectroscopy

FTIR technique is a highly suitable technique for the determination of molecular vibrations of the stratum corneum's components at the functional group level. As shown in Figure 2.14, the peaks near 2920 and 2850 cm^{-1} represented respectively asymmetric and symmetric stretching modes of the terminal methylene groups of the lipids (ceramides, phospholipids, etc.) that provide specific information about the interior composition of the lipid bilayer. The band positions change from trans-form (stable form) to gauche conformation indicates the fluidization of the lipid bilayer. A small band obtained at 1738 cm^{-1} position represents lipid ester carbonyl stretching in the stratum corneum. The bands observed near 1637 and 1550 cm^{-1} represent amide I (C═O stretching) and amide II (C–N stretching) linkages of the helical secondary structure found in epidermal keratin. The stratum corneum lipids can be examined by the investigation of the band representing lipid alkyl backbone through the CH_2 scissoring (1462–1474 cm^{-1}) that are indicators of lateral packing within the lamellae. A single methylene band at ∼1468 cm^{-1} represents hexagonal acyl chain packing of the lipids whereas orthorhombic (OR) chain packing is indicated by two components at 1472 cm^{-1} and 1464 cm^{-1} (Panchagnula et al., 2001, Mendelsohn et al., 2003, Kaushik and Michniak-Kohn, 2010). The spilt of the band that the scissoring width was ∼10 cm^{-1} indicated a high content of OR phase

(Boncheva et al., 2008). In previous study, the different types of analyzed skin, human heat, dermatomed abdominal porcine skin, and pig ear skin shows similar FTIR spectra, but the shape and the intensity of recorded spectra from pig skin are lower than human skin (Hasanovic et al., 2011).

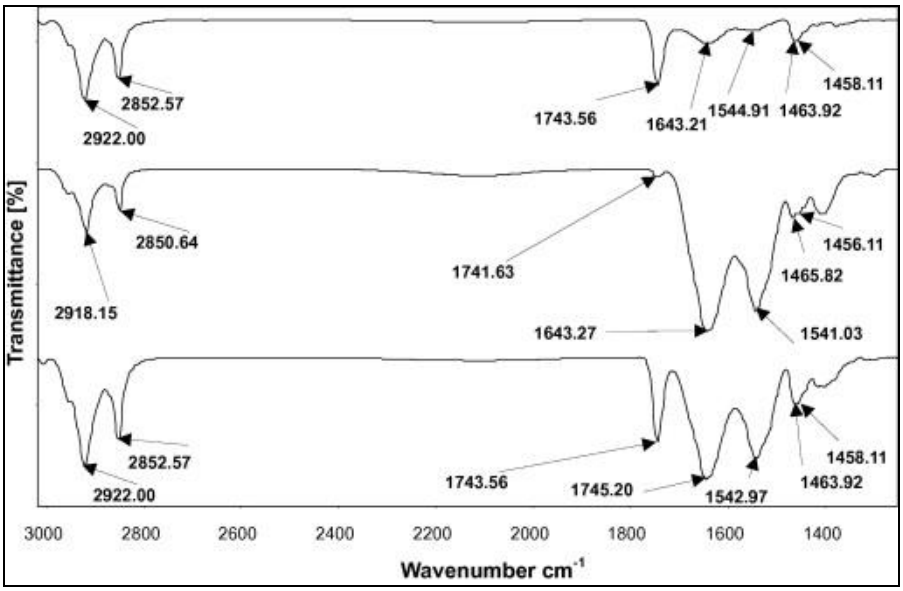

Figure 2.14 FTIR transmission spectra at 37 ˚C of pig abdominal dermatomed, pig ear, and human skin (from top to bottom).

Source: Hasanovic, A., et al. "Modification of the conformational skin structure by treatment with liposomal formulations and its correlation to the penetration depth of aciclovir." **European Journal of Pharmaceutics and Biopharmaceutics** 79, 1: 76 - 81.

2.3.1.2 Differential scanning calorimetry (DSC)

DSC has been commonly used to study the phase transitions (thermal phase properties) of the stratum corneum intercellular lipids. Thermal transitions in desiccated stratum corneum membranes have four endothermic transitions at 39–45 (T1), 68–74 (T2), 77–86 (T3), and 100-102 °C (T4). T1, T2 and T3 are attributed to phase changes in the intercellular lipid bilayers, while T4 is arisen after lipid extraction due to representation of protein denaturation. The transition peaks of human stratum corneum are summarized in Table 2.3 (Golden et al., 1986, Yamane et al., 1995, Al-Saidan et al., 1998).

Table 2.3 The transition peaks of human stratum corneum

Endothermic peak	Stratum corneum change
T1 (39–45°C)	Lipid melting of the sebaceous lipids together with cholesterol side chain motion, attributing to either lipid lamella phase transition from a crystalline to a gel like phase
T2 (68–74°C)	Lipid melting of the lipids chain portion buried within the bilayer structure, together within some non-polar material
T3 (77–86°C)	Break up of associated between lipid polar head groups together with disruption of cholesterol-stiffened regions
T4 (100-102°C)	Protein denaturation of intracellular keratin

The endothermic lipid phase transition profiles have been used to evaluate lipid phase alterations in enhancer-treated intact stratum corneum. Ibrahim et al. (2010) reported that the number of endothermic peaks in enhancer-treated stratum corneum was not equivalent to the number of endothermic peaks in the PBS control stratum corneum. 1-Octyl-2-pyrrolidinone treated stratum corneum samples showed two endothermic peaks, whereas oleic acid and n-octanol treated stratum corneum showed a single endothermic peak of the same temperature range. Moreover, a significant decrease in transition temperature occur a significant alteration of the gross fluidity of stratum corneum lipid domain due to enhancer intercalation into the stratum corneum intercellular lipids and subsequent lipid lamellae fluidization related to enhancer lipid concentration (Ibrahim and Li, 2010).

2.3.2 Visualization the skin permeation pathways

2.3.2.1 Confocal laser scanning microscopy (CLSM)

CLSM have been used to determine the mechanisms of diverse skin penetration enhancement strategies, such as chemical enhancement (De Rosa et al., 2000), iontophoresis (Brus et al., 2002), electroporation (Lombry et al., 2000), sonophoresis (Alvarez-Roman et al., 2003), and vesicle-mediated skin transport (Verma et al., 2003). CLSM can visualize skin structure and the localization of fluorescent probes within the tissue. The potential to recreate three-dimensional visualization of the tissue is another significant advantage relative to other

microscopic techniques. Xz-series images are a series of optical sections that take at successive focal planes along the z axis (Figure 2.15). To obtain depth information from a specific surface, it is first necessary to acquire a confocal image in the xy-plane (i.e. parallel to the plane of the membrane surface). To generate an xz-section, a horizontal line is drawn across a region of interest in the z = 0 μm-xy-plane and is then optically sliced through the digitized image data of the successive xy-sections (Figure 2.16) (Alvarez-Román et al., 2004).

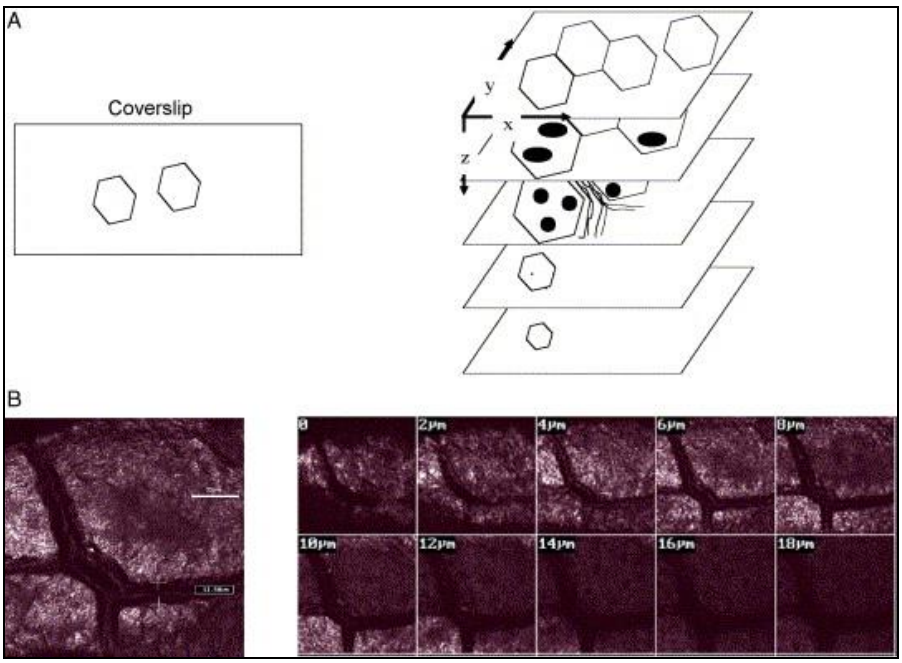

Figure 2.15 Confocal image: (A) a schematic of a z-series (sequential xy sections as a function of depth (z)), and (B) confocal images of a z-series through porcine skin.

Source: Alvarez-Román, R., et al. "Visualization of skin penetration using confocal laser scanning microscopy." **European Journal of Pharmaceutics and Biopharmaceutics** 58, 2: 301 - 316.

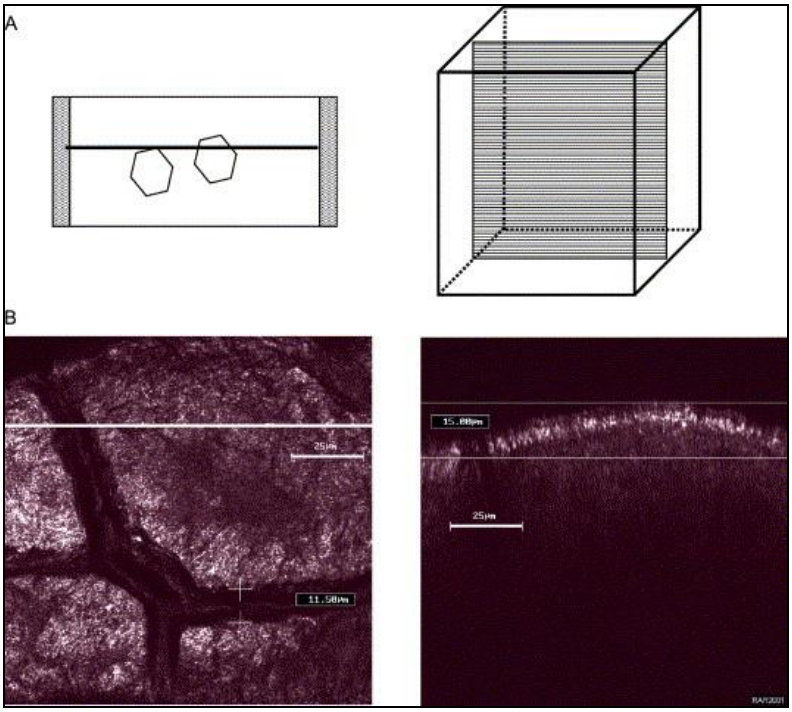

Figure 2.16 Confocal image: (A) schematic of an xz-planar optical cross-section, and (B) a confocal xz-image of porcine skin.

Source: Alvarez-Román, R., et al. "Visualization of skin penetration using confocal laser scanning microscopy." **European Journal of Pharmaceutics and Biopharmaceutics** 58, 2: 301 - 316.

CLSM provides valuable additional morphological information more than conventional microscopy. It is non-destructive nature, and the fact that little or no sample preparation is necessary, therefore CLSM offers a reasonably faithful representation of reality with few artefacts. CLSM has also been used to determine the distribution of a fluorophore in hair follicles (Grams, 2005). The relative accumulation in the stratum corneum, epidermis, dermis, outer root sheath, inner root sheath, cuticular area and hair shaft in non-fixed fresh human scalp skin was semi-quantitatively determined. Nevertheless, the important limitations of CLSM have been reported. First, only a restricted range of fluorophores are available for imaging and attachment of these markers. Second, the technique reveals at best only semi-quantitative information. Third, the images obtained are static views of reality captured at a particular point in time; thus, does a strongly fluorescent region imply a

key pathway through which a large fraction of the total transport is occurring, or does it suggest an area where the fluorophore has become tightly bound and/or immobilized (Alvarez-Román et al., 2004).

CHAPTER 3
MATERIALS AND METHODS

3.3.6 Data analysis

3.1 Materials

0.5 % Trypsin EDTA (No phenol red) (Gibco®, NY, USA)

1,6-Diphenyl-1,3,5-hexatriene (DPH) (Aldrich Chemical Co., Milwaukee, WI, USA)

Abdominal part of neonatal porcine skin (Obtained from the pigs that died naturally from pig farm in Nakhon Pathom)

Adhesion slides (MENZEL-GLÄSER® SuperFrost™ Plus, Braunschweig, Germany)

Cetyl palmitate (CP) (SABO SpA, Levate, Italy)

Cholesterol from lanolin (Chol purity 95%) (Fluka, Tokyo, Japan)

Disodium hydrogenphosphate dodecahydrate; $Na_2HPO_4.12H_2O$ (Ajax Finechem, Australia)

D-limonene (LI) (Sigma-Aldrich, MO, USA)

Egg phosphatidylcholine (PC) (Phopholipon® 90G, Lipoid GmbH, Ludwigshafen, Germany)

Frozen section medium (Neg 50, Microm International, Waldorf, Germany)

Hairless mouse skin (Hos: HR-1, 7 weeks old, Sankyo Labo Service, Tokyo, Japan)

Lissamine™ rhodamine B 1,2-dihexadecanoyl-sn-glycero-3-phosphoethanolamine triethylammonium salt (Rh-PE) (Invitrogen, CA, USA)

Na-salt N-(carbonyl-methoxypolyethylene glycol-2000)-1,2-distearoyl-sn-glycero-3-phosphoethanolamine (PEG2000-DSPE) (Lipoid GmbH, Ludwigshafen, Germany)

Potassium chloride; KCl (Ajax Finechem, Australia)

Potassium dihydrogenphosphate; KH_2PO_4 (Ajax Finechem, Australia)

Sodium chloride; NaCl (Ajax Finechem, Australia)

Sodium fluorescein (NaFI) (Sigma-Aldrich, MO, USA)

Span 20 (Sigma-Aldrich, MO, USA)

Triton® X-100 (Amresco®, Solon, Ohio, USA)

Tween 20 (Ajax Finechem, Auckland, New Zealand)

Tween 80 (NOF Corporation, Osaka, Japan)

3.2 Equipments

Aluminium foil

Analytical balance (Model CP224S and CP3202S, SARTORIUS, Germany)

Atomic Force Microscope (AFM; SPA400, SPI4000, SII Seiko Nanotechnology, Japan)

Centrifugal filters (Amicon® Ultra-0.5 ml, 3kDa)

Centrifuge (MULTIFUGE 1S-R, Kendro laboratory product, Hanau, Germany)

Centrifuge (Sorvall® Biofuge Stratos, Kendro laboratory product, Hanau, Germany)

Circulating water bath (WiseCircu WCH-8, Witeg®, Wertheim, Germany)

Confocal Laser Scanning Microscope (CLSM; Zeiss LSM510 META microscope, Jena, Germany)

Cryostat (Leica 1850, Leica Instrument, Nussloch, Germany)

Desiccator

Differential Scanning Calorimetry (DSC; Netzsch204 F1 Phoenix®, Selb, Germany, and DSC-60 Plus, Shimadzu, Kyoto, Japan).

Fluorescence spectrophotometer (FusionTM Universal Microplate Analyzer, Packard Instrument, USA)

Forceps and scissors

Fourier Transform Infrared Spectroscopy (FTIR; NICOLET4700; Thermo electron corporation, Madison, WI, USA, and FT/IR-4200; JASCO International Co., Ltd. Tokyo, Japan)

Franz diffusion cell (volume 6 ml)

Freeze-Dry System (FreeZone 2.5, Labconco, MO, USA)

Ice bath

Kimwipes® disposable wipers (Kimberly-Clark Professional, Australia)

Liquid N_2

Magnetic stirrer and Magnetic bar (RO 10 power IKAMAG®, IKA, Germany)

Microcentrifuge tube 1.5 ml (Eppendorf® tubes) and centrifuge tube 50 ml

Micropipette (2-20 µl, 20-200 µl, 100-1000 µl, 1-5 ml) and micropipette tip

N_2 gas in laminar hood

Nail varnish

Needle (27 gauge needle) (Nipro Medical Corporation, Bridgewater, NJ, USA)

Parafilm (BEMIS®, WI, USA)

pH meter

Probe sonicator (Sonics Vibra Cell™, Newtown, CT, USA)

Refrigerator, Freezer -20 ˚C and 4 ˚C

Scanning Electron Microscope (SEM; Camscan Mx2000, Obducat Camscan Ltd, UK)

Tape (3M, Hutchinson, Minnesota, USA)

Test tube (PYREX®, USA)

Thermometer

Transmission Electron Microscope (TEM; JEM 1230, JEOL Ltd, Tokyo, Japan)

VertiPureTM NYLON Syringes Filter, 13 mm, 0.45 μm (Vertical Chromatography, Nonthaburi, Thailand)

Vortex mixer (VX100, Labnet)

Zetasizer Nano ZS (Malvern Instruments, Malvern, UK)

3.3 Methods

3.3.1 Preparation of lipid nanocarriers

3.3.1.1 Liposomes

The liposome formulations (conventional liposomes (CL) and PEGylated liposomes (PL)) were prepared by controlled amount of PC and Chol, as well as various amounts of PEG2000-DSPE in the molar ratio: 10:2:0, 10:2:0.06, 10:2:0.12, 10:2:0.3, and 10:2:0.6 mM. NaFI was used as a model hydrophilic compound. Liposomes were prepared using thin film hydration and sonication method. Briefly, a mixture of lipid componants dissolved in chloroform/methanol (2:1, v/v) was added in a test tube, and the solvent was evaporated using a stream of nitrogen. The lipid film was placed in a desiccator until completely dried (6 h). Then NaFI was dissolved in phosphate-buffered saline (PBS; pH 7.4) at 0.2% (w/v) and added to the lipid film to give hydrated liposome vesicles. The liposome dispersion was probe-sonicated in ice-bath for 30 min to reduce the size of the vesicles. An

excess lipid composition was separated from vesicle formulation by centrifugation at 15,000 rpm at 4 ˚C for 15 min. The supernatant was collected for characterization.

3.3.1.2 Niosomes

The niosome formulations (niosomes (NI) and PEGylated niosomes (NIP)) were formulated by controlled amount of non-ionic surfactants (Span 20) and Chol, as well as various amounts of PEG2000-DSPE in the molar ratio: 5:5:0, 5:5:0.06, 5:5:0.12, 5:5:0.3, and 5:5:0.6 mM. The niosomes were prepared using the same method of liposome preparation. Brifly, a mixture of Span 20, Chol and various amount of PEG2000-DSPE was dissolved in an ethanol:chloroform mixture (1:1, v/v), and the solvent was evaporated using a stream of nitrogen. The film was placed in desiccator (6 h) until the thin film was completely dried. Then 0.2% (w/v) of NaFI solution was added to the lipid film to give hydrated niosomal vesicles and probe-sonicated in ice-bath for 30 min to reduce the vesicle size. An excess lipid composition was separated from vesicle formulation by centrifugation at 15,000 rpm at 4 ˚C for 15 min. The supernatant was collected for characterization.

In the case of terpene-containing nanocarriers, the liposome and niosome dispersions were prepared using the same procedure as described above. Then the dispersion was mixed with d-limonene (1%, w/v) and tween 20 (2%, w/v). All formulations were probe-sonicated for 30 min to reduce the vesicles size.

3.3.1.3 Solid lipid nanoparticles (SLN)

The SLN formulations (SLN and PEGylated SLN (SLNP)) were prepared using the *de-novo* emulsification method. The composition of oil phase containing a controlled amount CP (3%, w/v) and PC (0.12 %, w/v), and various amount of PEG2000-DSPE (0, 0.06, 0.12, 0.3, 0.6 mM) were formulated. For aqueous phase, NaFI (0.2%, w/v) and tween 80 (0.8% w/v) were dissolved in PBS. The oil and aqueous phase were heated at 65 $\pm$ 5 ˚C. Then the aqueous phase was added to the oil phase with stirring at 14,000 rpm for 5 min by magnetic stirrer. The emulsions were probe-sonicated for 15 min to reduce the particle size and then filtered through a 0.45-µm membrane filter to remove any precipitate matter.

In the case of terpene-containing SLN, d-limonene was added into melted oil phase at 50-55 ˚C. Tween 20 was added into aqueous phase and heated until 50-55 ˚C. Then the aqueous was added into oil phase with stirring at 14,000 rpm for 5 min. Probe-sonication was used to reduce the particle size for 15 min. Finally, SLN formulation was filtered through a 0.45-µm membrane filter to remove any precipitate matter.

Table 3.1 The composition of lipid nanocarrier formulations (%w/v)

Formulations	**PC**	**Cholesterol**	**Span20**	**CP**	**Tween80**	**PEG2000-DSPE**	**NaFI**
CL	0.773	0.077	-	-	-	0.000	0.2
PL1	0.773	0.077	-	-	-	0.015	0.2
PL2	0.773	0.077	-	-	-	0.030	0.2
PL3	0.773	0.077	-	-	-	0.075	0.2
PL4	0.773	0.077	-	-	-	0.150	0.2
NI	-	0.193	0.173	-	-	0.000	0.2
NIP1	-	0.193	0.173	-	-	0.015	0.2
NIP2	-	0.193	0.173	-	-	0.030	0.2
NIP3	-	0.193	0.173	-	-	0.075	0.2
NIP4	-	0.193	0.173	-	-	0.150	0.2
SLN	0.12	-	-	3	0.8	0.000	0.2
SLNP1	0.12	-	-	3	0.8	0.015	0.2
SLNP2	0.12	-	-	3	0.8	0.030	0.2
SLNP3	0.12	-	-	3	0.8	0.075	0.2
SLNP4	0.12	-	-	3	0.8	0.150	0.2

3.3.2 Characterization of nanocarriers

3.3.2.1 Particle size, size distribution and surface charge

Each formulation was diluted with an appropriate amount of water. The size distribution and zeta potential were measured using a Dynamic Light Scattering (DLS) particle size analyzer (Zetasizer Nano-ZS, Malvern Instrument, Worcestershire, UK) with a 4 mW He-Ne laser at a scattering angle of 173°. All measurements were carried out under ambient conditions in triplicate.

3.3.2.2 Entrapment efficiency and drug loading efficiency

The nanocarrier dispersion (0.5 mL) was placed in an ultrafiltration tube with a molecular weight cut-off of 3,000 Da (Microcon YM-3; Minipore, Billerica, Massachusetts, USA) and centrifuged at 4 °C at 10,000 xg for 60 min. The filtrate was discarded, and 0.25 mL of PBS was added to the retentate before further centrifugation at 4 °C at 10,000 xg for 40 min. The collected NaFI-loaded nanocarrier in the retentate were then disrupted with 0.2 mL of 0.1% (w/v) triton X-100 (for liposome and niosome formulations) or isopropyl alcohol (for SLN) and centrifuged at 4 °C at 10,000 xg for 10 min. The NaFI content of the supernatant was determined by fluorescence analysis.

The percent drug entrapment efficiency (%EE) and loading efficiency (%LE) were calculated with the equation (4 and 5) as follows:

$$\%EE = \frac{C}{Ci} \times 100 \quad (4)$$

where C is the concentration of NaFI in the formulation, and C_i is the initial concentration of NaFI added.

$$\%LE = \frac{C}{\text{Lipid composition}} \times 100 \quad (5)$$

3.3.2.3 Morphology

Transmission Electron Microscope (TEM; JEM 1230, JEOL Ltd, Tokyo, Japan) was used to visualize the particle. One drop of the vesicles was dropped onto a copper grid; then the excess suspension was adsorbed immediately using filter paper. The vesicles were air-dried on the copper grid. After drying, the

grid was observed using TEM under the microscope at 10-100k magnification with acceleration voltage of 80 kV.

3.3.3 Evaluation of the liposomes membrane fluidity

3.3.3.1 Atomic force microscope (AFM)

AFM (SPA400, SPI4000, SII Seiko Nanotechnology, Tokyo, Japan) operating in tapping mode at room temperature (25 ˚C) was used to determine the morphology and structure change of liposomal formulation. The formulation was diluted with distilled water before dropped onto a mica sheet. The cantilever tip have a resonant frequency + 10%, kHz = 210 and force constant + 20%, N/m = 6.1 (NT-MDT, Moscow, Russia). The AFM tapping mode data were analyzed using SPI4000 version 4.17E (SII Seiko Nanotechnology, Tokyo, Japan).

3.3.3.2 Fluorescence anisotropy

To evaluate the fluidity of liposome membrane, 1,6-diphenyl-1,3,5-hexatriene (DPH) was used to monitor in the hydrophobic regions of the lipid bilayer by measuring the fluorescence anisotropy from fluorescence spectrophotometer (Hitachi F-450, Hitachi Co., Ltd., Tokyo, Japan). The liposome was labeled with DPH by adding 10 µl of 10 mM DPH stock solution in tetrahydrofuran to 1000 µl of liposome dispersion and then incubated at room temperature for 2 h in the dark to complete the labeling. The fluorescence anisotropy of the samples was measured at an excitation wavelength of 350 nm and an emission wavelength 431 nm. Temperature was controlled at 25 ˚C and 32 ˚C by a circulating water bath. The anisotropy of DPH was then calculated by using the following equations:

$$r = \frac{(I_{vv} - (G \cdot I_{vh}))}{(I_{vv} + (G \cdot 2I_{vh})} \quad (6)$$

Where r is anisotropy, I_{vv} and I_{vh} are emission intensities perpendicular to the horizontally polarized light (90˚, 0˚) and parallel to the horizontally polarized light (90˚, 90˚), respectively. G is the correction factor ($G = I_{hv} / I_{hh}$) given by the ratio of the vertically to the horizontally polarized light.

3.3.4 *In vitro* skin penetration study

3.3.4.1 Preparation of the porcine skin

Abdominal porcine skin was taken from intrapartum stillborn animals from a farm in Nakhon Pathom. Subcutaneous fat was carefully removed using medical scissors and surgical blades. The skin thickness was approximately 0.6-0.7 mm. Samples were frozen at -20 ˚C until use and thawed at room temperature in PBS prior to experiments.

3.3.4.2 Skin penetration study

Permeation of NaFI through porcine skin was performed using Franz type diffusion cells. Briefly, approximately 2 mL of NaFI-loaded nanocarrier formulations was applied to the skin in the donor compartment. The receptor compartment of the cell was filled with 6 mL of PBS. At predetermined times (1, 2, 4, 6, 8, and 24 h), 0.5 mL of receiver medium was withdrawn for analysis using fluorescence detection, and the same volume of PBS was added to the receiver compartment to maintain a constant volume. Each sample was analyzed in triplicate.

Low frequency sonophoresis at 20 kHz was generated by using an ultrasonic transducer (Vibra-cellTM, VCX130 PB, Sonics and Materials, Inc., Newtown, CT, USA.), which the radiating diameter of transducer probe was 6 mm. The ultrasound transducer probe was placed inside the donor compartment with its active horn face located 3 mm above the skin surface. NaFI-loaded nanocarrier formulations were filled into the donor chamber. Then, the skin was sonicated for 2 min using intensity of 1.90 W/cm^2.

For *in vitro* penetration study, cumulative amount was plotted against time and steady-state flux determined as the slope of the linear portion of the plot. Lag time was obtained by extrapolating the linear portion of the penetration profile to the abscissa. The skin permeation of model drug was analyzed using the mathematical model based on the Fick's law of diffusion. The permeability coefficients (K_p) were calculated from the cumulative skin permeation profile using the steady-state flux (J), and the donor concentration (C_d) of the formulations by equations (7)

$$K_p = \frac{J}{C_d} \quad (7)$$

The enhancement ratio (ER) is calculated with the following equation:

$$ER = \frac{\text{Flux of nanocarrier formulation}}{\text{Flux of NaFI solution}} \quad (8)$$

3.3.4.3 Skin deposition study by tape stripping

After the *in vitro* permeation studies at 8 h, tape stripping was performed to collect the stratum corneum for each formulation. The skin was washed with PBS and blotted dry with soft tissue. Visible hair was removed with scissors. Transparent adhesive tape (3 M, Hutchinson, Minnesota, USA) was pressed onto the skin (1.96 cm^2) with the thumb using a vinyl glove. Approximately 20 strips were applied, quickly removed and collected. After stripping, the skin was cut into small pieces. The collected stratum corneum and remaining skin (epidermis and dermis) were added to 20 mL of PBS, probe-sonicated for 20 min, and then centrifuged for 10 min at 12,000 rpm. The NaFI-containing stratum corneum and epidermis and dermis were analyzed using fluorescence detection. Each sample was analyzed in triplicate.

3.3.4.4 Fluorescence analysis

The NaFI concentration was analyzed using a fluorescence spectrophotometer (FusionTM Universal Microplate Analyzer, Packard Instrument Company, Inc., Downers Grove, Illinois, USA). The excitation wavelength was 485 nm, and the emission wavelength was 535 nm. Samples (100 µL) were pipetted into a black 96-well plate, and fluorescence was determined in triplicate.

3.3.5 Mechanistic characterization of nanocarriers permeated through skin

3.3.5.1 Confocal laser scanning microscopy (CLSM)

After *in vitro* skin penetration at 4 h of Rh-PE labeled liposome and niosome membranes or SLN core, the depth of the NaFI permeation through the skin was visualized by using cross section images. The whole skins were taken cross-sectioned using a cryostat (Leica 1850, Leica Instrument). Each skin sample was

mounted on a metal sample holder by using frozen section medium (Neg50, Microm International, Waldorf, Germany). The frozen skin was sectioned into 10 μm slices and placed on glass microscope slides. The skin tissues were mounted with mounting medium and covered with a cover slip. Confocal images were obtained from the x10 objective lens system.

Xz sectioning confocal images were obtained using the ×20 objective lens system of an inverted Zeiss LSM 510 META microscope (Carl Zeiss, Jena, Germany) equipped with He-Ne (excitation wavelength 543 nm; emission wavelength 580 nm), Ar (excitation 488 nm; emission 514 nm) and diode lasers (excitation 358 nm; emission 461 nm). A piece of tissue was placed on a coverslip (22 x 50 mm) with the stratum corneum facing up toward the microscope condenser. Sufficient methyl salicylate was added to immerse the tissue. Confocal images were illustrated as x-z axis serial optical sections. Fluorescence intensity was evaluated at the middle horizontal line of each image using Zeiss LSM 5 operating software. Mean fluorescence intensity was plotted against skin depth.

3.3.5.2 Selectively block hair follicle technique

All hair follicles in the skin sample were blocked by using the follicular closing technique. Each skin had hair follicle density average between 30 to 40 follicles per application area (1.96 cm^2). One micro drop of nail varnish using a blunt 27 gauge needle was carefully placed beside each hair follicle orifice and dried for 5 min to completely block the follicular shunt. Then, the skin samples were washed in PBS and mounted on Franz cells for *in vitro* penetration study using the same as describe above.

3.3.5.3 Scanning electron microscopy (SEM)

After the *in vitro* skin penetration study at a time of 4 h, porcine skin was visualized. Each skin sample was cut into pieces (1 mm x 2 mm) from the central area. The samples were rapidly frozen in liquid nitrogen and dried by Freeze-Dry System, (FreeZone 2.5; Labconco, Kansas City, MO) for 24 h. The dried specimens were gold-coated on a by using sputtering device. Specimens were then observed

under SEM (Camscan Mx2000, ObducatCamscan Ltd, Cambridge, UK). Photographs were taken of suitably representative skin regions.

3.3.5.4 Stratum corneum modification

3.3.5.4.1 Fourier transform infrared spectroscopy (FTIR)

FTIR was used for characterization of the stratum corneum at a molecular level. The stratum corneum layer of porcine skin was separated from the epidermis using trypsin digestion method. The whole skin (stratum corneum side facing downward) was placed on 0.1% w/v trypsin solution in PBS pH 7.4 at 4 ˚C (overnight) and then at 37 ˚C for 4 h. Next, stratum corneum sheet from viable epidermis was carefully removed, rinsed with distilled water, and dried in a desiccator for 24 h. Nanocarrier formulations were applied on the stratum corneum sheets for 4 h at 32 ˚C. The treated sheets were dried and investigated by FTIR spectrophotometer (NICOLET4700; Thermo electron corporation, Madison, WI, USA) between 4,000 and 1,000 cm^{-1}. All data were analyzed by version 8 of OMNIC software (Thermo electron corporation, Madison, WI, USA).

3.3.5.4.2 Thermotropic behavior of stratum corneum lipids

The stratum corneum layer of hairless mice skin was separated by the same method as above. The formulations treated sheets were rinsed with distilled water, dried, and investigated by FTIR spectrophotometer (FT/IR-4200; JASCO International Co., Ltd. Tokyo, Japan) between 4,000 and 600 cm−1. The spectra were collected in transmission mode. In order to detect phase transitions the temperature was increased at a heating rate of 1 ˚C/min and collected between 20 ˚C and 100 ˚C**.**

3.3.5.4.3 Differential scanning calorimetry (DSC)

To confirm the phase transition temperature, DSC (DSC-60 Plus, Shimadzu, Kyoto, Japan) was used to investigate the mechanism of the treated stratum corneum sheet of hairless mice skin. The sample was weighed approximately 1-3 mg and sealed in aluminum pan. The thermal analysis process was performed using an aluminium pan as reference pan. The heating rate was at 10 ˚C/min over the

temperature range of 20 to 100 ˚C. The transition midpoint temperature (T_m) was defined as the temperature at the peak of endothermic curve.

3.3.5 Data analysis

All experimental measurements were collected in triplicate. The values were expressed as the mean and standard deviation (S.D.). Statistical significance was analyzed using analysis of variance (ANOVA) followed by Tukey's post hoc test. The significance level was set at $p < 0.05$.

CHAPTER 4
RESULTS AND DISCUSSION

4.4.4.3 Thermal phase transition of lipid organization in the stratum corneum

4.1 Lipid nanocarrier formulations and characterizations

Three types of lipid nanocarriers such as liposomes, niosomes, and SLN were successfully formulated for entrapment of a hydrophilic compound NaFI. Liposomes and niosomes were prepared by thin film hydration and sonication method. SLN was prepared by *de-novo* emulsification method. Various amounts of PEG2000-DSPE were used as a hydrophilic polymer for modification of the surface of lipid nanocarriers. Terpene was added into lipid nanocarriers for enhancement of the skin penetration.

4.1.1 The physicochemical characteristics

4.1.1.1 Effect of different lipid nanocarriers

The physicochemical characteristics of the different lipid nanocarrier formulations are presented in Table 4.1. The particle size of all formulations was nano-meter scale with a narrow size distribution (polydispersity index; PDI < 0.3). The average particle size of CL was smaller than SLN and NI, respectively. For zeta potential, all formulations exhibited negative surface charge.

4.1.1.2 Effect of different concentrations of PEG2000-DSPE

In the result of the liposome formulations, the grafting PEG onto the liposome surfaces significantly reduced the particle sizes. PL2 showed the smallest particle size, following by PL4, PL3, PL1, and CL, respectively. The average particle sizes of niosomes also decreased in the order: NI > NIP1> NIP2 > NIP3 > NIP4. These results suggested the intercalation of PEG2000-DSPE molecule into the liposome and niosome lipid bilayers. The hydrophilic components, PEG2000, were outside the bounds of the vesicles and the lipid components, while DSPE were inside the membrane bilayer. With such an orientation, the PEG molecules strongly reduced attractive van der Waals forces and increased repulsive force (steric, electrostatic, and hydration) resulting in decreased the vesicle aggregation (Kenworthy, Simon, and McIntosh, 1995). For the surface charge, liposome formulations had zeta potential value between -8.74 and -14.1 mV. Because PC is a zwitterionic compound with the isoelectric point (pI) approximately 6 to 6.7, at the higher pH values of the liposome formulations (pH 7.4) PC vesicles exhibit a negative charge (Chain and Kemp, 1934). For niosome formulations, the zeta potentials were between -17.93 to -35.2 mV.

PEGylation significantly decreased the negative surface charge of the niosome vesicles. According to Okore et al. (2011), the increasing of PEG chain length and concentration ratio dramatically decreased negative surface charge. Moreover, the magnitude of the surface charge is depended on the acidic or basic strength of the surface groups and the pH of the solution. At pH 7.4 of niosome formulations, a basic surface takes on a positive charge, therefore PEG-modified surface might decrease a negative charge of niosome surfaces.

For SLN formulations, non-PEGylated SLN significantly showed smaller particle size than PEGylated SLN, while the zeta potential of SLN was lower negative surface charge than SLNP1-4. This suggested that PEG molecules might be a brush layer over the surface of nanoparticles, which using various concentrations of PEG2000-DSPE significantly affected on the particle sizes and zeta potentials. (Bocca et al., 1998; Madan et al., 2013).

Table 4.1 The physicochemical characterizations of the lipid nanocarrier formulations. Each value represents the mean ± S.D. (n=3). * indicates significant difference between group ($p < 0.05$).

Formulations	**Particle size (nm)**	**PDI**	**Zeta potential (mV)**	**%EE**	**%LE**
CL	106.43 ± 0.40	0.25 ± 0.01	-9.06 ± 0.58	17.08 ± 0.60	4.52 ± 0.20
PL1	71.69 ± 0.60*	0.24 ± 0.01	-9.73 ± 0.30*	27.81 ± 0.09*	6.90 ± 0.02*
PL2	68.82 ± 0.60*	0.22 ± 0.01	-8.74 ± 0.20	21.74 ± 2.5*	5.31 ± 0.36
PL3	71.35 ± 0.30*	0.29 ± 0.01	-14.10 ± 0.40*	26.14 ± 0.14*	6.51 ± 0.03*
PL4	69.91 ± 0.60*	0.18 ± 0.01	-9.09 ± 1.00	22.94 ± 1.70*	5.73 ± 0.40
NI	228.07 ± 0.60	0.20 ± 0.01	-35.20 ± 1.30	40.87 ± 0.50	22.34 ± 0.30
NIP1	163.43 ± 1.70*	0.28 ± 0.01	-24.23 ± 0.60*	28.97 ± 7.60*	15.84 ± 4.20*
NIP2	129.43 ± 0.30*	0.24 ± 0.01	-21.23 ± 0.90*	31.76 ± 4.47	17.36 ± 2.40
NIP3	125.13 ± 0.10*	0.26 ± 0.01	-17.93 ± 0.60*	28.64 ± 3.50*	15.66 ± 1.90*
NIP4	105.16 ± 5.50*	0.27 ± 0.01	-19.30 ± 0.60*	33.16 ± 2.30	15.66 ± 1.90
SLN	142.17 ± 1.80	0.15 ± 0.01	-25.23 ± 1.00	45.11 ± 2.10	2.80 ± 0.10
SLNP1	199.97 ± 1.20*	0.17 ± 0.01	-11.27 ± 0.60*	44.25 ± 0.60	1.47 ± 0.02*
SLNP2	197.33 ±1.90*	0.17 ± 0.01	-11.87 ± 0.90*	51.49 ± 0.29*	1.72 ± 0.01*
SLNP3	202.13 ± 0.60*	0.15 ± 0.01	-15.63 ± 1.20*	45.19 ± 0.04	1.50 ± 0.01*
SLNP4	197.03 ± 1.50*	0.18 ± 0.01	-16.47 ± 0.40*	56.47 ± 0.95*	1.88 ± 0.03*

4.1.1.3 Effect of d-limonene-containing PEGylated nanocarrier formulations

In this study, the amount of PEG2000-DSPE as 1% of lipid composition from liposome formulation was formulated for entrapping 1% (w/v) d-limonene. D-limonene-containing PL (PL-LI) showed significantly smaller particle size than d-limonene-containing NIP (NIP-LI) and d-limonene-containing SLNP (SLNP-LI), respectively (Table 4.2). The particle size of d-limonene containing formulation was significantly smaller than those without d-limonene, because the particle size was affected by adding tween 20 and d-limonene (Subongkot et al., 2012). For incorporating d-limonene into liposomes and niosomes bilayer, tween 20 had to be a solubilizing agent. Also, it can be an edge activator for interacting with bilayers, leading to disrupted lipid packing (El Maghraby, Williams, and Barry, 2000) and reduced the vesicle size. In case of SLN, the adsorption of tween 20 onto solid surfaces decreased the surface tension and aggregation of particles driven by reducing hydrophobic attraction between insufficiently covered lipid crystal surfaces (Helgason, 2009). Moreover, all formulations showed a narrow size distribution (PDI < 0.3) and exhibited a negative surface charge.

Table 4.2 The physicochemical characterizations of d-limonene-containing lipid nanocarrier formulations. Each value represents the mean ± S.D. (n=3). * indicates significant difference from those without d-limonene ($p < 0.05$).

Formulations	Particle size (nm)	PDI	Zeta potential (mV)	%EE	%LE
PL-LI	31.46 ± 0.30*	0.21 ± 0.00	-10.25 ± 1.80	30.30 ± 0.70*	7.55 ± 0.20*
NIP-LI	104.02 ± 7.20*	0.19 + 0.00	-16.03 ± 2.30*	50.32 ± 4.80*	27.51 ± 2.60*
SLNP-LI	126.10 ± 1.10*	0.23 ± 0.00	-14.70 ± 0.50*	44.98 ± 0.04*	1.50 ± 0.01*

4.1.2 Entrapment efficiency and loading efficiency

4.1.2.1 Effect of different lipid nanocarriers

The %EE and %LE of NaFI-loading lipid nanocarrier formulations is shown in Table 4.1. The %EE was in the following order: SLN > NI > CL, and the %LE was in the following order: NI > CL > SLN. SLN had the highest %EE but the

lowest %LE because these particles had higher lipid compositions to form drug carriers system wherein more NaFI could be entrapped.

4.1.2.2 Effect of different concentration of PEG2000-DSPE

The grafting of PEG onto the liposome surfaces exhibited significantly higher %EE and %LE than CL, where as various PEG concentrations did not affect %EE and %LE. This result suggested that the polarity of the bilayer vesicles in the presence of PEGylated-lipids was more than that of the non-PEG modified liposomes, leading to increased the incorporation efficiency of hydrophilic drugs (Knudsen et al., 2012).

For the niosomes formulations, non-PEG niosome formulation was higher %EE than PEGylated niosomes (NIP1-4). This could be that the PEG chain might make the niosome structure more rigid and resulting in decreased drug entrapment. The presence of cholesterol decreased the niosome bilayer fluidity but increased the drug loading efficiency. Additionally, the affinity of the drug with the niosome material, the thickness of the niosome bilayer, drug solubility in water, and drug–drug interactions affected the drug loading efficiency (Shi, Fang, and Pei, 2005).

SLN with the highest PEG concentration (SLNP4) had a significantly higher %EE than non-PEG modified SLN, suggesting that PEG molecules covalently attached to the nanoparticle surface and provided a hydrophilic steric barrier around the SLN (Acar et al., 2005). This barrier likely helped to retain hydrophilic drugs within SLN more than other formulations.

4.1.2.3 Effect of d-limonene-containing PEGylated nanocarrier formulations

For liposome and niosome formulations, the %EE and %LE of PL-LI and NIP-LI were significantly higher than those without d-limonene. NIP-LI also showed higher %EE and %LE than other formulations. This indicated that d-limonene and tween 20 affected the entrapment of hydrophilic compound into lipid bilayer vesicles (Table 4.2). The content of edge activator may have led to formation of pores in the bilayer (Jain et al., 2003), thus resulting in increased incorporation efficiency of the hydrophilic drug in the aqueous compartment of bilayer vesicles. SLNP-LI

showed lower %EE and %LE than SLN without d-limonene, however no significant difference was found.

4.1.3 Morphology

TEM was used to visualize the particle size and shape of NaFl-loaded lipid nanocarrier formulations. Figure 4.1 shows particle size and shape of lipid nanocarriers, PEGylated nanocarriers, and d-limonene-containing nanocarrier formulations. All formulations were spherical in shape and nano-scale sized relating to the results from DLS analysis.

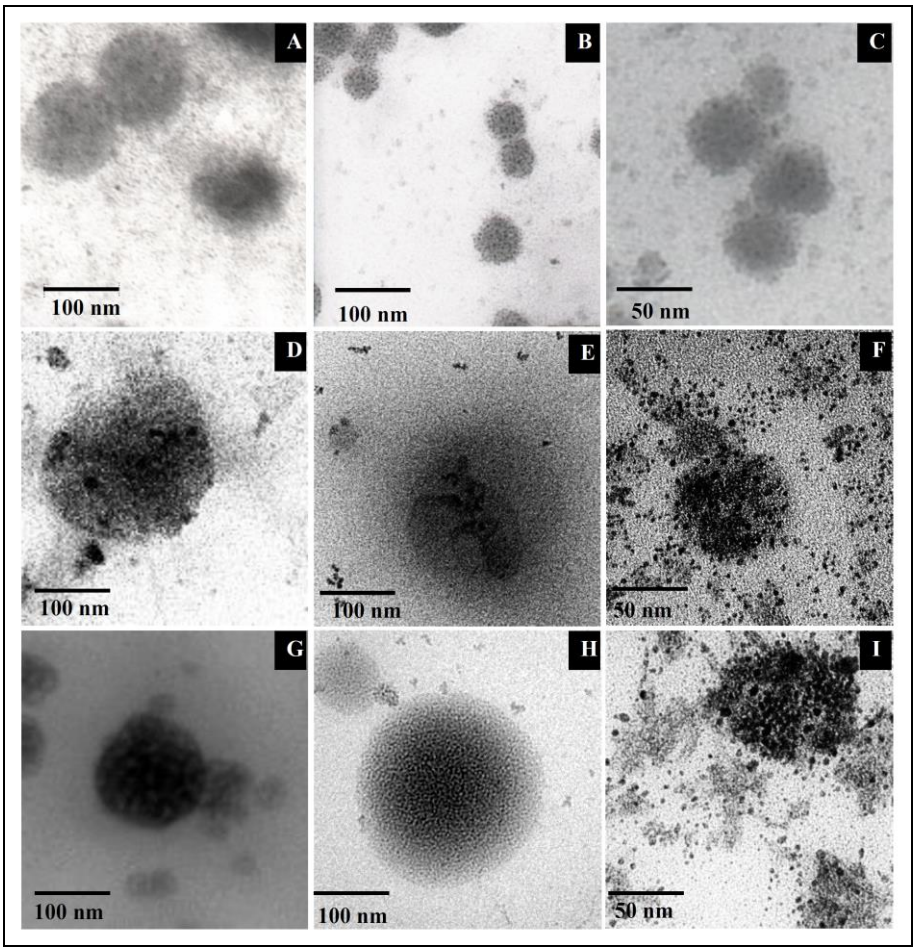

Figure 4.1 TEM images of lipid nanocarriers: liposomes [(A) CL, (B) PL, and (C) PL-LI], niosomes [(D) NI, (E) NIP2, and (F) NIP-LI], and SLN [(G) SLN, (H) SLNP2, and (I) SLN-LI]. The scale bars represent 50 nm and 100 nm.

4.1.4 Membrane fluidity of liposome vesicles

Liposomes containing phospholipid and edge activator are called as phospholipid based elastic nanocarriers, which can exhibit more deformable than conventional liposomes (Romero and Morilla, 2013). The AFM images of liposomal formulations are shown in Figure 4.2. The liposomal morphology (shape, structure, surface morphology and size measurement) was obtained using AFM. All formulations were spherical structure of the small unilamellar vesicles. The geometric mean diameter of CL, PL, PL-Tween 20, and PL-LI were 132.35 ± 1.97 nm, 45.67 ± 4.31 nm, 30.11 ± 8.39 nm, and 31.36 ± 5.09 nm, respectively. The height of CL, PL, PL-Tween20, and PL-LI from 3D images were 27.40 ± 1.97 nm, 9.70 ± 0.91 nm, 6.53 ± 2.23 nm, and 6.28 ± 1.67 nm, respectively. The diameter in each liposome formulation was higher than the height values. Because of the flattening of vesicles, the shape of liposomes could change after deposited on the mica support. The deformation of liposomes was induced by the interaction between the liposome vesicles and the support, as well as the continuous movement of the AFM tip. Therefore, the vesicle composition such as edge activators and terpenes might destabilize the lipid bilayers of liposome vesicles and increase the flexibility of the membrane (Honeywell-Nguyen and Bouwstra, 2005, Ruozi et al., 2011, Maheshwari et al., 2012).

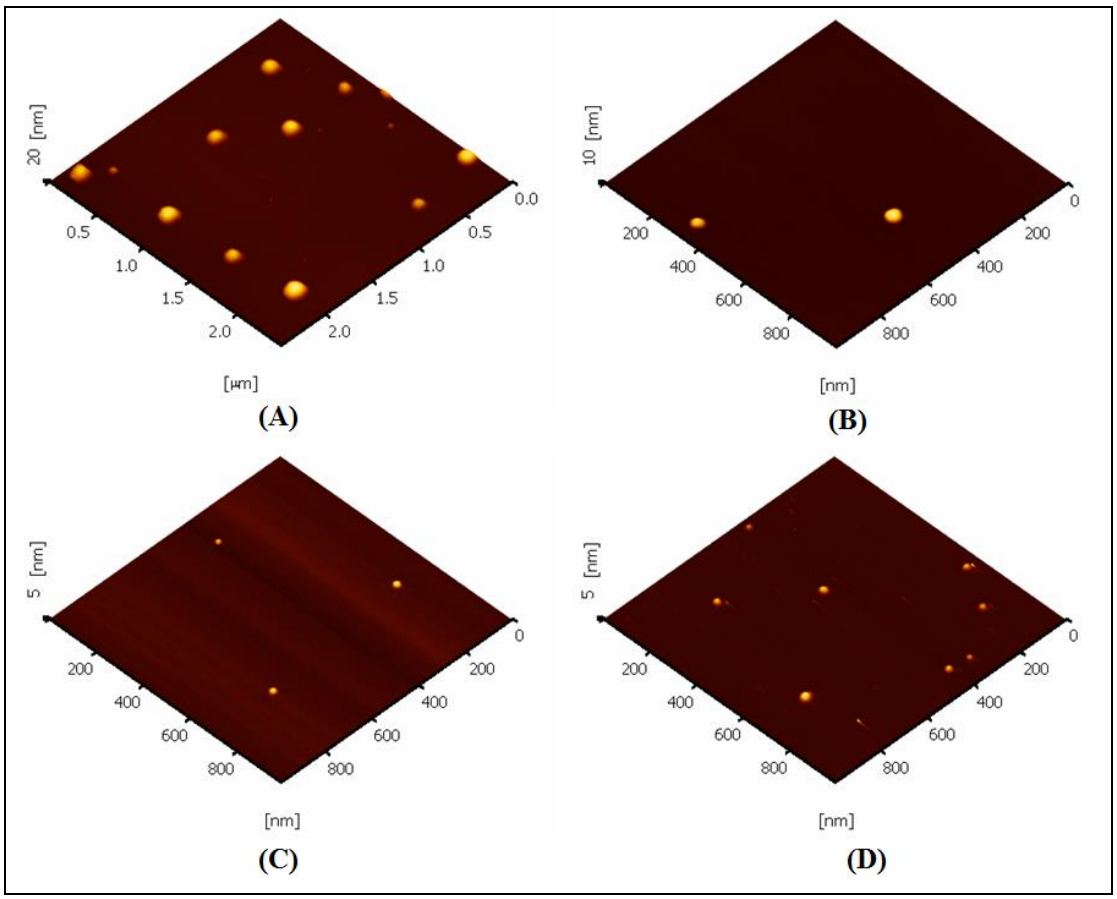

Figure 4.2 AFM image of (A) CL, (B) PL, (C) PL-Tween 20, and (D) PL-LI

The fluorescence anisotropy presents the structural and orientation in the lipid bilayer that are inversely proportional to liposomes membrane fluidity. The fluorescence probe, DPH is incorporated in the hydrophobic regions of lipid bilayer. A high value represents a high structural order or low membrane fluidity (Marczak, 2009). As shown in Figure 4.3, the fluorescence anisotropy of liposome formulations at 25 ˚C and 32 ˚C was evaluated. All liposome formulations at the temperature of the skin (32 ˚C) showed lower anisotropy value than at 25 ˚C, indicating the high fluidity of liposome membrane. Various amounts of d-limonene (0.1, 1, and 2 %w/v) in PL formulation showed different anisotropy value. The value of fluorescence anisotropy of PL was significantly higher than PL-LI 1% and PL-LI 2%, but it was not significantly different from PL-LI 0.1%. This result indicated that d-limonene might increase membrane fluidity of liposome membrane, which 1% and 2 % of d-limonene in liposome vesicles showed higher membrane fluidity than 0.1% of d-limonene. In

this study, tween 20 molecules were localized near the polar head group of the liposomal bilayer leading to increased the fluidity of the acyl chain near the polar head group of the phospholipid bilayer, but the fluidity of the acyl chain near the hydrophobic region was not increased. While terpene molecules were localized in the phospholipid acyl chain near the lipophilic region of the vesicle bilayer leading to increased the fluidity at the C16 atom of the phospholipid acyl chain (Badran, Shazly, and El-Badry, 2012, Subongkot and Ngawhirunpat, 2015). Therefore, PL with tween 20 exhibited higher anisotropy value of DPH than PL without tween 20. The anisotropy value was decreased by adding d-limonene into liposomes membrane. However, no significant difference between 1% and 2% of limonene in liposomes formulations was found.

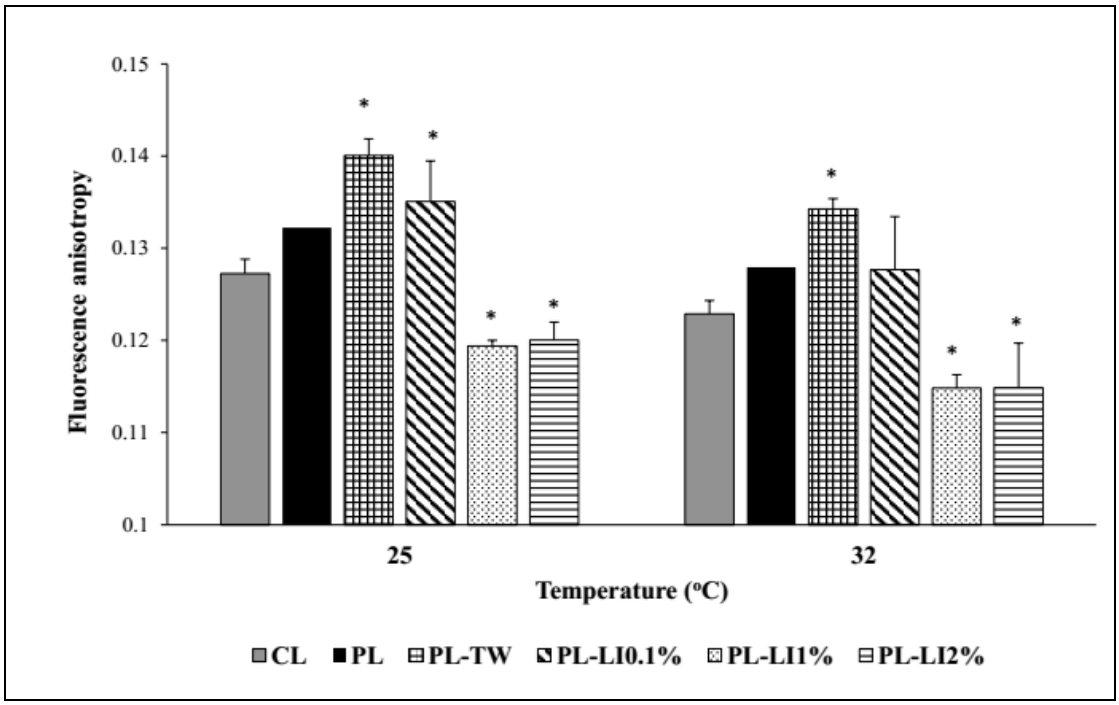

Figure 4.3 Fluorescence anisotropy of DPH added to the liposome formulations at the temperature of 25 and 32 °C. Results denote the mean ± S.D. (N = 3). *indicates significant difference from PL ($p < 0.05$).

4.2 Influence of SN on *in vitro* skin permeation

In vitro skin penetration studies were performed using Franz type diffusion cells. The amount of NaFI delivered from different lipid nanocarrier formulations into the

abdominal porcine skin was plotted against time. The rate of absorption, or flux, of any substance across the skin is proportional to its concentration difference across that barrier. The permeability coefficient (K_p), calculated from the proportionality constant, is related to ratio of the flux and the concentration of solute in donor phase (Franz, 1983). After skin penetration study at 8 h, tape stripping technique was performed to examine the distribution of substances within the skin (Escobar-Chavez et al., 2008).

4.2.1 NaFI-loaded lipid nanocarriers

Low frequency SN is a more effective technique for enhancing transdermal delivery of small hydrophilic molecules (Boucaud et al., 2001, Sarheed and Abdul Rasool, 2011). In this study, ultrasound energy at 20 kHz was generated inside a coupling medium onto the skin surface. The skin was continuous sonicated for 2 min (100% duty cycle, 25% amplitude, and 1.90 W/cm^2 acoustic intensity). The cumulative amount versus time profile and penetration parameters of the different formulations are shown in Figure 4.4 and Table 4.3, respectively. Using NaFI solution as a coupling medium, the skin permeation and the steady-state flux of NaFI were higher than those without SN. SN significantly increased the NaFI flux of NaFI solution from 0.0058 (without SN) to 0.2999 $\mu g.cm^{-2}.h^{-1}$ (51.7-fold enhancement). This suggested that the acoustic cavitation of SN might be the defects mechanism of the stratum corneum structure, leading to creation of intercellular lipid channels at discrete sites and transportation of hydrophilic drug through aqueous permeation pathways (Alvarez-Román et al., 2003, Morimoto et al., 2005). Moreover, temperature also affects the solute diffusivity. Thermal energy provides a doubling of permeability for every 1 0 ˚C of increase in temperature (Merino et al., 2003). However, the donor solutions in contact with the sonicated skin of this study were increased just around 1-2 ˚C (no significant rise in temperature). Therefore, the NaFI diffusity might be mainly due to cavitation from SN.

In case of using lipid nanocarrier system, the NaFI-loaded lipid nanocarriers showed higher NaFI permeated through the skin than NaFI solutions. The enhancement ratio from NaFI solution was in the order: SLN (33.10-fold) > NI (17.84-fold) > CL (1.34-fold). SLN showed the highest NaFI permeation through the

skin, because of the higher NaFI entrapment into SLN than other formulations. Moreover, the solid structure of lipid particles was more lipophilic and could closely contact the skin, leading to formation of a thin film of lipid nanoparticles on the skin surface and then providing an occlusive effect to increase skin hydration. Consequently, the penetration of the drug into the skin was enhanced (Pardeike, Hommoss, and Müller, 2009). Therefore, it was anticipated that a greater amount of solid lipids in the formulation might lead to greater skin penetration.

Niosomes showed higher NaFI flux through the skin than liposomes. This suggested that niosomes altered horny layer properties by reducing transepidermal water loss and increasing smoothness via the replenishment of lost skin lipids (Hofland et al., (1995). Because nonionic surfactants and cholesterol containing in niosome vesicles could provide a higher chemical and physical stabilities (Vora, Khopade, and Jain, 1998), a greater availability of surfactant classes (Manconi et al., 2006), and a higher amount of entrapped substances penetrated across the skin (Schneider et al., 2009). Therefore, niosome are an alternative drug delivery system to conventional liposome-based delivery methods. While liposomes are of little or no value as carriers for transdermal drug delivery due to their inability to deeply penetrate the alteration of the stratum corneum lipid structure. Hence, these vesicles remain confined to the stratum corneum layer (Touitou et al., 2000).

The effect of SN on the skin transportation of NaFI-loaded in different lipid nanocarriers was investigated. The flux rate was in the following order: NI > CL > SLN, however, NaFI flux of all of those formulations were significantly lower than NaFI solution with SN. From the result, NI alone had a slightly higher NaFI flux than NI treated with SN. When applying the SN with NI, the niosomal vesicles might break and release entrapped NaFI prior to contacting the skin surface (Vyas, Singh, and Asati, 1995). The membrane bilayers might adsorb and cover the defect skin surface, which caused a reduction in transport of the hydrophilic compound through skin.

The flux of CL with SN was significantly higher than CL alone (5.36-fold enhancement). The lag time of CL with SN was significantly lower than CL without SN, suggesting that the SN increased penetration rate of CL. According to Vyas, Singh, and Asati (1995), the sonication energy could break the lamellae of liposomes.

The entrapped drugs were then released and transported through the stratum corneum (Subongkot et al., 2013). Moreover, liposomes made from phospholipids, e.g., fluid-state l-α-phosphatidylcholine from egg yolk (EPC), may diffuse into the stratum corneum by adsorption onto and fusion with the defect skin surface, resulting in enhanced drug penetration through the skin and repaired ultrasound-induced skin disruption (Dahlan, Alpar, and Murdan, 2009, Kirjavainen et al., 1999).

In the result of SLN, the SN reduced the skin penetration of NaFI. SLN alone had a significantly higher NaFI flux than SLN with SN (6.32-fold). The extreme cavitation transient in the medium was produced by ultrasound energy, leading to increased medium temperature by expanding and producing energetic shock waves from a bubble implosion. However, maintaining the temperature of the dispersion above the melting point of SLN lipids is essential to facilitate the breakup of oil droplets (Siddiqui et al., 2014). In this study, cetyl palmitate was used as a solid core of SLN (the melting point of cetyl palmitate is 54 ˚C). At the end of a 2-min of SN application, the temperature of the donor solutions resulted in increase of ~ 2 ˚C from 32 ± 0.5 ˚C. Although the temperature of the SLN dispersion was lower than the melting point of the solid core, the sonication energy could break the solid core of the lipid nanoparticles. Therefore, the skin surface was covered by a solid lipid fraction, leading to reduced NaFI transport through skin.

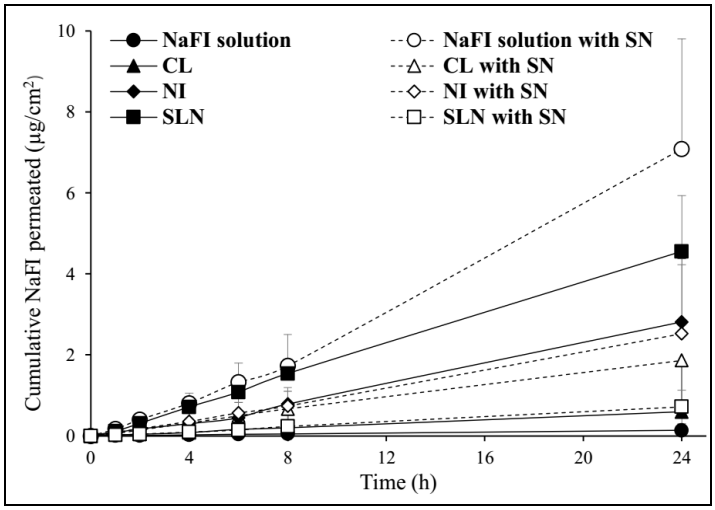

Figure 4.4 The cumulative amount and time profiles of NaFI from NaFI solution and different lipid nanocarrier formulations (CL, NI, and SLN) with and without SN. Each value represents the mean ± S.D. (n=3).

Table 4.3 The penetration parameters of NaFI-loaded different lipid nanocarrier formulations. Each value represents the mean ± S.D. (n=3). *indicates significant difference from those without SN ($p < 0.05$).

Formulations	**Flux (μg.cm^{-2}.h^{-1})**	**ER**	**Lag time (h)**	**K_p (cm/h) (x 10^{-6})**
NaFI solution	0.0058 ± 0.00	-	0.54 ± 0.19	2.90 ± 0.95
NaFI solution with SN	0.2999 ± 0.12*	51.71	0.37 ± 0.06	149.93 ± 58.44*
CL	0.0078 ± 0.00	1.34	1.00 ± 0.35	3.90 ± 2.91
CL with SN	0.0418 ± 0.01	7.21	0.20 ± 0.20*	20.90 ± 3.49
NI	0.1035 ± 0.08	17.84	0.58 ± 0.33	51.77 ± 41.06
NI with SN	0.0666 ± 0.01	11.48	0.50 ± 0.35	33.32 ± 3.44
SLN	0.1920 ± 0.06	33.10	0.43 ± 0.23	95.98 ± 30.70
SLN with SN	0.0304 ± 0.02*	5.24	0.50 ± 0.26	15.20 ± 8.89*

4.2.2 NaFI-loaded PEGylated nanocarriers

PEGylated lipid nanocarriers were formulated by modifying lipid carrier surface with hydrophilic polymer, polyethylene glycol. As shown in Figure 4.5 and Table 4.4, the PEG-grafted liposome vesicles provided a slightly higher NaFI flux through skin than non-PEGylated liposomes (CL). The NaFI penetrated through skin of PL2 was higher than PL3, PL1, and PL4, respectively. There was several explanations for the preserved permeation in this study. Firstly, a smaller vesicle size and higher NaFI entrapment of the grafting PEG onto liposome surfaces (PL1-PL4) provided higher NaFI delivery through skin than CL. According to Verma et al. (2003), a hydrophilic fluorescent compound (carboxyfluorescein; CF) loaded into the smaller liposome vesicles (120 nm) showed statistically enhanced the skin penetration of CF as compared to larger ones (191 nm, 377 nm, and 810 nm, respectively). The higher amount of CF incorporated into liposome vesicles also exhibited a higher penetration than those with lower %EE (Verma et al., 2003). Secondly, the physicochemical properties of liposome vesicles were depended on the concentration of PEG2000-DSPE in liposome formulations. The grafting of 1%mol PEG2000-DSPE onto liposome surface have been expected to adopt a mushroom-like configuration, while PEG-DSPE more than 4 mol% exhibited the brush structure of the polymer (Garbuzenko et al, 2005), leading to decreased the drug permeability

across the liposomal bilayer and slow released of entrapped drug from the liposomes. And thirdly, the hydrophilicity of PEG-DSPE molecule might bind with water molecules in the stratum corneum leading to increased the skin hydration and enhancing the skin permeability of hydrophilic compound across the skin barrier (Knudsen et al., 2012).

Using SN with PEGylated liposomes, SN increased NaFI flux of the lowest concentration of PEG in liposomal formulation (PL1), but it decreased NaFI flux of PL2-4. However, the NaFI flux of all PEGylated liposome formulations was not significantly different between the formulations with and without SN. This result indicated that SN had no effect on the penetration route of PEGylated liposomes.

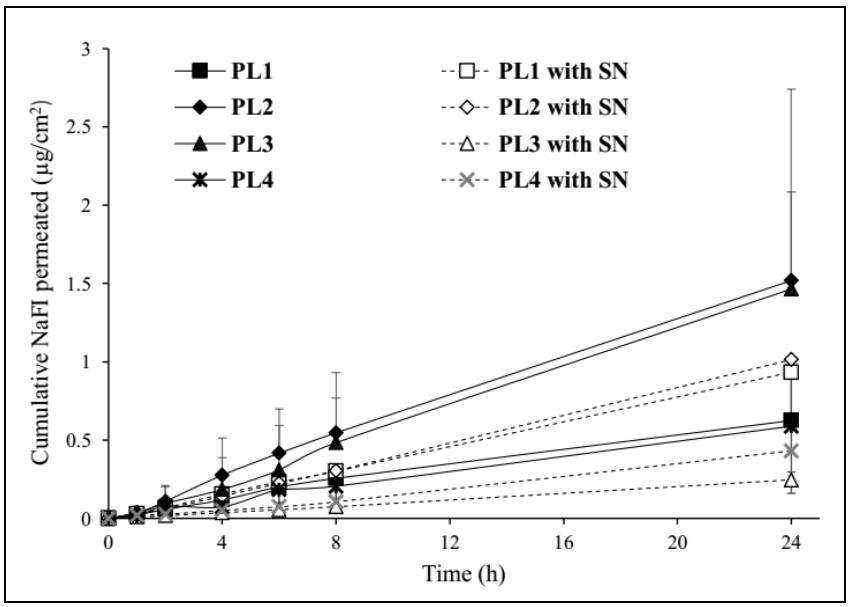

Figure 4.5 The cumulative amount and time profiles of NaFI from different concentrations of PEG2000-DSPE in PEGylated liposome formulations. Each value represents the mean ± S.D. (n=3).

Table 4.4 The penetration parameters of NaFI from different concentrations of PEG2000-DSPE in PEGylated liposome formulations. Each value represents the mean ± S.D. (n=3.).

Formulations	**Flux (μg.cm^{-2}.h^{-1})**	**ER**	**Lag time (h)**	**K_p (cm/h) (x 10^{-6})**
CL	0.0078 ± 0.00	1.34	1.00 ± 0.35	3.90 ± 2.91
Without SN				
PL1	0.0258 + 0.00	4.45	0.50 ± 0.10	12.89 ± 1.46
PL2	0.0639 ± 0.05	11.02	0.86 ± 0.00	32.00 ± 25.53
PL3	0.0620 ± 0.03	10.69	0.70 ± 0.26	31.00 ± 13.50
PL4	0.0244 ± 0.00	4.21	0.40 ± 0.20	12.22 ± 1.33
With SN				
PL1 with SN	0.0391 ± 0.03	6.74	0.47 ± 0.29	19.53 ± 13.43
PL2 with SN	0.0427 ± 0.02	7.36	0.37 ± 0.15	21.33 ± 8.68
PL3 with SN	0.0165 ± 0.01	2.84	0.40 ± 0.09	8.25 ± 5.50
PL4 with SN	0.0189 ± 0.00	3.26	0.32 ± 0.30	6.30 ± 0.36

For niosome formulations, the NaFI flux of the PEGylated niosomes (NIP1-4) was lower than that of non-PEGylated niosomes (Figure 4.6 and Table 4.5), indicating that the size and %EE of PEGylated niosomes were smaller than non-PEG niosomes. Junyaprasert et al. (2012) explained the effect of vesicle size and %EE of different niosome formulations entrapping ellagic acid that the penetration enhancement properties of different niosome formulations were caused by the particle size, % EE, and interaction of the solubilizer in the niosomes with the skin.

For the influence of SN, SN slightly increased NaFI flux of NIP1. Higher concentration of PEG2000-DSPE (NIP2-4) combined with SN significantly decreased NaFI flux compared to NI alone. However, the results of all NIP formulations were not significantly different between NIP with and without SN, suggesting that the main effect on the skin permeation might depend on niosomal formulation.

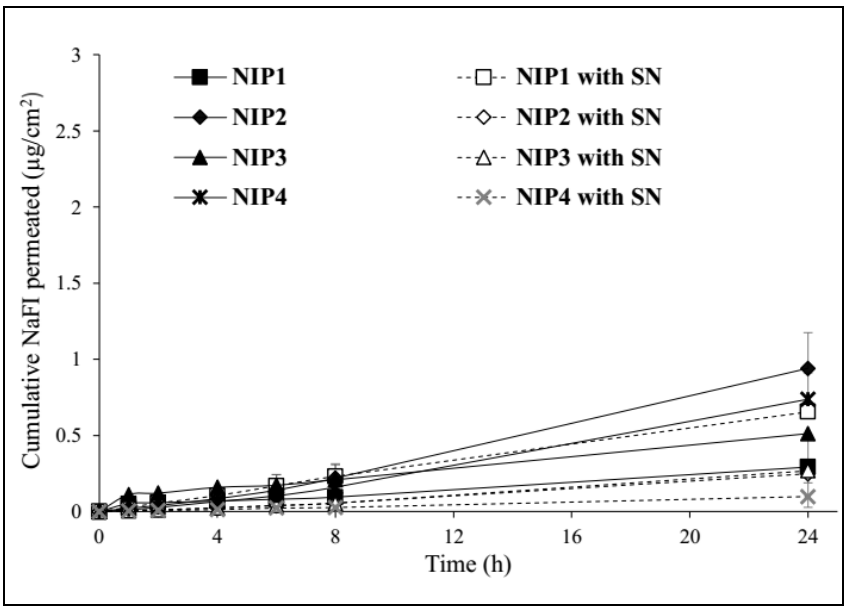

Figure 4.6 The cumulative amount and time profiles of NaFI from different concentrations of PEG2000-DSPE in PEGylated niosome formulations. Each value represents the mean ± S.D. (n=3).

Table 4.5 The penetration parameters of NaFI from different concentrations of PEG2000-DSPE in PEGylated niosome formulations. Each value represents the mean ± S.D. (n=3.). *indicates significant difference between NI ($p < 0.05$).

Formulations	**Flux (µg.cm^{-2}.h^{-1})**	**ER**	**Lag time (h)**	**K_p (cm/h) (x 10^{-6})**
NI	0.1035 ± 0.08	17.84	0.58 ± 0.33	51.77 ± 41.06
Without SN				
NIP1	0.0111 ± 0.01*	1.91	0.30 ± 0.30	5.58 ± 4.71*
NIP2	0.0433 ± 0.01	7.47	0.85 ± 0.30	20.00 ± 5.12
NIP3	0.0190 ± 0.01	3.28	0.38 ± 0.33	9.49 ± 6.50
NIP4	0.0314 ± 0.01	5.41	0.35 ± 0.35	15.72 ± 3.81
With SN				
NIP1 with SN	0.0274 ± 0.00	4.72	0.37 ± 0.40	13.70 ± 1.50
NIP2 with SN	0.0105 ± 0.01*	1.81	0.70 ± 0.17	5.23 ± 2.83*
NIP3 with SN	0.0114 ± 0.00*	1.97	0.60 ± 0.17	5.70 ± 1.82*
NIP4 with SN	0.0041 ± 0.00*	0.71	0.73 ± 0.12	2.07 ± 0.89*

In the case of the SLN, the particle size and % EE of PEGylated SLN (SLNP 2-4) were significantly higher than non-PEGylated SLN. However, the NaFI flux for all PEGylated SLN formulations significantly decreased when compared with that of non-PEGylated SLN (Figure 4.7 and Table 4.6). The NaFI permeated through skin of SLNP1 was higher than SLNP3, SLNP2, and SLNP4, respectively, suggesting that the grafting of hydrophilic polymer onto SLN surface might decrease the film formation onto the skin surface, thus resulting in reduced the encapsulated drug onto the skin surface. The combination of SN and SLNP formulations significantly decreased NaFI flux compared to SLN alone, but it was not significantly different between SLN with and without SN of the same formulation.

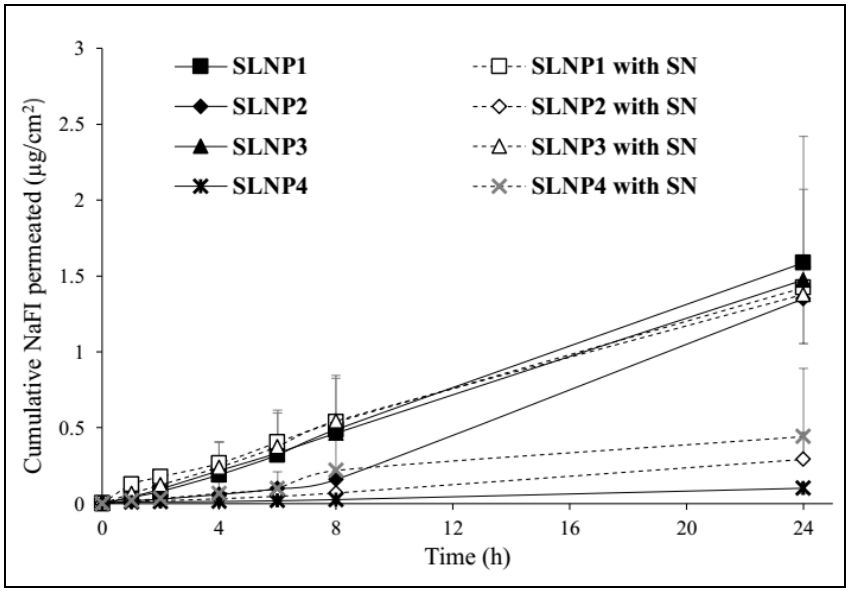

Figure 4.7 The cumulative amount and time profiles of NaFI from different concentrations of PEG2000-DSPE in PEGylated SLN formulations. Each value represents the mean ± S.D. (n=3).

Table 4.6 The penetration parameters of NaFI from different concentrations of PEG2000-DSPE in PEGylated SLN formulations. Each value represents the mean ± S.D. (n=3.). *indicates significant difference between SLN ($p < 0.05$).

Formulations	**Flux (μg.cm^{-2}.h^{-1})**	**ER**	**Lag time (h)**	**K_p (cm/h) (x 10^{-6})**
SLN	0.1920 ± 0.06	33.10	0.43 ± 0.23	95.98 ± 30.70
Without SN				
SLNP1	0.0461 ± 0.04*	7.95	0.73 ± 0.31	23.07 ± 20.34*
SLNP2	0.0577 ± 0.04*	9.95	0.57 ± 0.23	28.87 ± 20.93*
SLNP3	0.0184 ± 0.02*	3.17	0.73 ± 0.31	9.22 ± 11.47*
SLNP4	0.0041 ± 0.00*	0.71	0.23 ± 0.21	2.05 ± 0.74*
With SN				
SLNP1 with SN	0.0578 ± 0.01*	9.97	0.23 ± 0.21	28.92 ± 25.42*
SLNP2 with SN	0.0115 ± 0.00*	1.98	0.57 ± 0.31	5.73 ± 1.36*
SLNP3 with SN	0.0574 ± 0.01*	9.90	0.27 ± 0.23	28.72 ± 7.11*
SLNP4 with SN	0.0188 ± 0.02*	3.24	0.60 ± 0.10	9.40 ± 9.60*

4.2.3 NaFI-loaded d-limonene-containing PEGylated nanocarriers

As shown in Figure 4.8 and Table 4.7, the cumulative NaFI permeation from PL-LI was significantly higher than NIP-LI and SLNP-LI, respectively. The lag time for each formulation was not significantly different. For the flux rate, the greatest skin permeation of PL-LI was 8.33-fold, whereas PL-Tween 20 was 2.10-fold enhancement compared to PL2 (data not shown). This result may reveal that incorporation of tween 20 and a terpene (d-limonene) into liposomes gave a synergistic enhancement of the skin penetration (Subongkot et al., 2012). The membrane fluidity of liposome vesicles was increased by adding tween 20 and d-limonene into bilayer structure, leading to enhanced NaFI penetration though skin (Subongkot et al., 2013). D-limonene has been used extensively for topical delivery of both hydrophilic and lipophilic drugs, because it can break the network of hydrogen bonds between ceramides and then modify the organization of lipids in the stratum corneum (Badran, Shazly, and El-Badry, 2012, Jain, Thomas, and Panchagnula, 2002). Tween 20 is an edge activator that increased deformability of neutral or

negatively charged conventional liposomes (Oh et al., 2006). In addition, the small size of the liposome provided an enhancement effect on the skin permeation. Smaller PL vesicles gave higher skin penetration of NaFI than the larger ones (Verma et al., 2003). For d-limonene containing niosomes, the NaFI flux was slightly higher than those without d-limonene. This result was quiet the same with liposomal formulation result, which the effect of d-limonene played an important role on the skin penetration. However, the NaFI permeated through skin of SLNP-LI showed lower than those without d-limonene, suggesting that d-limonene was intercalated in the lipid part of particles and might not be released from lipid particles to the skin surface.

For the combination effect of SN, d-limonene (as a chemical enhancer), and lipid nanocarriers on the skin penetration of NaFI, the cumulative amount of NaFI permeated into the skin of PL-LI with SN was higher than NIP-LI with SN and SLNP-LI with SN, respectively. However, SN significantly decreased the NaFI flux of PL-LI from 0.5380 $\mu g.cm^{-2}.h^{-1}$ (without SN) to 0.1914 $\mu g.cm^{-2}.h^{-1}$, indicating that using SN resulted in a 2.81-fold decrease in skin permeation compared with passive delivery. According to Vyas et al. (1995), the application of SN with liposomal ointment exhibited an enhancement effect of the encapsulated diclofenac permeated across the skin better than that without SN. They explained that the diffusion improvement was probably due to the breaking of liposome lamellae on sonication. After that, the entrapped hydrophilic molecules were released and transported through the pore pathway in the stratum corneum (Kenworthy, Simon, and McIntosh, 1995). When sonication energy was terminated, phospholipid bilayer fragments were rapidly fused and closed to form liposome vesicles (Subongkot et al., 2013). Some liposome bilayers repaired ultrasound-induced skin disruption by adsorption onto and fusion with the skin surface's defect resulting in reduced the skin permeability of any compound (Dahlan, Alpar, and Murdan, 2009). In the previous report, the penetration pathway of ultradeformable liposomes with d-limonene was transfollicular pathway rather than intercellular or intracellular pathway. Therefore, if ultrasound can lead to changes in the structure of the skin surface, the penetration route of NaFI-loaded PL-LI will also be affected. However, PL-LI with SN showed higher NaFI permeated through the skin than CL with SN and PL with SN, because d-limonene caused greater skin disruption than that can be repaired by liposome vesicles.

For niosome formulations, the NaFI flux of NIP-LI with SN was lower than those without SN, but higher than NIP with SN. Similarly to liposome vesicles, SN might break the lamellar structure of niosome vesicles, therefore the broken vesicles adsorbed and covered the defect skin surface causing a reduction in transport of the hydrophilic compound through skin (Vyas et al., 1995). However, chemical enhancer-containing vesicles might also affect the skin penetration of NaFI.

For SLN formulation, the NaFI flux of SLNP-LI with SN was higher than SLNP and SLNP-LI, respectively. From the result of SLNP-LI, d-limonene might not be released from lipid particles to skin surface. Therefore, the combination of SN and SLNP-LI exhibited higher NaFI permeated than other condition, indicating that SN might break solid particles and release d-limonene into the skin for enhancing NaFI permeation.

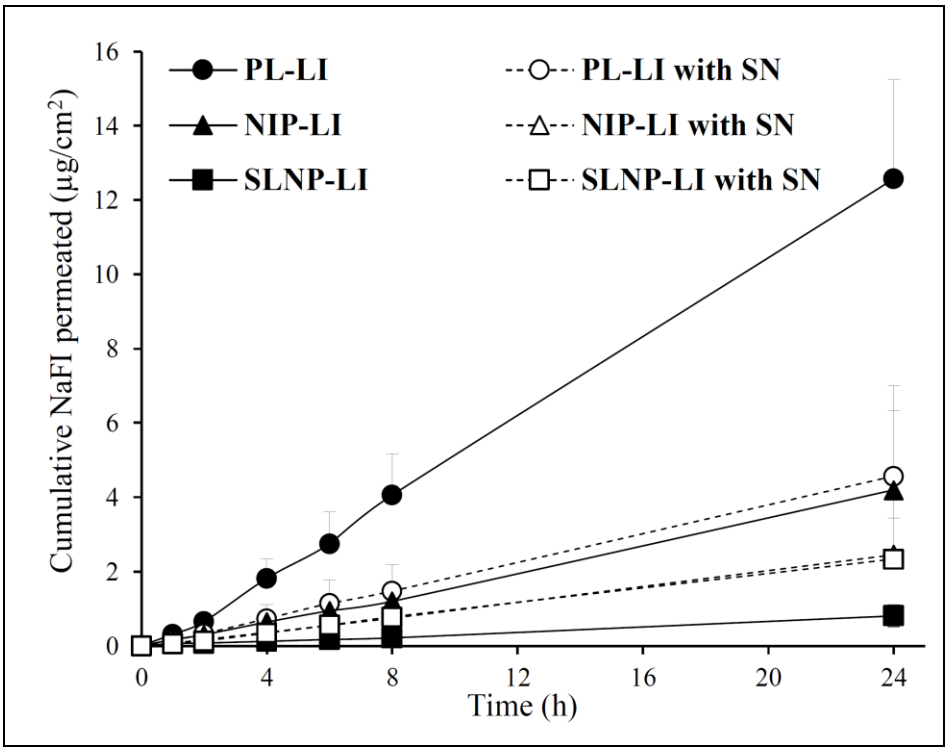

Figure 4.8 The cumulative amount and time profiles of NaFI from difference lipid nanocarrier formulations: PL-LI, NIP-LI, and SLNP-LI with and without SN at 32 ± 0.5 ˚C. Each value represents the mean ± S.D. (n=3.)

Table 4.7 The penetration parameters of NaFI-loaded difference lipid nanocarrier formulations: PL-LI, NIP-LI, and SLNP-LI with and without SN. Each value represents the mean ± S.D. (n=3). *indicates significant difference between those without SN ($p < 0.05$).

Formulations	**Flux ($\mu g.cm^{-2}.h^{-1}$)**	**ER**	**Lag time**	**K_p (cm/h) (x 10^{-6})**
Without SN				
PL-LI	0.5381 ± 0.11*	92.78	0.48 ± 0.16	269.03 ± 55.76*
NIP-LI	0.1753 ± 0.09	30.22	0.35 ± 0.35	87.63 ± 45.11
SLNP-LI	0.0332 ± 0.01	5.72	0.93 ± 0.40	16.58 ± 5.47
With SN				
PL-LI with SN	0.1914 ± 0.10	33.00	0.33 ± 0.06	95.68 ± 51.55
NIP-LI with SN	0.1476 ± 0.06	25.45	0.57 ± 0.08	73.80 ± 31.95
SLNP-LI with SN	0.0689 ± 0.04	11.88	0.83 ± 0.25	34.47 ± 20.81

4.3 Influence of SN on the skin deposition of nanocarriers

The amount of NaFI deposited in the different skin layers were evaluated by tape stripping technique. Using NaFI solution as a coupling medium, the amount of NaFI in the stratum corneum treated with SN was lower than that without SN, while NaFI in the epidermis and dermis layer was higher than that without SN (Figure 4.9). SN increased the penetration of NaFI into the deeper skin layer and through skin into receiver compartment. Alvarez-Román et al. (2003) reported that SN could remove a fraction of the intercellular lipids (~30%) of the stratum corneum. Therefore, it might decrease the amount of NaFI deposited in the statum corneum layer and increase NaFI pass through the defect skin barrier into the deer layer.

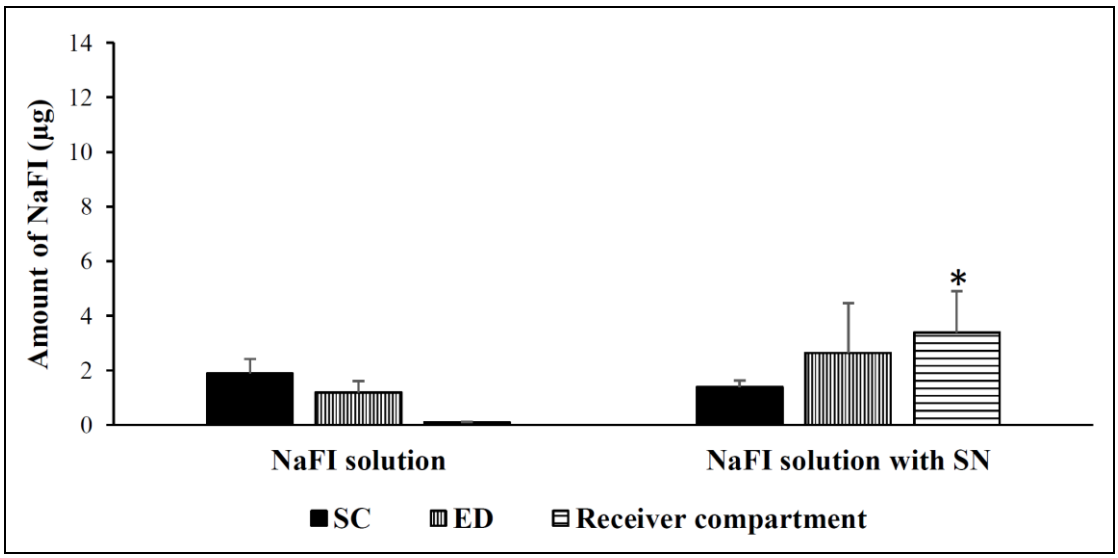

Figure 4.9 Comparison of NaFI-remaining stratum corneum (SC), epidermis and dermis (ED), and receiver compartment from NaFI solution with and without SN after 8 h *in vitro* skin permeation. Each value represents the mean ± S.D. (n=3). * indicates significant difference from NaFI solution ($p < 0.05$).

For liposome formulations as shown in Figure 4.10, the amount of NaFI in the stratum corneum was in the following order: CL (3.24 ± 0.45 µg) > PL2 (3.22 ± 0.39 µg) > PL2 with SN (2.37 ± 0.39 µg) > PL-LI (2.36 ± 0.16 µg) > CL with SN (2.24 ± 0.22 µg) > PL-LI with SN (1.18 ± 0.26 µg). SN and d-limonene significantly reduced the amount of NaFI deposited in the stratum corneum layer. The amount of NaFI in the epidermis and dermis was in the following order: PL-LI (6.48 ± 2.12 µg) > PL2 (1.90 ± 0.60 µg) > PL-LI with SN (1.76 ± 0.77 µg) > CL (1.46 ± 0.16 µg) > PL2 with SN (1.15 ± 0.06 µg) > CL with SN (0.69 ± 0.16 µg). The NaFI penetrated into the deeper skin layer and through the skin into the receiver compartment of the Franz diffusion cell of PL-LI was significantly higher than other formulations. This indicated that d-limonene provided a main enhancing effect on the skin penetration of NaFI from liposome formulation. Badran, Shazly, and El-Badry (2012) reported that d-limonene can disrupt the stratum corneum lipids leading to creation of voids and empty spaces in the upper epidermal region and then enhance drug penetrated into the

skin. Therefore, PL-LI delivered more NaFI to the epidermis and dermis and across the skin than remaining into the stratum corneum.

Moreover, the high elasticity of deformable liposomes can increase skin permeability (Cevc and Blume, 1992). Ultradeformable vesicles, prepared by adding tween 20 (as an edge activator) into PL2 formulation penetrated skin better and delivered more NaFI to the receiver compartment than PL (data not shown). Therefore, the use of ultradeformable liposomes with skin penetration enhancers exhibited a synergistic effect for enhancing the skin penetration of NaFI (Subongkot et al., 2012). In addition, the NaFI depositions in the epidermis and dermis of PL2 was higher than CL. Conventional liposomes containing phospholipids and cholesterol did not penetrate skin deeply. Instead, these liposomes remained confined in the stratum corneum (Touitou et al., 2000). Liposomes prepared by using PEG (hydrophilic polymer) conjugated with phospholipids enhanced NaFI delivery into the deeper skin layers, because these vesicles provided better stratum corneum hydration than phospholipids without PEG (Knudsen et al., 2012), thus resulting in improved the skin permeability of hydrophilic compound.

SN significantly decreased the amount of NaFI in the stratum corneum layer of all formulations when compared to those without SN. Although the combination of SN with PL-LI provided deeper skin penetration of NaFI than other formulation, the skin treated with PL-LI and SN was significantly lower amount of NaFI penetrated into and through skin than that without SN. This suggested that SN might break the ultrastructure of stratum corneum and change the transcellular pathway of NaFI in the defect skin. Moreover, some broken vesicles might repair the sonicated skin by adsorbing and fusing with the stratum corneum surface, leading to decreased NaFI penetrated into the skin

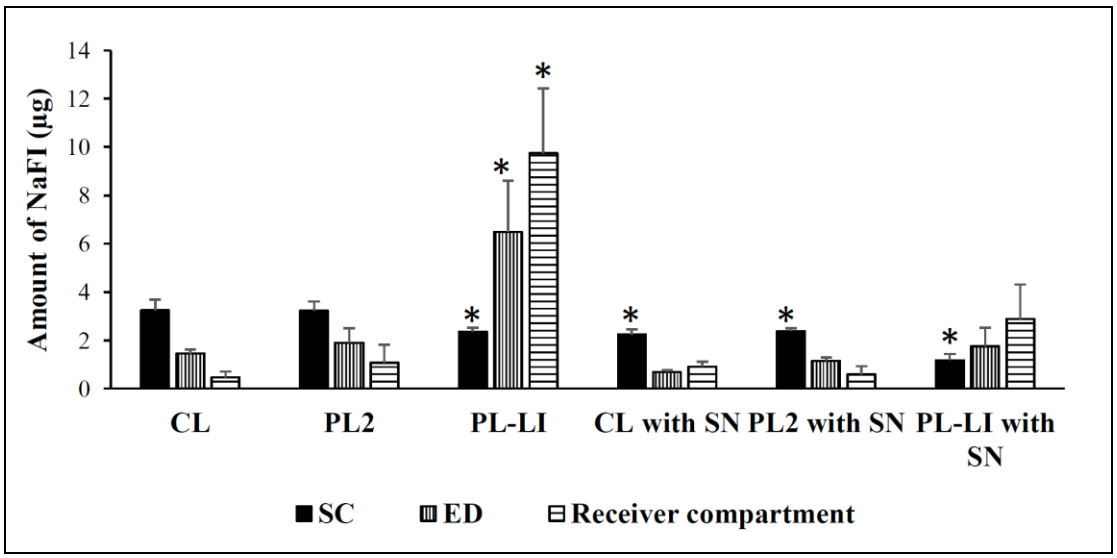

Figure 4.10 Comparison of NaFI-remaining stratum corneum (SC), epidermis and dermis (ED), and receiver compartment from liposome formulations (CL, PL, and PL-LI) with and without SN after 8 h *in vitro* skin permeation. Each value represents the mean ± S.D. (n=3). * indicates significant difference from CL ($p < 0.05$).

For niosomes formulations as shown in Figure 4.11, the amount of NaFI in the stratum corneum was in the following order: NI (3.68 ± 0.18 µg) > NIP2 (3.25 ± 0.68 µg) > NIP-LI (2.79 ± 0.65 µg) > NIP-LI with SN (1.46 ± 0.11 µg) > NIP2 with SN (1.46 ± 0.69 µg) > NI with SN (1.44 ± 0.03 µg). SN significantly reduced the amount of NaFI deposited in the stratum corneum layer. The amount of NaFI in the epidermis and dermis was in the following order: NI (1.11 ± 0.09 µg) > NIP-LI with SN (0.81 ± 0.59 µg) > NIP2 (0.79 ± 0.02 µg) > NIP2 with SN (0.70 ± 0.13 µg) > NIP-LI (0.69 ± 0.09 µg) > NI with SN (0.53 ± 0.05 µg). The amount of NaFI in all formulations was not significantly different. However, NaFI permeated through skin of NIP-LI was higher than other conditions, suggesting that d-limonene provided enhancing effect on the skin permeation of entrapped NaFI.

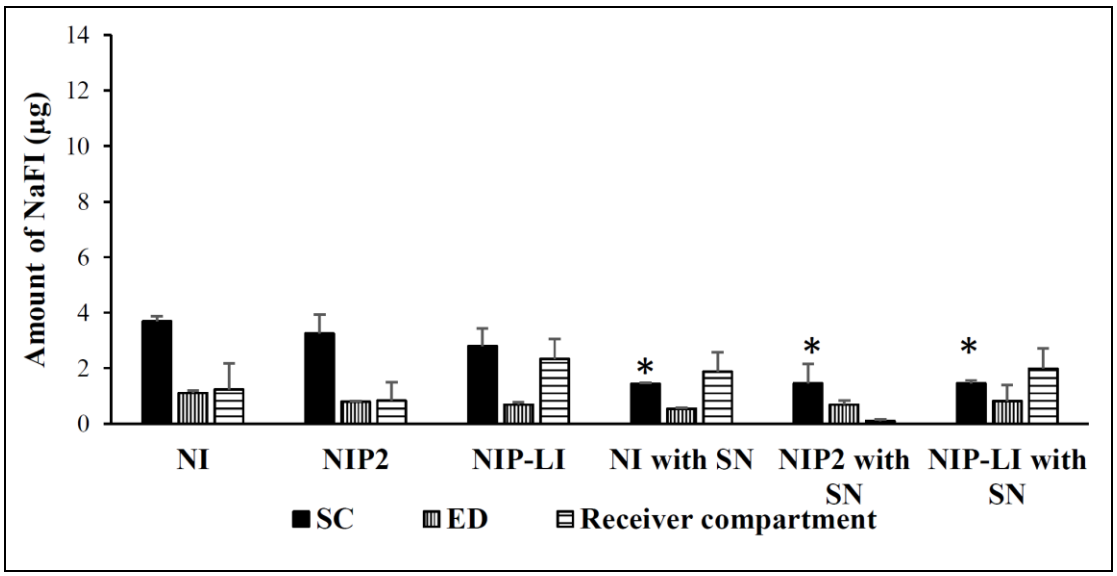

Figure 4.11 Comparison of NaFI-remaining stratum corneum (SC), epidermis and dermis (ED), and receiver compartment from niosome formulation (NI, NIP, and NIP-LI) with and without SN after 8 h *in vitro* skin permeation. Each value represents the mean ± S.D. (n=3). * indicates significant difference from NI ($p < 0.05$).

For SLN formulations as shown in Figure 4.12, the amount of NaFI in the stratum corneum was in the following order: SLNP-LI (2.99 $\pm$ 1.13 µg) > SLNP2 (2.86 $\pm$ 0.62 µg) > SLN (2.22 $\pm$ 0.43 µg) > SLNP-LI with SN (1.73 $\pm$ 0.17 µg) > SLN with SN (1.37 $\pm$ 0.07 µg) > SLNP2 with SN (1.29 $\pm$ 0.33 µg). SN decreased the amount of NaFI deposited in the stratum corneum layer. The amount of NaFI in the epidermis and dermis was in the following order: SLNP-LI with SN (0.96 $\pm$ 0.09 µg) > SLN with SN (0.91 $\pm$ 0.09 µg) > SLN (0.79 $\pm$ 0.25 µg) > SLNP-LI (0.69 $\pm$ 0.13 µg) > SLNP2 with SN (0.69 $\pm$ 0.09 µg) > SLNP2 (0.39 $\pm$ 0.12 µg). The amount of NaFI in all formulations was not significantly different. In these results, the amounts of NaFI deposited in the stratum corneum was higher than those in the epidermis and dermis layers. Although SLN are known to have beneficial properties for topical drug therapy, including biocompatible ingredients, drug release modifications, skin adhesion, and film formation with the subsequent hydration of superficial skin layers, their penetration and permeation into and across deeper skin layers are restricted due to the barrier function of the stratum corneum (Lauterbach and Müller-Goymann,

2015). A few intact SLN form an occlusive film on the top layer of the skin surface; these SLN was observed in the first tape-stripped stratum corneum layer. Therefore, the drug permeation enhancement of SLN was likely due to particle occlusion properties (Baroli, 2010). The PEG-grafted SLN surface showed lower amounts of NaFI deposits in the epidermis and dermis than the non-PEG modified SLN, suggesting that a hydrophilic steric barrier around the SLN surfaces may have reduced the ability for the entrapped NaFI to deeply penetrate into the skin layer.

The amount of NaFI in the combination of SLNP-LI with SN was higher than those without SN, suggesting that the synergistic effect of SN and d-limonene might enhance the penetration of NaFI into the deep skin layer and through skin. Applying the SN with SLN, the ultrasound energy disrupted the lipid particles, leading to released penetration enhancer into the skin (Siddiqui et al., 2014).

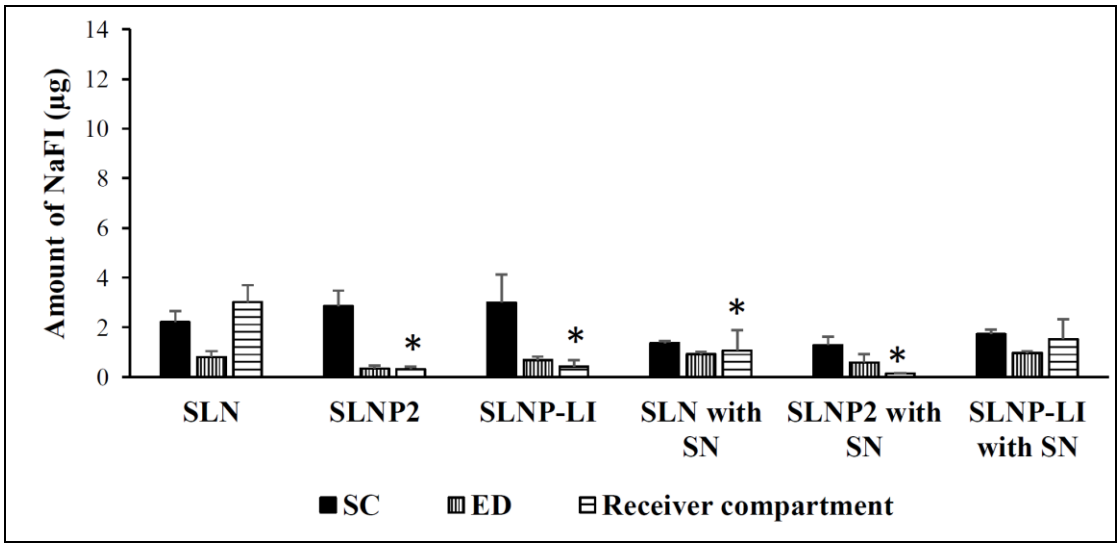

Figure 4.12 Comparison of NaFI-remaining stratum corneum (SC), epidermis and dermis (ED), and receiver compartment from solid lipid nanoparticle formulations (SLN, SLNP, and SLNP-LI) with and without SN after 8 h *in vitro* skin permeation. Each value represents the mean ± S.D. (n=3). *indicates significant difference from SLN ($p < 0.05$).

The amounts of NaFI in the stratum corneum from the niosomes and liposomes were not significantly different. The deposition of NaFI in the stratum corneum of SLN was lower than niosomes and liposomes, and the deposition of NaFI in the

epidermis and dermis of all formulations was lower than the NaFI deposited in the stratum corneum. NIP-LI and SLNP-LI provided higher NaFI deposited in stratum corneum than PL-LI, but lower NaFI penetrated into the deeper skin layer and through skin. This suggested that d-limonene can increase free NaFI penetrated into the high fluidity of intercellular lipid in the stratum corneum. While rigid nanocarrier can not transport as intact carriers passed through the stratum corneum.

4.4 Mechanistic characterization of nanocarriers permeated through skin

4.4.1 Visualization of the skin penetration pathway by CLSM

4.4.1.1 NaFI-loaded liposomes

The cross-sectioned skin images of samples obtained 4 h after the deposition of NaFI-loaded-Rh-PE-labeled liposome formulations were visualized as shown in Figure 4.13. The skin with SN of CL and PL showed brighter fluorescence intensity of both NaFI and Rh-PE-labeled liposome membrane than the skin without SN. The fluorescence was deposited in the stratum corneum surface, covered the hair and in the follicle opening, but did not penetrate into the deep follicular duct and the deep skin layer. Applying SN with CL or PL onto the skin, the damaged skins were repaired by the adsorption of liposome bilayers. Because phospholipid-based liposomes have the same properties of stratum corneum lipids, their adhesion onto the skin surface and fusion or mixing with the lipid matrix of the stratum corneum might be found. Moreover, this effect might lead to enhanced NaFI permeated into skin (Kirjavainen et al., 1996).

For visualization the effect of SN on the skin permeation of d-limonene-containing PL, the result of PL-LI without SN showed brighter fluorescence intensity of NaFI and Rh-PE in the skin and the hair follicle than PL-LI with SN and other liposome formulations. The skin image of PL-LI with SN exhibited high fluorescence intensity on the top of hair outside the skin, while PL-LI without SN showed bright fluorescence intensity at a depth of 10 – 40 μm of the stratum corneum and exhibited deeper penetration around the hair follicle orifice than other regions. The fluorescence along the length of hair inside the skin indicated the follicular penetration route as the main penetration route. Moreover, the deposition of Rh-PE-labeled PL-LI membrane was at the same region of NaFI and in the deepest layer of

skin, indicating that the intact vesicles combined with entrapped NaFI might penetrate into skin. However, the fluorescence of NaFI was only observed in some parts of the skin, suggesting that some vesicles might release the entrapped drug before attaching to any part of the skin. Therefore, three mechanisms might be explained the skin penetration of NaFI-loaded PL-LI: i) penetration associated with the liposomal bilayer (intact vesicles), ii) penetration associated with a liposomal bilayer fragment, or iii) penetration solitarily (Grams YY, 2005).

When using SN, the fluorescence intensity of NaFI-loaded-Rh-PE-labeled PL-LI in skin decreased, indicating that the mechanical effect of ultrasound changed the transport pathway of drug-loaded lipid vesicles. Morimoto et al. (2005) reported that the differences in the physicochemical properties of the solutes, such as lipophilicity or hydrophilicity, affected low frequency ultrasound. Because ultrasound increases water transport across the skin, the distribution of more lipophilic compounds may not be influenced. Thus, PL-LI as a lipid vesicle carrier might not penetrate through hydrophilic transport routes in the intercellular space of the stratum corneum. In addition, the adsorption of liposomes onto the skin damage might cause the high fluorescence intensity of both NaFI and Rh-PE-labeled CL and PL at the top of the skin layer

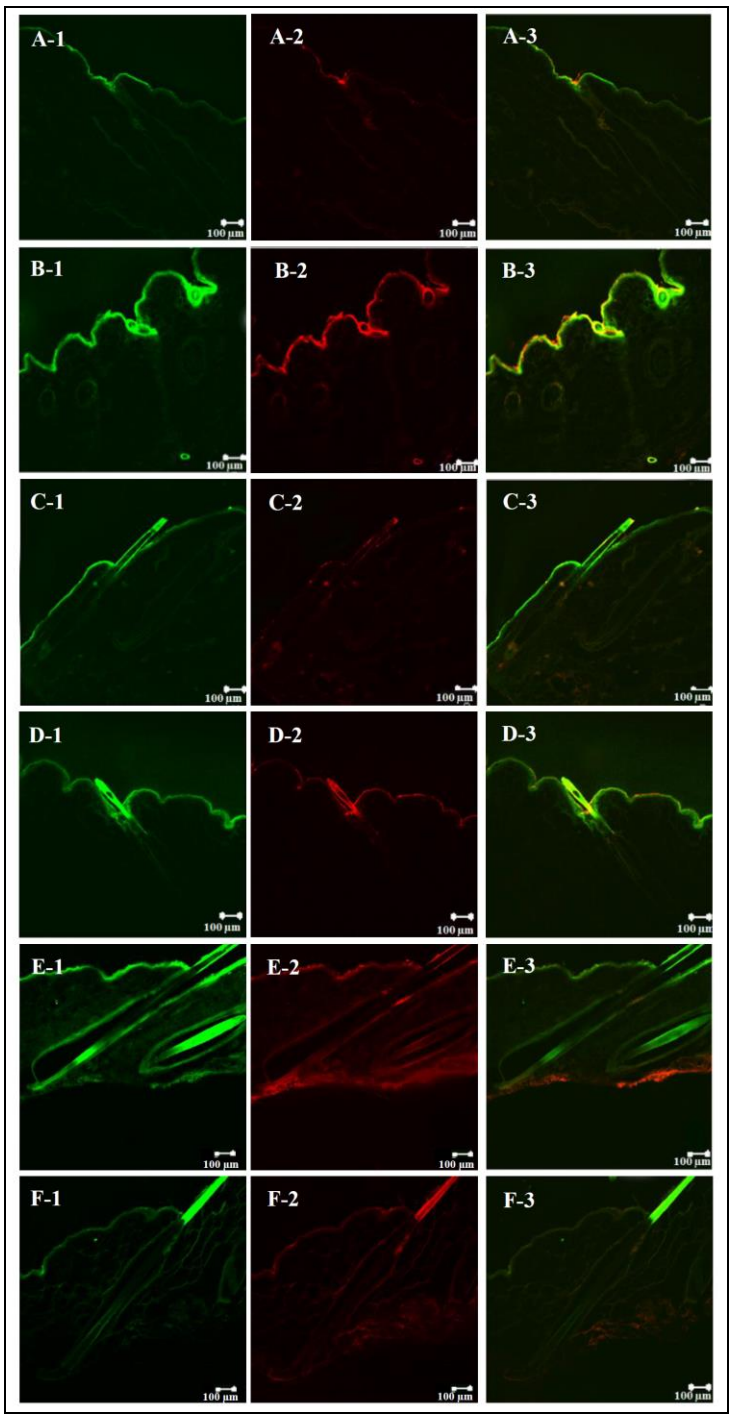

Figure 4.13 Confocal images of the skin cross section obtained at 4 h after deposition of NaFI-loaded-Rh-PE-labeled liposome formulations: CL without (A) and with SN (B), PL2 without (C) and with SN (D), and PL-LI without (E) and with SN (F). The image is divided in three parts, with (1) green fluorescence of NaFl, (2) red fluorescence of Rh-PE and (3) overlay of (1)

and (2). The scale bar represents 100 μm. All confocal images were obtained at a magnification of ×10.

4.4.1.2 NaFI-loaded niosomes

For the confocal images of all niosome formulations treated skin, Rh-PE-labeled niosome membranes were not found in the skin. Only NaFI permeated into the skin surface but niosome membranes were unable to form vesicles within the skin. This indicated that NaFI might be released from these nanocarriers before permeation. After applying ultrasound energy into NI and NIP, confocal image of the skin showed the brightest fluorescence intensity for the Rh-PE-labeled niosome membrane covering the stratum corneum surface, which NI exhibited brighter fluorescence intensity than NIP. However, NaFI did not permeate deeply into the skin (Figure 4.14). These results suggested that the ultrasound energy might disrupt the niosomes vesicles. The lipid fractions from niosome vesicles adsorbed onto the damage skin and covered the skin surface, resulting in reduced the skin penetration of hydrophilic compound.

For d-limonene-containing NIP, CLSM images showed NaFI deposited on the top layer of skin, while NIP-LI with SN showed NaFI distributed into the deeper skin layer. This result suggested that SN might disrupt NIP-LI vesicle leading to released d-limonene into the skin and increase the skin deposition of NaFI into the deep skin layer.

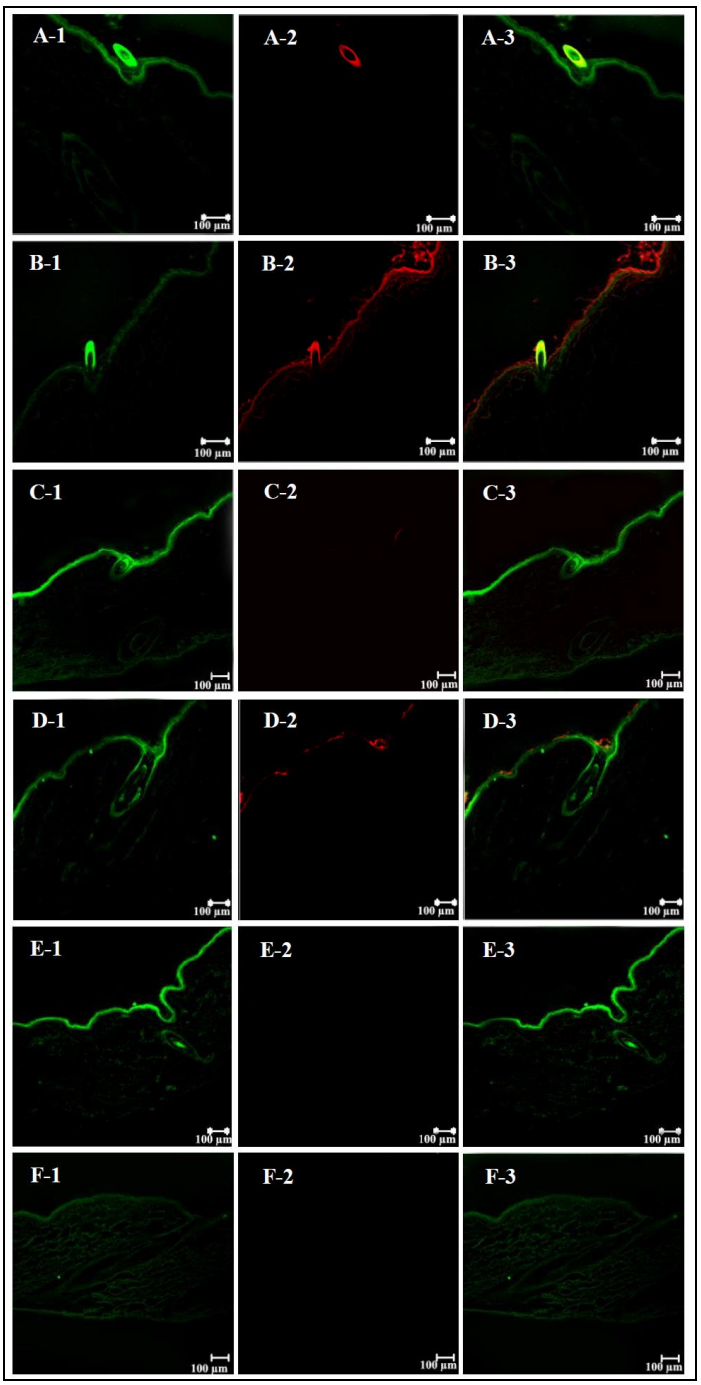

Figure 4.14 Confocal images of the skin cross section obtained at 4 h after deposition of NaFI-loaded-Rh-PE-labeled niosome formulations: NI without (A) and with SN (B), NIP2 without (C) and with SN (D), and NIP-LI without (E) and with SN (F). The image is divided in three parts, with (1) green fluorescence of NaFl, (2) red fluorescence of Rh-PE and (3) overlay of (1) and (2). The scale bar represents 100 µm. All confocal images were obtained at a magnification of ×10.

4.4.1.3 NaFI-loaded SLNs

SLN particles were not permeated into the skin as shown in Figure 4.15. Similarly to niosomes, SLN were unable to form vesicles within the skin. CLSM images showed only the NaFI distributed into the skin surface, suggesting that NaFI might be released from these nanocarriers before permeated through the skin. After that, NaFI deposited along the length of hair follicles inside the skin more than other lipid nanocarriers, indicating that the transfollicular pathway may be a skin penetration route for NaFI-loaded SLN. For PEG-grafted SLN surface showed lower amount of NaFI deposits in the epidermis and dermis than the non-PEG modified SLN, suggesting that a hydrophilic steric barrier around the SLN surfaces may have reduced the ability of the entrapped NaFI to deeply penetrate into the skin layer. Particulate drug carriers, e.g., lipid nanoparticles, have been reported to penetrate and preferentially accumulate in hair follicles. The lipophilic properties of the carriers provided high local concentrations of a drug on the skin surface and improved drug uptake via hair follicles (Lauterbach and Müller-Goymann, 2015, Wosicka-Frąckowiak et al., 2015). Therefore, the surface modification of SLN using hydrophilic polymers may reduce NaFI penetration through hair follicles.

For SLN, the ultrasound energy disrupted the lipid particles at a lower temperature than the melting point of the solid core. Therefore, the fragments of solid lipids might not be covered by surfactant (Siddiqui et al., 2014). Moreover, the separation of solid lipid (wax) were irreversible. The skin after applying SN into donner compartment of SLN formulation showed no value of red fluorescence because the Rh-PE probe may have been released before skin contacted by the SLN disruption. Only fragments of solid wax from the disrupted SLN might have covered the skin surface, leading to reduced the NaFI transport through skin via transdermal and transfollicular pathway.

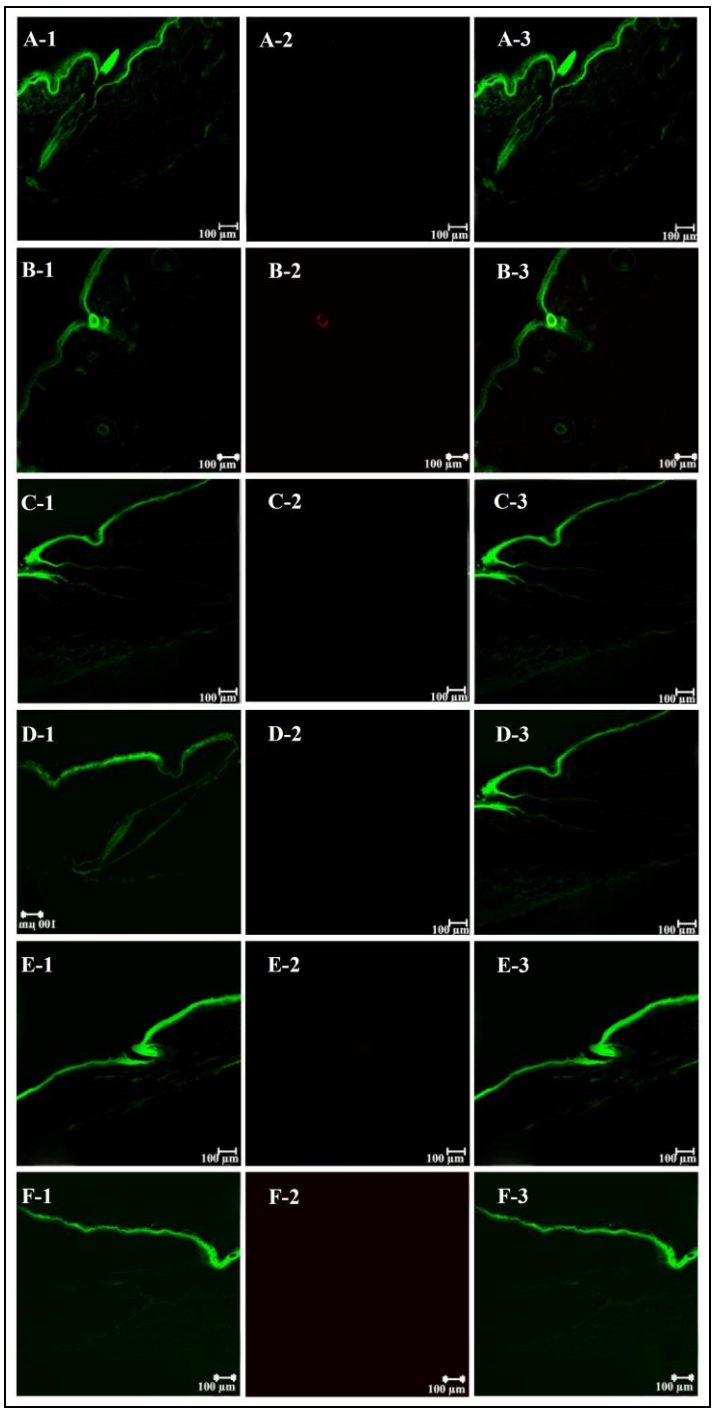

Figure 4.15 Confocal images of the skin cross section obtained at 4 h after deposition of NaFI-loaded-Rh-PE-labeled SLN formulations: SLN without (A) and with SN (B), SLNP2 without (C) and with SN (D), and SLNP-LI without (E) and with SN (F). The image is divided in three parts, with (1) green fluorescence of NaFl, (2) red fluorescence of Rh-PE and (3)

overlay of (1) and (2). The scale bar represents 100 μm. All confocal images were obtained at a magnification of ×10.

4.4.2 Skin surface topography by SEM

The SEM images of the porcine skin surface after applying SN with the different lipid nanocarriers were used to observe the effect of SN on the ultrastructure of skin. As shown in Figure 4.16, SN treated skin showed lifted up and crack-like structures of the skin surface, while the surface of the stratum corneum without SN showed relatively flat, intact, and confluent. The low-frequency SN induced disruption of the stratum corneum structure and enhanced the skin permeability for hydrophilic molecules in solution into the viable epidermis via an intracellular pathway (Morimoto, 2005).

The combination of the lipid nanocarriers with SN onto the skin showed small corneocytes lifting because the lipid compositions could cover and repair the damaged skin. In this result, the sonicated skin with the SLN had a thick lipid layer of solid wax (cetyl palmitate). The formation of the lipid film on the skin surface might have decreased the skin permeation of hydrophilic compound.

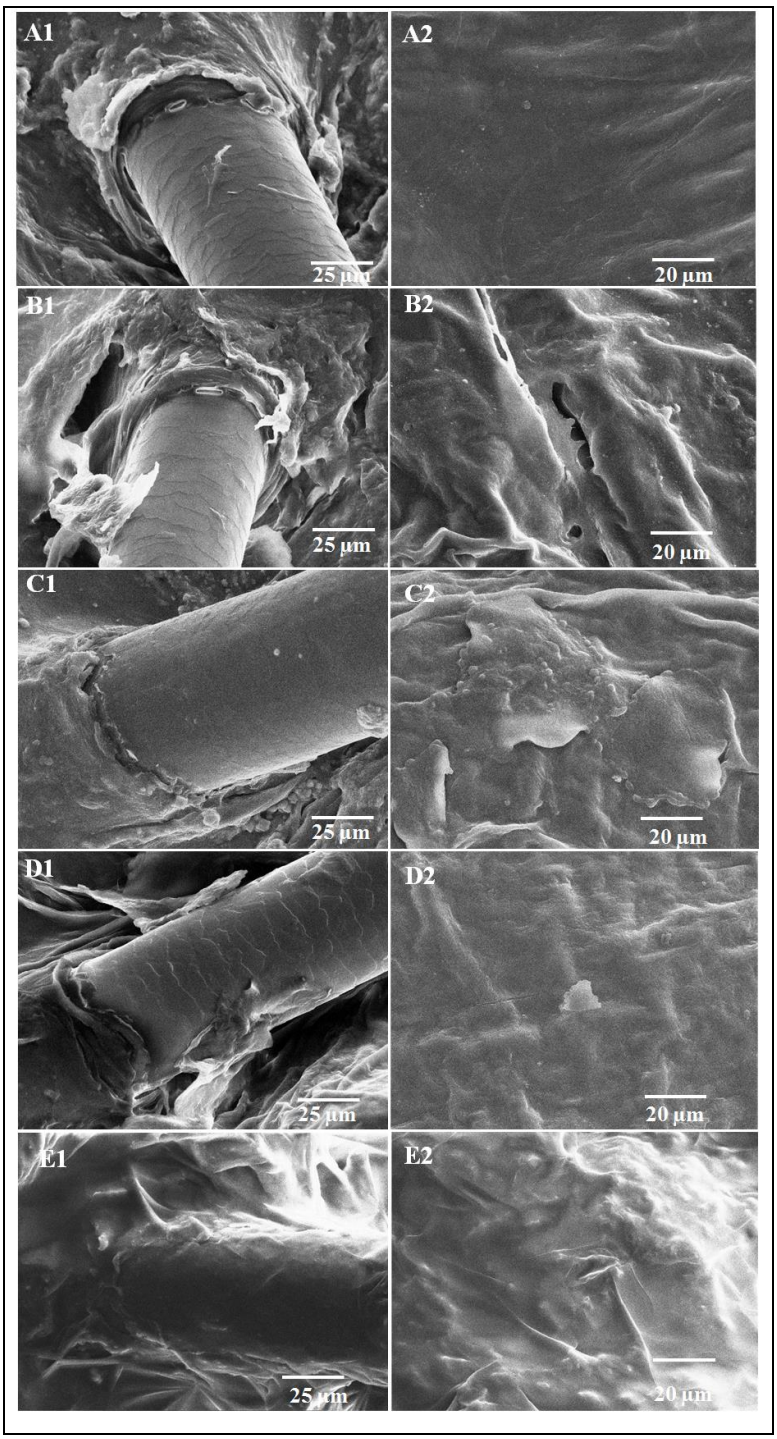

Figure 4.16 SEM images of the porcine skin surface at (1) the follicular region (original magnification × 400) and (2) nonfollicular region (original magnification × 500): control (PBS) without SN (A) and with SN (B), CL with SN (C), NI with SN (D), and SLN with SN (E).

With SN, the skin permeation of NaFI of PL-LI was higher than other formulations. However, SN significantly reduced the skin penetration of NaFI from PL-LI. The combination of all liposome formulations with SN showed small corneocytes lifting (Figure 4.17), indicating that the lipid membrane of liposomes could fill and cover the skin damage. Although liposomes can repair the skin damage, the combination of using a chemical penetration enhancer (d-limonene) in liposomal formulation (PL-LI) and SN exhibited a greater disruption of the skin stratum corneum, so some part of skin damage could not be repaired by liposomes (Vyas, 1995, Essa, 2003).

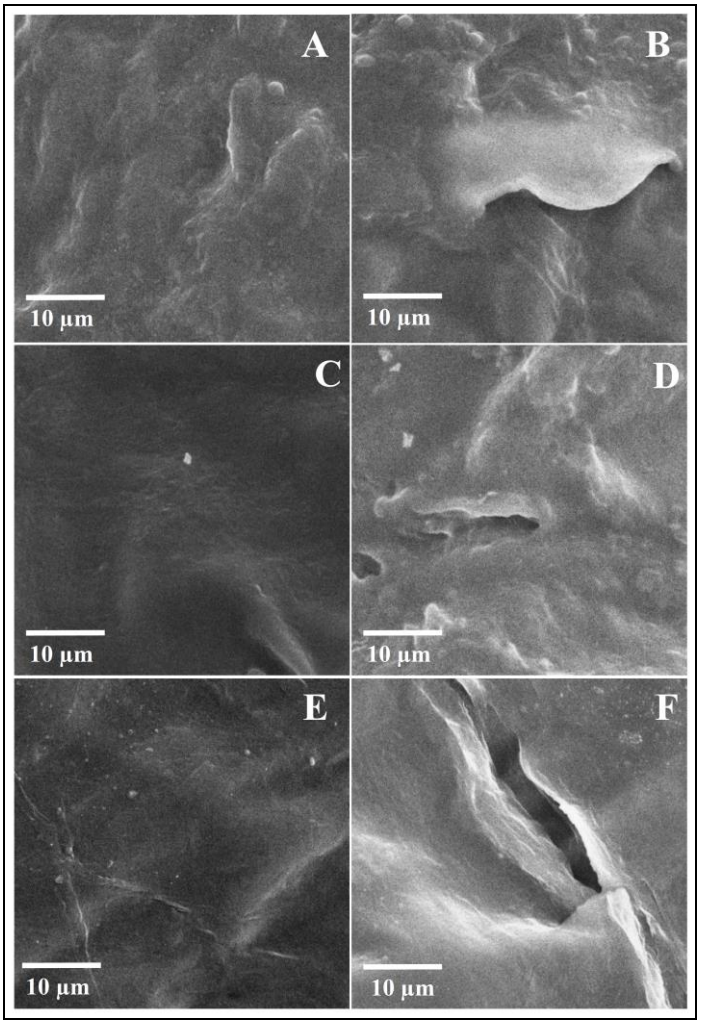

Figure 4.17 SEM images of porcine skin surface at nonfollicular region (original magnification 1000x): CL without (A) and with SN (B), PL without (C) and with SN (D), and PL-LI without (E) and with SN (F).

Figure 4.18 shows scanning electron micrographs of the skin surface view at the follicular region of CL, PL and PL-LI with and without SN. In the absence of SN, only PL-LI were clearly found to be deposited on the top of hair follicles, covering hair follicle orifices (Figure 34 (G), white arrow), indicating the follicular route was a major penetration route. Therefore, SN provided lower amount of NaFI permeated through the skin than without SN because the ultrasound changes the ultrastructure of the stratum corneum by dislocating the top layer of corneocytes (Sarheed and Abdul Rasool, 2011). Moreover, the hair follicles have a very tiny fraction (≤0.1% approximately) of the total skin surface area; therefore, a large number of detached corneocytes might partially slough off the hair follicle opening (Sarheed and Frum, 2012), closing the main penetration pathway of NaFI-loaded-PL-LI. Therefore, ultrasound energy altering the ultrastructure of stratum corneum might reduce the absorption of NaFI and PL-LI by closing the main penetration pathway of these carriers.

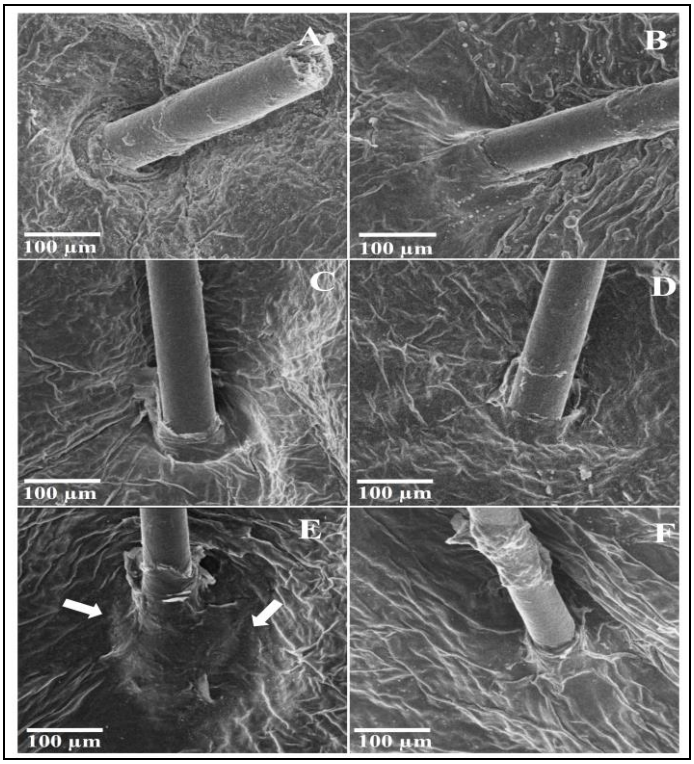

Figure 4.18 SEM images of porcine skin surface at follicular region (original magnification 120x): CL without (A) and with SN (B), PL without (C) and with SN (D), and PL-LI without (E) and with SN (F).

4.4.3 Follicular penetration pathway of d-limonene-containing PEGylated nanocarriers

The NaFI permeated through skin of PL-LI was higher than other formulations. SN had significantly effect on the skin penetration of this formulation. The cross section image from CLSM showed brighter fluorescence intensity of NaFI deposit in the skin, especially along the length of hair follicle, than other formulations. Therefore, selectively block hair follicle technique was used to confirm the penetration pathway of PL-LI. According to Lasic (1998), the delivery of the substances into the skin primarily occurs by two routes, the transfollicular route and the transepidermal routes (intercellular and intracellular penetration). Therefore, the blocked hair follicles skin presented only the transepidermal route. The difference in permeated flux between the open hair follicles skin (both transfollicular and transepidermal route) and the blocked hair follicles skin (only transepidermal route) was a permeated flux of transfollicular route (Manosroi et al., 2012). For comparison of the blocked and open hair follicles skin, the cumulative amount and the flux of NaFI-loaded PL-LI between with SN and without SN were evaluated (Figure 4.19). In the blocked hair follicles skins, the flux of NaFI showed small value and seemed to be no significant difference between that NaFI-loaded PL-LI with and without SN, indicating that NaFI-loaded PL-LI may transport via the transfollicular pathway.

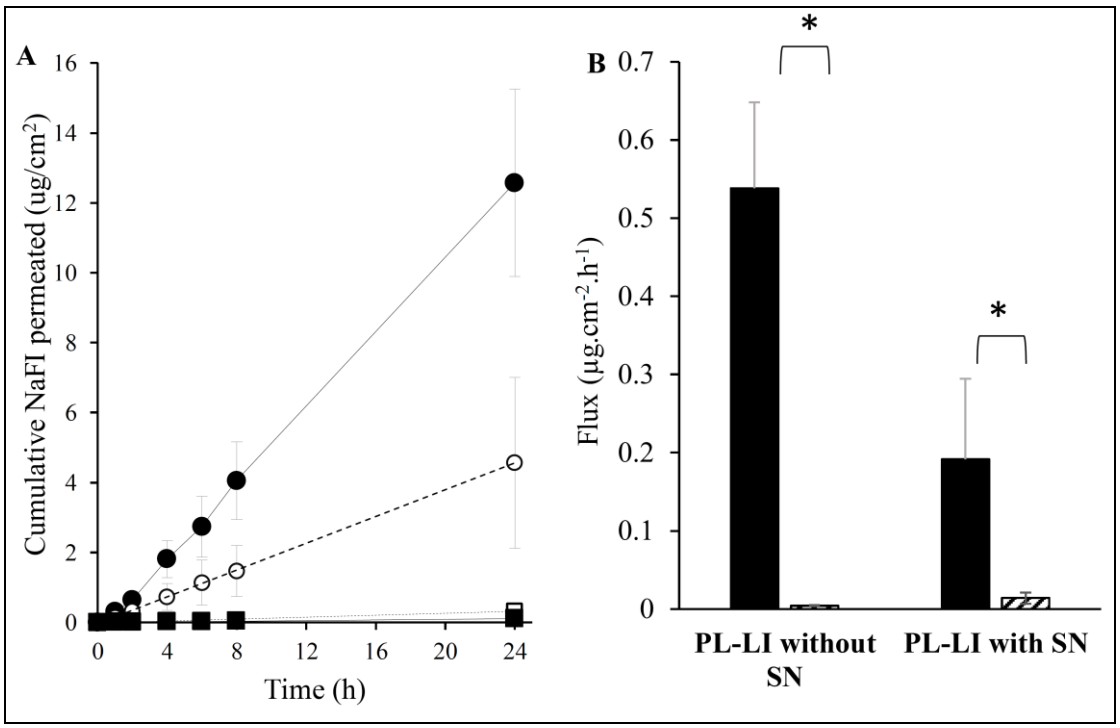

Figure 4.19 (A) The cumulative amount and time profiles of NaFI-loaded PL-LI permeated through blocked hair follicles skin (with SN (---□---) and without SN (—■—)) and open hair follicles skin (with SN (---○---) and without SN (—●—)). (B) Comparison of NaFI flux (µg.cm^{-2} .h^{-1}) of NaFI-loaded PL-LI permeated through blocked hair follicles skin (▨) and open hair follicles skin (■). Each value represents the mean ± S.D. (n=3). *indicates significantly different from other groups ($p < 0.05$).

PL-LI without SN significantly exhibited higher cumulative amounts of NaFI than those with SN. PL-LI might have a transfollicular pathway as a major pathway and an intercellular and intracellular pathways as a minor pathways. Using ultrasound leads to changes in the corneocyte layers at the uppermost layer of skin. The opening up of the continuous surface together with partially sloughing off of the hair follicle orifices referred to reduce the absorption of drug through the follicular route (Sarheed and Frum, 2012, Alvarez-Roman et al, 2003). Therefore, PL-LI had a higher passive permeability than SN. While the flux of NaFI solution treated with SN and without SN was not significantly different between the open and blocked hair follicle skin (data not shown), suggesting a transepidermal route as a major route.

To confirm these result, CLSM images were used to evaluate in term of semi-quantitative fluorescence intensity of NaFI and Rh-PE-probes in phospholipid membranes at the different skin penetration depths of follicular and nonfollicular region. The fluorescent compound from PL-LI could penetrate into deeper skin layers with higher fluorescence intensity at a given depth both nonfollicular and follicular regions than from PL and CL (data not shown). The skin depth of maximum NaFI and Rh-PE intensity in the nonfollicular regions was 40 μm, while in the follicular region was 60 and 55 μm for NaFI and Rh-PE intensity, respectively (Figure 4.20). Follicular region showed higher fluorescence intensity and deeper penetration of NaFI than nonfollicular regions, while Rh-PE showed higher fluorescent intensity in nonfollicular than follicular regions. Rh-PE was used as a fluorescence dye to probe phospholipid vesicles, so higher fluorescence intensity in nonfollicular regions indicated better permeation through the stratum corneum than in follicular regions. The high fluorescence intensity for both NaFI and Rh-PE suggested the co-migration of the phospholipid vesicle and entrapped NaFI transport through the stratum corneum. Subongkot et al. (2013) suggested that liposome vesicles may attach to some part of the skin (i.e., surface or hair follicles) before releasing the entrapped drug. After released, hydrophilic drugs are transported through pores in the stratum corneum lipid bilayer and through hair follicles and sweat ducts by the shunt pathway. In case of CL and PL, there was no difference in the fluorescence intensity of NaFI or Rh-PE between follicular and nonfollicular regions. All niosome and SLN formulation had a little bit different in the fluorescence intensity and skin depths (data not shown). Moreover, deformable liposomes and ethosomes improved skin delivery (permeation and deposition) of the model hydrophilic drug ketotifen fumarate, with greater improvement of deposition than permeation (Elsayed et al, 2006).

For the effect of SN, PL-LI with SN showed lower fluorescence intensity at the same skin layer and lower skin penetration depths than those without SN, however, Rh-PE in the nonfollicular region was the same intensity of PL-LI without SN. In this result, at follicular and nonfollicular region seemed to be the same fluorescence intensity value, suggesting that follicular region might not be the main penetration pathway of PL-LI with SN.

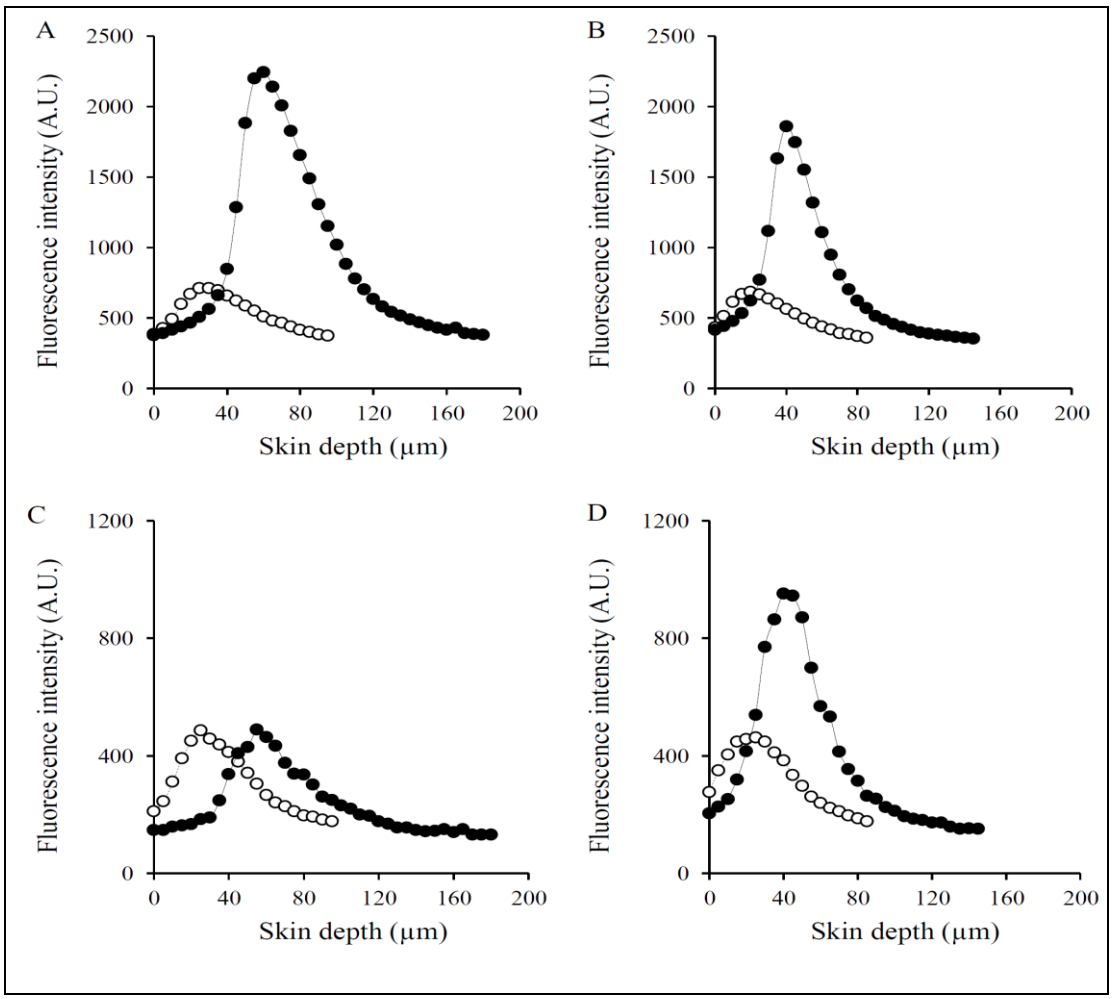

Figure 4.20 Fluorescence intensity profile of (A) NaFI in follicular region, (B) NaFI in nonfollicular region, (C) Rh-PE in follicular region, and (D) Rh-PE in nonfollicular region from PL-LI (with SN (---o---) and without SN (—●—)).

Xz axis serial images from CLSM (Figure 4.21) showed the different penetration depths of NaFI and Rh-PE from PL-LI. In follicular regions, PL-LI penetrated deeper (180 μm) than in nonfollicular regions (145 μm). The penetration pathway of ultradeformable liposomes with d-limonene was reported to be transfollicular rather than the intercellular or transcellular pathways (Subongkot et al, 2013). Therefore, three possible mechanisms may improve the skin delivery of PEGylated liposomes with terpenes. Firstly, deformable vesicles might act as drug carriers, whereby intact vesicles enter the stratum corneum carrying vesicle-bound drugs into the skin. Secondly, surfactant-based elastic vesicles might act as

penetration enhancers, whereby vesicle bilayers enter the stratum corneum and modify intercellular lipid lamellae. So, free drug molecules would be facilitated into and across the stratum corneum (Honeywell-Nguyen and Bouwstra, 2005). And thirdly, water-binding PEG molecules might increase the skin hydration. Maitani et al (2012) reported that PEG layers covered and extended the fluorescence of laurdan (a hydrophilic probe) in the head groups of OH in cholesterol molecules, indicating that the grafting of PEG onto liposomes increased the hydration at the surface. The permeability of skin depended on changing in the water gradient, which the hydration-induced structural alterations in stratum corneum lipids and/or corneocytes showed the swelling of the stratum corneum referring to reduce the effective solubility of nonpolar drugs in the membrane (Bjorklund et al., 2010).

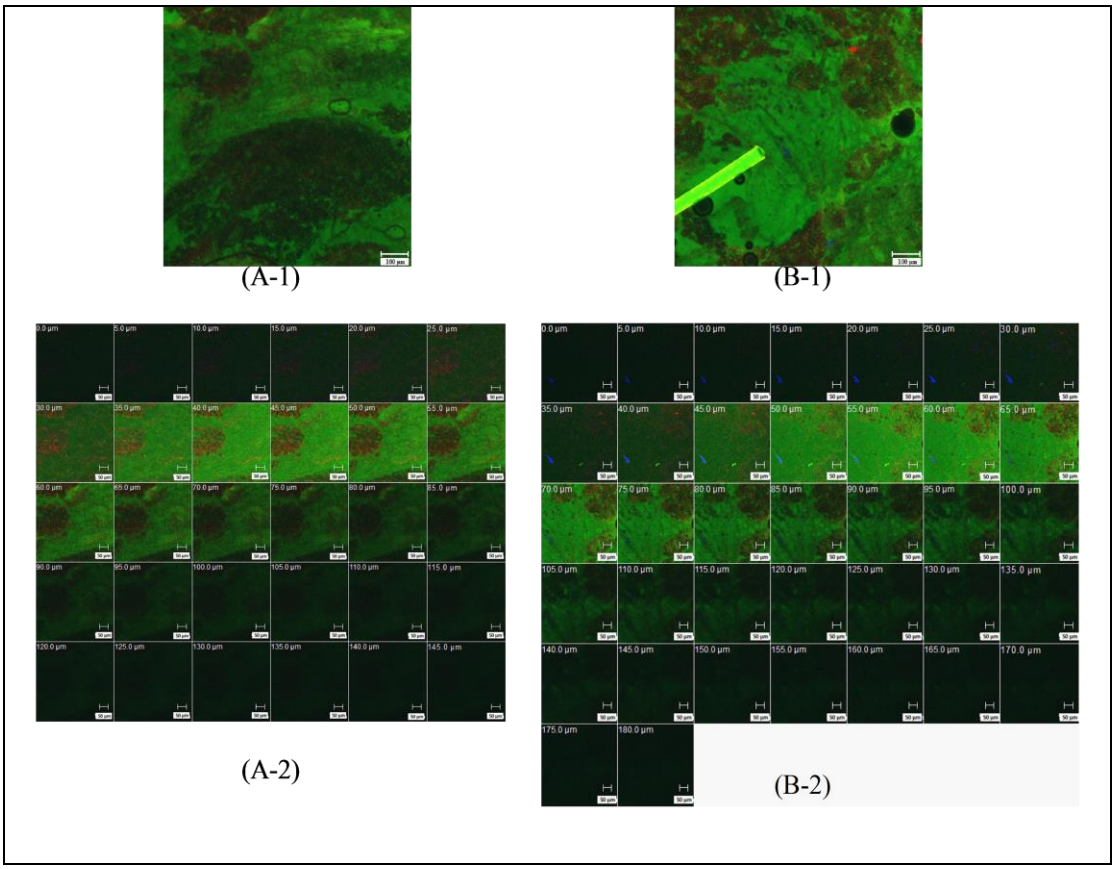

Figure 4.21 CLSM images of porcine skin treated with NaFI-loaded Rh-PE-probed PL-LI at a time of 4 h shows: xy plane image (10x objective lens) at (A-1) nonfollicular region and (B-1) follicular region, and x-z axis serial images (20x objective lens) at (A-2) nonfollicular region and (B-2)

follicular region. The images show green fluorescence of NaFI, red fluorescence of Rh-PE, and blue autofluorescence of skin.

4.4.4 Stratum corneum modification

To investigate the greatest enhancing mechanism of PL-LI on the modifying stratum corneum barrier, FTIR was used to evaluate. The stratum corneum sheets treated with different liposome formulations both with and without SN were determined as shown in Figure 4.22. The asymmetric and symmetric stretching modes of the terminal methylene groups (near 2920 and 2850 cm^{-1}, respectively) represent the lipid component in the stratum corneum (ceramides, phospholipids, etc.). An increase/decrease in the band position of these signals provided the specific information about the interior composition of the lipid bilayer. CH_2 scissoring vibration (1466.2 and 1457.3 cm^{-1}) provides information about the lateral packing of the lipid alkyl chains in the stratum corneum that the spilt of the band width around 10 cm^{-1}indicates a high content of the orthorhombic phase. Amide I ($C{=}O$) vibration (1640 cm^{-1}), amide II (C–N) vibration (1540 cm^{-1}), and fatty acids (1740 cm^{-1}) were also investigated. Additionally, the height intensity of the bands represent the amount of lipid and proteins in the stratum corneum. Any change in the peak intensity suggests the extraction or strengthening of the lipid stratum corneum (Panchagnula et al., 2001, Mendelsohn et al., 2003, Boncheva et al., 2008, Kaushik et al., 2010, Obata et al., 2010, and Hasanovic et al., 2011).

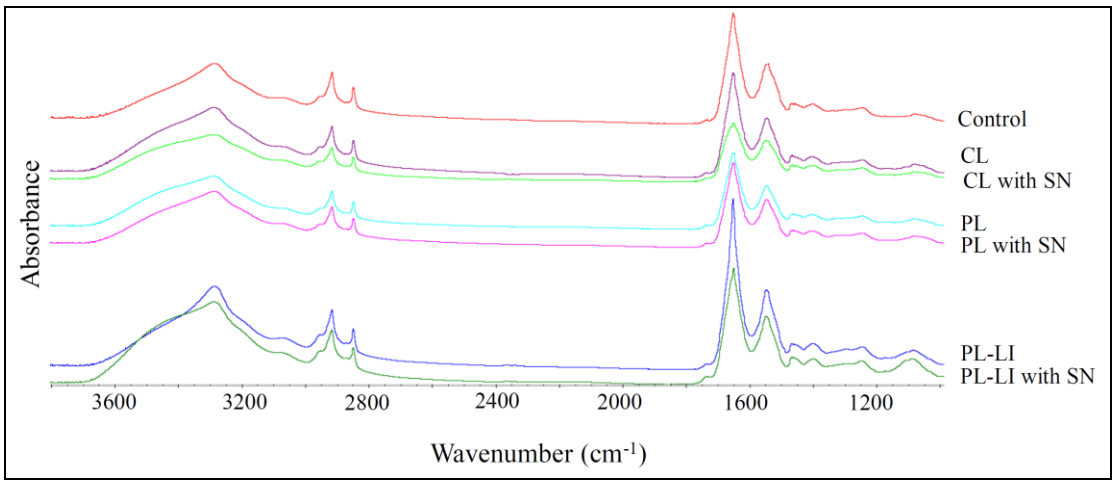

Figure 4.22 FTIR spectra of the stratum corneum from porcine skin after being treated with the different liposome formulation with and without SN compared to control (untreated stratum corneum) at room temperature.

4.4.4.1 Skin hydration study by FTIR spectroscopy

FTIR spectroscopy was used to determine changes in hydration of the stratum corneum. The intensity ratio of the amide I /amide II band is called as the moisture factor, and hydration increases the ratio between amide-I and amide-II peaks in FTIR (Shah et al., 2008). Figure 4.23 shows the intensity ratio of the amide I (~ 1652.3 cm^{-1}) /amide II (~1541.8 cm^{-1}) band in FTIR spectra of different liposome formulations. PL-LI showed higher intensity ratio than PL2 and CL, respectively, suggesting that d-limonene could increase the skin hydration by forming new polar pathways. The stranger intermolecular hydrogen bonding of ceramide amide group was broken by terpenes, leading to increased the breadth of existing polar pathway (Narishetty and Panchagnula, 2005). Moreover, grafting PEG onto liposome surface increased hydration of the stratum corneum, because the hydrophilic PEG molecule might have bound the water molecules to penetrate the skin.

However, only liposomes showed an enhancing effect by PEG. The modifying niosomes and SLN by PEG had a lower skin hydration level than SLN without PEG and PL2 (data not shown). Although cholesterol can act as emollients to fill in spaces between corneocytes on the skin surface and increase skin hydration (Wan, 2014), the steric stabilized barrier of PEG molecules around the niosome surfaces led to reduced the cholesterol released into the skin, resulting in reduced the

skin hydration and decreased the skin permeability (Knudsen et al., 2012). For SLN, the skin hydration depended on the occlusive factor by film formation on the skin surface. The grafting of PEG molecules onto SLN surfaces could prevent particle agglomeration by altering the surface hydrophobicity of the particles and inducing a hydrophilic steric barrier (Acar et al., 2005, Uner and Yener, 2007). The film formation on the skin surface and the skin hydration was decreased, and the skin penetration of entrapped drug from NIP and SLNP also decreased. Therefore, the skin hydration may be a factor affecting the skin penetration of NaFI in PEGylated liposomes and CL.

For the influence of SN, the intensity ratios were lower than those without SN, suggesting that SN might remove some fraction of the stratum corneum (Alvarez-Román et al., 2003). However, PL2 with SN treated the stratum corneum sheets showed higher intensity ratio than those without SN, indicating that the repairing sonicated skin by PEG liposomes might increase bounding of PEG molecule and water molecules, leading to increased hydration of the stratum corneum. PL-LI showed large different between with and without SN, suggesting that the combination of SN and d-limonene might remove the fraction of stratum corneum more than other condition.

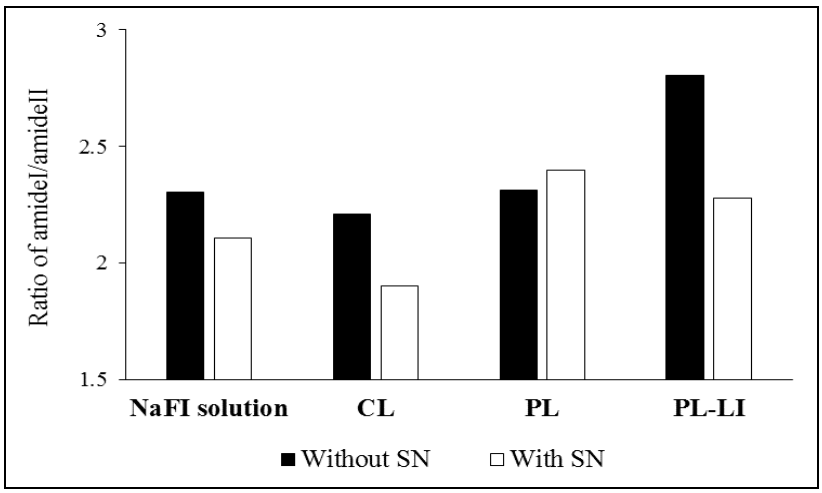

Figure 4.23 The ratio of the amide I /amide II band from FTIR spectra of the stratum corneum treated with different liposome formulations with and without SN.

4.4.4.2 Stratum corneum lipid organization change

As shown in Figure 4.22, all formulations showed no or little change in the band position of the CH_2 symmetric and asymmetric stretching and CH_2 scissoring vibration compared with untreated stratum corneum. However, the band intensity of CL and PL was lower than untreated stratum corneum, indicating that the stratum corneum lipids were extracted, leading to enhanced NaFI permeation through skin. While PL-LI showed the shifting of CH_2 asymmetric band position into higher wavenumber than PL, CL, and untreated stratum corneum, respectively, suggesting that terpene might disrupt the highly ordered lipid organization structure referring to partial disorder in the lipid alkyl chains (Narishetty and Panchagnula, 2005).

Applying with SN, PL-LI showed lower band intensity than PL-LI without SN, but no effect on the stratum corneum lipid ordering. The ultrasound energy may extract the membrane lipid from the stratum corneum. In the same time, the membrane bilayer of vesicles might fuse and repair the skin damage caused by SN. Alvarez-Román et al. (2003) reported that low-frequency SN significantly removed the intercellular lipid's fraction of the stratum corneum. The disruption of barrier properties led to increased the transportation of the hydrophilic via discrete permeabilized regions. Additionally, the indirect cavitational effect in solution that is the collapse of cavitation bubbles on the surface of skin might play an important role in enhancement of sonophoretic solute permeation (Ueda et al., 2009). Therefore, SN might discrete and remove some part of the stratum corneum sheet from the epidermis but no change of lipid organization.

4.4.4.3 Thermal phase transition of lipid organization in the stratum corneum

In order to determine the thermotropic response of the conformational ordering of the stratum corneum lipid tails, the CH_2 stretching depicted from 20 ˚C to 100 ˚C of stratum corneum was observed as shown in Figure 4.24. The stretching frequency was shifted into higher position when increasing the temperature. At the skin temperature (32 ˚C), the information about conformational order (trans-gauche isomerization) of the lipid alkyl chains are shown in Table 4.8. To clearly explain the effect of d-limonene on the intercellular lipid organization, the

different concentrations of d-limonene-containing liposome formulations were treated with the stratum corneum sheets. The symmetric and asymmetric CH_2 stretching bands were shifted to a significantly higher values when treated with PL-LI2%, PL-LI1%, PL, and CL, respectively, while SN treated stratum corneum showed a little shifted to a higher value. D-limonene containing liposomes significantly induced the disordering of the stratum corneum lipid organization and increased the fluidity of stratum corneum lipids. Moreover, the liposome with highest concentration of d-limonene significantly increased lipid organization change more than liposome without d-limonene. However, the result of CH_2 stretching depicted at 25 ˚C was not significant different among formulations, suggesting that the temperature influenced on the conformational ordering of the stratum corneum lipid.

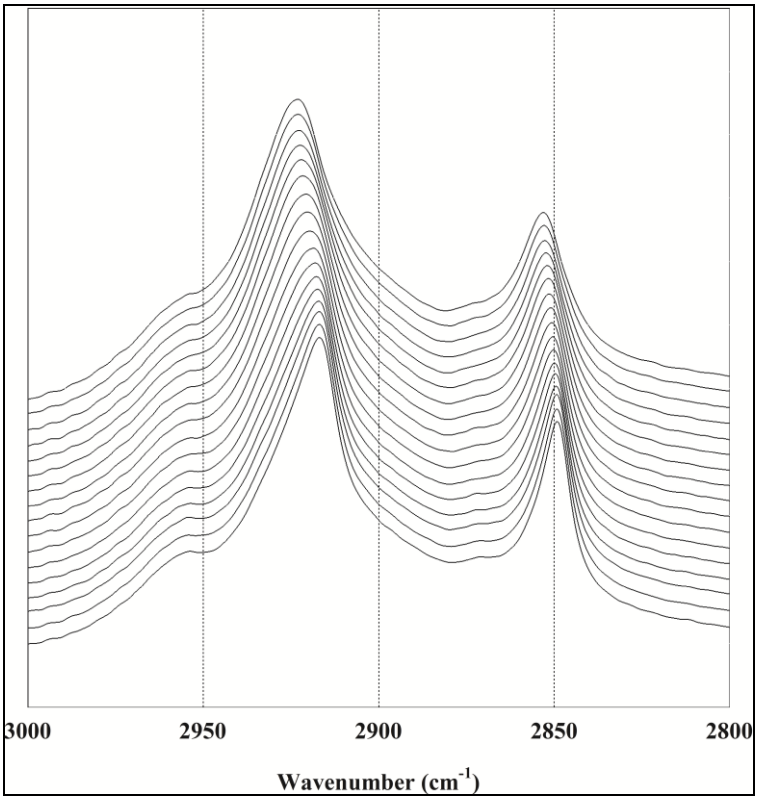

Figure 4.24 FTIR CH_2 asymmetric and symmetric spectra versus temperature of untreated stratum corneum. The temperature was in the range of 20 ˚C to 100 ˚C (top).

Table 4.8 Alterations on the CH_2 asymmetric and symmetric stretching absorbance shifts on the acyl chains of stratum corneum lipids at 32 ± 2 ˚C upon the application of different formulations. Mean ± S.D. (N=3). *significantly different from untreated stratum corneum ($p < 0.05$). **significantly different from PL ($p < 0.05$)

Formulation treated skin	**CH_2 asymmetric stretching**	**CH_2 symmetric stretching**
Untreated stratum corneum	2916.81	2849.15
SN treated stratum corneum	2917.13	2849.31
CL	2916.97	2849.31
PL	2917.77	2849.63
PL-LI1%	2918.25*	2849.95
PL-LI2%	2918.90*, **	2850.27*

As shown in Figure 4.25, the untreated stratum corneum showed the first stretching frequency shift from 2848.83 to 2851.07 cm^{-1} between 25 ˚C to 60 ˚C, indicating a transition from orthorhombic to hexagonal lateral packing, and the second shift to 2852.36 cm^{-1} at 80 ˚C, indicating the formation of a liquid phase (Groen et al., 2011). For the effect of SN on the stratum corneum lipid organization, no significant difference from untreated stratum corneum was observed. However, the stratum corneum treated with SN at the temperature from 45 ˚C to 100 ˚C showed lower CH_2 asymmetric peak value than untreated stratum corneum (Figure 4.25 (B)), suggesting that SN might increase the conformational ordering of the lipid bilayer. In this study, the stratum corneum area under the SN probe cannot be characterized due to the disruption of stratum corneum fraction after applying ultrasound energy, suggesting that SN might create the transportation route in the interlamellar water layer and decrease lipid bilayer thickness (Quinn and Wolf, 2009). Therefore, the skin permeability for hydrophilic molecules in solution was enhanced via an intracellular pathway. Moreover, the large aqueous channel might be created in the intercellular lipid of the stratum corneum area under the SN probe leading to dislocated and

removed the corneocytes in the stratum corneum (Morimoto et al., 2005, Sarheed and Abdul Rasool, 2011).

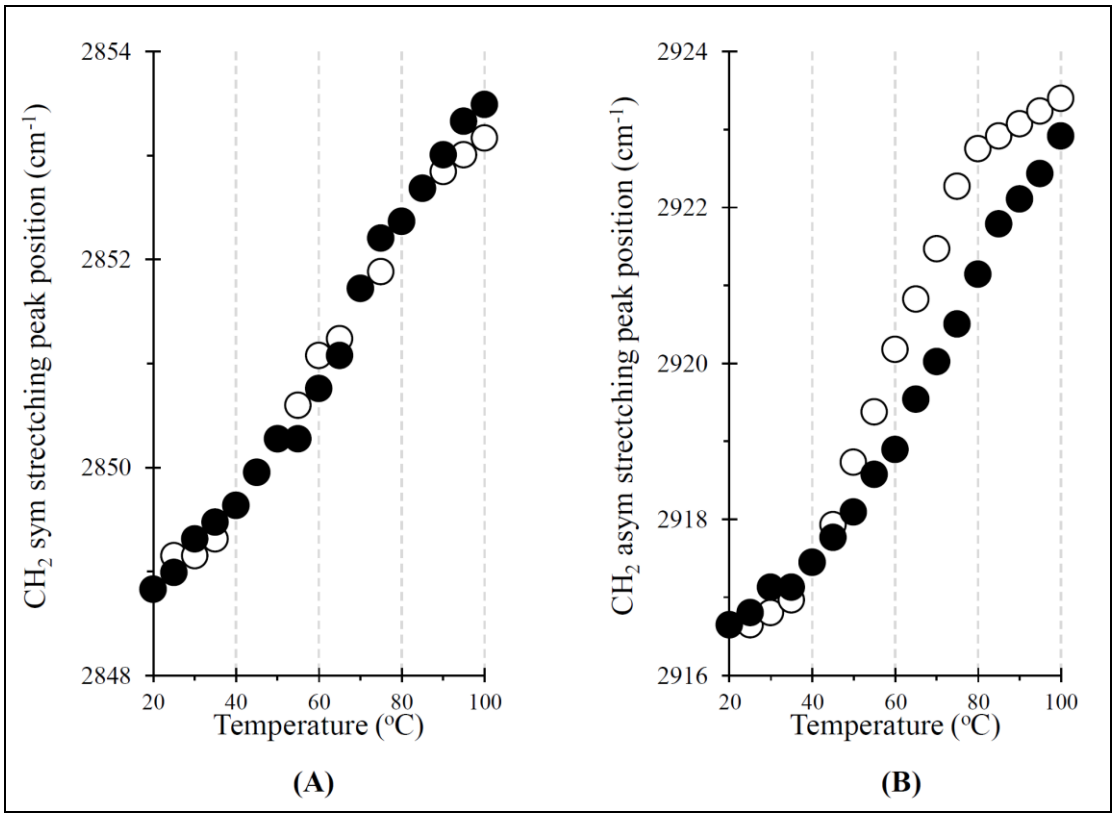

Figure 4.25 FTIR CH_2 symmetric (A) and asymmetric (B) stretching frequency versus temperature of stratum corneum treated with SN (•), compared with untreated stratum corneum (o).

For the effect of liposomes formulations on the phase transition of the stratum corneum, CH_2 asymmetric stretching peak position of all formulations was higher than untreated stratum corneum (Figure 4.26). CL showed no or little change from untreated stratum corneum, while PL exhibited higher shift than CL. PL provided the blue shift of CH_2 asymmetric stretching from 2917.29 to 2921.79 cm^{-1} between 25 ˚C to 45 ˚C for the first shift and to 2923.40 cm^{-1} at 65 ˚C for the second shift, indicating that the lower phase transition temperature with higher lamellar organization change than untreated stratum corneum.

The peak position shift of stratum corneum treated with d-limonene-containing PL formulations was higher than liposomes without d-limonene. PL-LI1%

provided the stretching peak position shift from 2917.45 to 2920.02 cm^{-1} between 20 ˚C and 35 ˚C for the first shift and to 2922.11 cm^{-1} at 50 ˚C for the second shift, while stratum corneum treated with PL-LI 2% showed the stretching peak position shift from 2917.29 to 2921.63 cm^{-1} between 20 ˚C and 40 ˚C for the first shift and to 2923.23 cm^{-1} at 50 ˚C for the second shift. This result indicated that d-limonene-containing PL induced stronger disorder of lipid lamellar structure with the lower phase transition temperature than those without limonene.

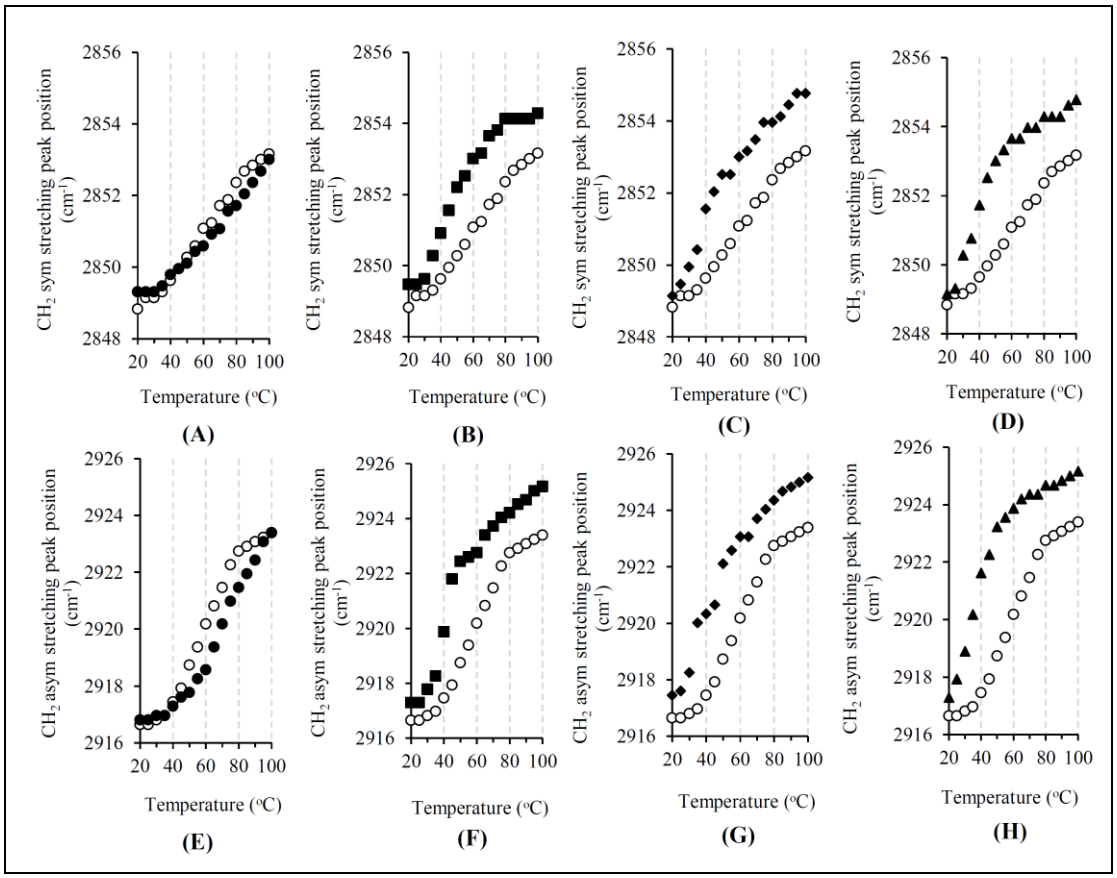

Figure 4.26 FTIR CH_2 symmetric and asymmetric stretching frequency versus temperature of stratum corneum treated with liposomes formulations: CL (●) (A and E), PL (■) (B and F), PL-LI 1% (♦) (C and G), and PL-LI 2% (▲) (D and H), compared with untreated stratum corneum (o).

To confirm the effect of liposome formulations on the lipid organization in the stratum corneum, DSC was used to determine thermal alteration in the stratum corneum as shown in Figure 4.27. The results correlated with phase

transition in the lipid lamellar-structures and other skin components modifications such as proteins or the interaction between lipid and these composition (Tanojo et al., 1999). The endothermic transitions between 20 and 100 ˚C have been used to identify the organization of stratum corneum lipid that the peak around 55-75 ˚C is associated with the melting of lipids chain portion buried within the bilayer structure. From the result, all formulations exhibited the endothermic peak around 63 ˚C, suggesting the destabilization of the lamellar phase at this temperature. However, the endothermic peak of stratum corneum treated with limonene-containing PL formulations was between 32 ˚C to 44 ˚C, while other samples had broad peak with higher temperature. This endothermic peak represented the lipid melting of the sebaceous lipids together with cholesterol side chain motion, attributing to a transition from solid lipids to a liquid ordered phase (Al-Saidan et al., 1998, Brief et al., 2009), so the clear endothermic peak of PL-LI 2% might be caused by a strong lipid organization change in the stratum corneum leading to increase the gross fluidity of stratum corneum lipid domain (Hashida and Yamashita, 2000, Ibrahim et al., 2010)

In this result, the greatest concentration of limonene-containing liposomes showed the strongest modification effect on the barrier function of the stratum corneum. According to Hatta et al. (2010), the structural change of intercellular lipid matrix after applying d-limonene has been reported by using synchrotron X-ray diffraction technique. D-limonene intercalated into hydrophobic region of intercellular lipid providing the swelling of the long lamellar structure and strongly disrupting the hexagonal hydrocarbon chain packing structure. The drastic change in the lamellar organization had a higher impact on the skin barrier function (Groen et al., 2011).

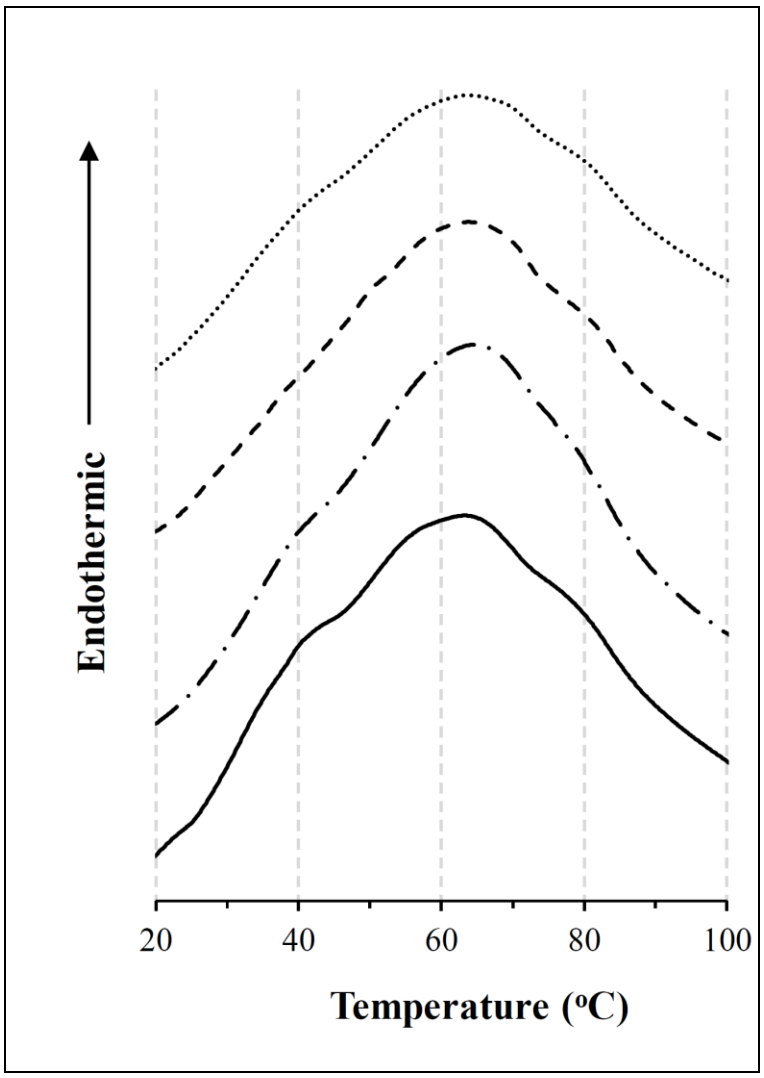

Figure 4.27 DSC Thermograms of stratum corneum treated with different formulations: untreated stratum corneum (·····), PL (– – –), PL-LI 1% (— · —), PL-LI 2% (———). (n=3)

In this study, d-limonene-containing liposomes formulations provided stronger effect on the skin permeation of NaFI than those without limonene. The possible penetration mechanism for enhancing transdermal delivery of these vesicles can be explained as follows; firstly, ultra-deformable vesicles induced by an edge activator (Tween 20) and d-limonene, whereby intact vesicles carrying vesicle-bound drugs passed through the stratum corneum. The smaller particle size of elastic vesicles can be partitioned through the channel-like regions of the startum corneum than larger one (Honeywell-Nguyen et al., 2002). Secondly, d-limonene is a chemical

penetration enhancer that can intercalate into stratum corneum intercellular lipids and increase lipid lamellae fluidity. Dragicevic-Curic et al. (2008) reported that some of the terpene-containing liposomes vesicles (invasomes) were fragmented during their penetration through the stratum corneum, while some of the small and deformable invasomes could penetrate to the deeper stratum corneum layers intact. Therefore, the released terpenes from some vesicles were localized into intercellular lipids of the stratum corneum barrier, leading to enhanced skin permeability of drug via an intercellular pathway (Hashida and Yamashita, 2000, Ibrahim et al., 2010).

CHAPTER 5
CONCLUSION

In this study, three types of lipid nanocarriers (liposomes, niosomes, and SLN) were successfully formulated for entrapped hydrophilic compound. The effect of PEG2000-DSPE and terpene in nanocarriers were evaluated in term of the physicochemical properties, morphology, and membrane fluidity of liposome vesicles. For the influence of using SN with lipid nanocarrier formulations on transdermal delivery of hydrophilic compound, *in vitro* skin permeation study was determined. The possible penetration mechanism was also clarified. It can be concluded as follows,

5.1 The influence of formulations on the physicochemical properties

All nanocarrier formulations showed small particle size in nanometer scale, spherical shape, and negative surface charge. The entrapped NaFI into SLN was higher than NI and CL, respectively. Liposome formulations with PEGylation had a significantly smaller size with higher %EE and %LE than non-PEGyted liposomes. As LI was added into the formulations, the particle size of nanocarriers decreased, but the NaFI entrapment efficiency increased. Moreover, the membrane fluidity of LI containing carriers was higher than those without LI.

5.2 The influence of using SN and nanocarrier formulations on the skin penetration of sodium fluorescein

SN significantly increased the NaFI flux of NaFI solution (51.1-fold enhancement), but it decreased the NaFI flux of almost lipid nanocarrier formulation. Although PL-LI had the highest NaFI penetrated into and through the skin, the NaFI penetration of the combination of SN with PL-LI was lower than NaFI solution and PL-LI without SN, respectively.

5.3 The mechanism of SN and nanocarrier formulations on skin penetration

Applying SN on the skin can disrupt the barrier properties of stratum corneum, leading to enhance the transportation of hydrophilic compound via discrete site. PL-LI enhanced NaFI transport via transfollicular and intercellular pathway due to the physicochemical properties of these vesicles and the effect of penetration enhancer on the disruption of intercellular lipid in the stratum corneum. After applying SN, both skin structure and lipid nanocarriers were affected. The sonicated skin were repaired by disrupted lipid nanocarriers, leading to decreased NaFI permeated through skin.

Our results led to the better understanding of the skin penetration mechanism of the combination of SN and different types of lipid nanocarrier system. The useful fundamental information can be utilized to develop the treatment condition for improving skin delivery of hydrophilic drug.

REFERENCES

Abdelkader, H., et al. (2014). "Recent advances in non-ionic surfactant vesicles (niosomes): self-assembly, fabrication, characterization, drug delivery applications and limitations." **Drug Delivery** 21, 2: 87 - 100.

Acar, H., et al. (2005). "Superparamagnetic nanoparticles stabilized by polimerized PEGylated coatings." **Journal of Magnetism and Magnetic Materials** 293: 1 - 7.

Aldwaikat, M., and Alarjah, M. (2015). "Investigating the sonophoresis effect on the permeation of diclofenac sodium using 3D skin equivalent." **Ultrasonics Sonochemistry** 22: 580 – 587.

Allen, T. M., et al. (1991). "Liposomes containing synthetic lipid derivatives of poly(ethylene glycol) show prolonged circulation half-lives in vivo." **Biochimica et Biophysica Acta** 1066, 1: 29 - 36.

Al-Saidan, S. M., et al. (1998). "Differential scanning calorimetry of human and animal stratum corneum membranes." **International journal of pharmaceutics** 168, 1: 17 - 22.

Alvarez-Román, R., et al. (2003). "Skin permeability enhancement by low frequency sonophoresis: lipid extraction and transport pathways." **Journal of Pharmaceutical Sciences** 92:1138 – 1146.

Alvarez-Román, R., et al. (2004). "Visualization of skin penetration using confocal laser scanning microscopy." **European Journal of Pharmaceutics and Biopharmaceutics** 58, 2: 301 - 316.

Ammar, H. O., et al. (2011). "Proniosomes as a carrier system for transdermal delivery of tenoxicam." **International Journal of Pharmaceutics** 405, 1-2: 142 - 152.

Andega, S., et al. (2001). "Comparison of the effect of fatty alcohols on the permeation of melatonin between porcine and human skin." **Journal of Controlled Release** 77, 1–2: 17 - 25.

Anigbogu, A. N. C., et al. (1995). "Fourier transform raman spectroscopy of interactions between the penetration enhancer dimethyl sulfoxide and human stratum corneum." **International Journal of Pharmaceutics** 125, 2: 265 - 282.

Azagury, A., et al. (2014). "Ultrasound mediated transdermal drug delivery." **Advanced Drug Delivery Reviews** 72: 127 - 143.

Badran, M., Shazly, G., and El-Badry, M. (2012). "Effect of terpene liposomes on the transdermal delivery of hydrophobic model drug, nimesulide: Characterization, stability and in vitro skin permeation." **African Journal of Pharmacy and Pharmacology** 6: 3018 - 3026.

Balakrishnan, P., et al. (2009). "Formulation and in vitro assessment of minoxidil niosomes for enhanced skin delivery." **International Journal of Pharmaceutics** 377, 1-2: 1 - 8.

Bariya, S. H., et al. (2012). "Microneedles: an emerging transdermal drug delivery system." **Journal of Pharmacy and Pharmacology** 64, 1: 11 - 29.

Baroli, B. (2010). "Penetration of nanoparticles and nanomaterials in the skin: fiction or reality?" **Journal of Pharmaceutical Sciences** 99, 1: 21 - 50.

Barry, B. W. (2001). "Novel mechanisms and devices to enable successful transdermal drug delivery." **European Journal of Pharmaceutical Sciences** 14, 2: 101-114.

Benson, H. A. (2005). 'Transdermal drug delivery: penetration enhancement techniques." **Current Drug Delivery** 2, 1: 23 - 33.

Bjorklund, S., et al. (2010). "A water gradient can be used to regulate drug transport across skin." **Journal of Controlled Release** 143, 2: 191 - 200.

Blume-Peytavi, U., et al. (2010). "Follicular and percutaneous penetration pathways of topically applied minoxidil foam." **European Journal of Pharmaceutics and Biopharmaceutics** 76, 3: 450 - 453.

Bocca, C., et al. (1998). "Phagocytic uptake of fluorescent stealth and non-stealth solid lipid nanoparticles." **International Journal of Pharmaceutics** 175, 2: 185 - 193.

Boncheva, M., et al. (2008). "Molecular organization of the lipid matrix in intact Stratum corneum using ATR-FTIR spectroscopy." **Biochimica et Biophysica Acta (BBA) - Biomembranes** 1778, 5: 1344 - 1355.

Boucaud, A., et al. (2001). "*In vitro* study of low-frequency ultrasound-enhanced transdermal transport of fentanyl and caffeine across human and hairless rat skin." **International Journal of Pharmaceutics** 228, 1 – 2: 69 – 77.

Bouwstra, J. A., et al. (2003). "Structure of the skin barrier and its modulation by vesicular formulations." **Progress in Lipid Research** 42, 1: 1 - 36.

Brief, E., et al. (2009). "Phase behavior of an equimolar mixture of N-palmitoyl-D-erythro-sphingosine, cholesterol, and palmitic acid, a mixture with optimized hydrophobic matching." **Langmuir** 25, 13: 7523 - 7532.

Brus, C., et al. (2002). "Distribution and quantification of polyethylenimine oligodeoxynucleotide complexes in human skin after iontophoretic delivery using confocal scanning laser microscopy." **Journal of Controlled Release** 84, 3: 171 - 181.

Cal, K., et al. (2001). "In vitro studies on penetration of terpenes from matrix-type transdermal systems through human skin." **International Journal of Pharmaceutics** 224, 1-2: 81 - 88.

Cameli, N., et al. (1994). "Expression of integrins in human nail matrix." **British Journal of Dermatology** 130, 5: 583 - 588.

Cevc, G. and Vierl, U. (2010). "Nanotechnology and the transdermal route: A state of the art review and critical appraisal." **Journal of Controlled Release** 141, 3: 277 - 299.

Cevc, G., and Blume, G. (1992). "Lipid vesicles penetrate into intact skin owing to the transdermal osmotic gradients and hydration force." **Biochimica et Biophysica Acta (BBA) - Biomembranes** 1104, 1: 226 – 232.

Cevc, G., Schätzlein, A., and Blume, G. (1995). "Transdermal drug carriers: Basic properties, optimization and transfer efficiency in the case of epicutaneously applied peptides." **Journal of Controlled Release** 36, 1 – 2: 3 - 16.

Chain, E., and Kemp, I. (1934). "The isoelectric points of lecithin and sphingomyelin." **Biochemical Journal** 28: 2052 -2055.

Chen, M., Liu, X., and Fahr, A. (2011). "Skin penetration and deposition of carboxyfluorescein and temoporfin from different lipid vesicular systems: In vitro study with finite and infinite dosage application." **International Journal of Pharmaceutics** 408, 1 – 2: 223 – 234.

Chen, Y., et al. (2014). "Novel chemical permeation enhancers for transdermal drug delivery." **Asian Journal of Pharmaceutical Sciences** 9, 2: 51 - 64.

Cornwell, P. A. and Barry, B. W. (1994). "Sesquiterpene components of volatile oils as skin penetration enhancers for the hydrophilic permeant 5-fluorouracil." **Journal of Pharmacy and Pharmacology** 46, 4: 261 - 269.

Dahlan, A., Alpar, H.O., and Murdan, S. (2009). "An investigation into the combination of low frequency ultrasound and liposomes on skin permeability." **International Journal of Pharmaceutics** 379, 1: 139 – 142.

Dayan, N. and Touitou, E. (2000). "Carriers for skin delivery of trihexyphenidyl HCl: ethosomes vs. liposomes." **Biomaterials**. 21, 18: 1879 - 1885.

de Leeuw, J., et al. (2009). "Liposomes in dermatology today." **Journal of the European Academy of Dermatology and Venereology** 23, 5: 505 - 516.

De Rosa, F. S., et al. (2000). "A vehicle for photodynamic therapy of skin cancer: influence of dimethylsulphoxide on 5-aminolevulinic acid in vitro cutaneous permeation and in vivo protoporphyrin IX accumulation determined by confocal microscopy." **Journal of Controlled Release** 65, 3: 359 - 366.

Denet, A. R., et al. (2004). "Skin electroporation for transdermal and topical delivery." **Advanced Drug Delivery Reviews** 56, 5: 659 - 674.

Donnelly, R. F., et al. (2014). "Microneedle-iontophoresis combinations for enhanced transdermal drug delivery." **Methods in Molecular Biology** 1141: 121 - 132.

Dragicevic-Curic, N., et al. (2008). "Temoporfin-loaded invasomes: development, characterization and in vitro skin penetration studies." **Journal of Controlled Release** 127, 1: 59 - 69.

Dubey, V., Mishra, D., and Jain, N. K. (2007). "Melatonin loaded ethanolic liposomes: Physicochemical characterization and enhanced transdermal delivery." **European Journal of Pharmaceutics and Biopharmaceutics** 67, 2: 398 - 405.

El Maghraby, G. M., Barry, B. W., and Williams, A. C. (2008). "Liposomes and skin: From drug delivery to model membranes." **European Journal of Pharmaceutical Sciences** 34, 4 – 5: 203 - 222.

El Maghraby, G. M., Campbell, M., and Finnin, B.C. (2005). "Mechanisms of action of novel skin penetration enhancers: Phospholipid versus skin lipid

liposomes." **International Journal of Pharmaceutics** 305, 1 – 2: 90 - 104.

El Maghraby, G. M., Williams, A. C., and Barry, B. W. (1999). "Skin delivery of oestradiol from deformable and traditional liposomes: mechanistic studies." **Journal of Pharmacy and Pharmacology** 51, 10: 1123 - 1134.

El Maghraby, G. M., Williams, A. C., and Barry, B. W. et al. (2000). "Skin delivery of oestradiol from lipid vesicles: importance of liposome structure." **International Journal of Pharmaceutics** 204(1–2): 159-169.

El Maghraby, G. M., Williams, A. C., Barry, B. W. (2006). "Can drug-bearing liposomes penetrate intact skin?" **Journal of Pharmacy and Pharmacology** 58, 4: 415 - 429.

El-Laithy, H. M., et al. (2011). "Novel sugar esters proniosomes for transdermal delivery of vinpocetine: preclinical and clinical studies." **European Journal of Pharmaceutics and Biopharmaceutics** 77, 1: 43 - 55.

Elsayed, M. M. A., et al. (2006). "Deformable liposomes and ethosomes: Mechanism of enhanced skin delivery." **International Journal of Pharmaceutics** 322, 1 – 2: 60 – 66.

Elsayed, M. M., et al. (2007). "Deformable liposomes and ethosomes as carriers for skin delivery of ketotifen." **Pharmazie** 62, 2: 133 - 137.

Escobar-Chávez, J. J., et al. (2008). "The tape-stripping technique as a method for drug quantification in skin." **Journal of Pharmaceutical Sciences** 11: 104 – 130.

Esposito, E., Menegatti, E., and Cortesi, R. (2004). "Ethosomes and liposomes as topical vehicles for azelaic acid: a preformulation study." **Journal of Cosmetic Science** 55, 3: 253 - 264.

Fang, J. Y., et al. (2001). "In vitro skin permeation of estradiol from various proniosome formulations." **International Journal of Pharmaceutics** 215, 1–2: 91 - 99.

Fang, J. Y., et al. (2002). "Transdermal iontophoresis of sodium nonivamide acetate: V. Combined effect of physical enhancement methods." **International Journal of Pharmaceutics** 235, 1 – 2: 95 – 105.

Fang, J. Y., et al. (2004). "Enhancement of topical 5-aminolaevulinic acid delivery by erbium:YAG laser and microdermabrasion: a comparison with iontophoresis and electroporation." **British Journal of Dermatology** 151, 1: 132 - 140.

Franz, T. J. (1983). "Kinetics of cutaneous drug penetration." **International Journal of Dermatology** 22, 9: 499 - 505.

Friend, D., et al. (1988). "Transdermal delivery of levonorgestrel I: Alkanols as permeation enhancers in vitro." **Journal of Controlled Release** 7, 3: 243 - 250.

Funke, A. P., et al. (2002). "Transdermal delivery of highly lipophilic drugs: in vitro fluxes of antiestrogens, permeation enhancers, and solvents from liquid formulations." **Pharmaceutical Research** 19, 5: 661 - 668.

Ganesan, M. G., et al. (1984). "Influence of liposomal drug entrapment on percutaneous absorption." **International journal of pharmaceutics** 20, 1–2: 139 - 154.

Garbuzenko, O., et al. (2005). "Effect of grafted PEG on liposome size and on compressibility and packing of lipid bilayer." **Chemistry and Physics of Lipids** 135, 2: 117 - 129.

Gennes, P. G. (1980). "Conformations of Polymers Attached to an Interface." **Macromolecules** 13, 5: 1069 - 1075.

Gloor, M., et al. (2001). "Clinical effect of salicylic acid and high dose urea applied according to the standardized New German Formulary." **Pharmazie** 56, 10: 810 - 814.

Golden, G. M., et al. (1986). "Lipid thermotropic transitions in human stratum corneum." **Journal of Investigative Dermatology** 86, 3: 255 - 259.

Grams, Y. Y. (2005). "Influence of molecular properties and delivery system design on the transfollicular transport across the skin". Division of Drug Delivery Technology of the Leiden/Amsterdam Center for Drug Research: Leiden University.

Groen, D., et al. (2011). "Is an orthorhombic lateral packing and a proper lamellar organization important for the skin barrier function?" **Biochimica et Biophysica Acta** 1808, 6: 1529 - 1537.

Guo, L., et al. (2013). "Enhanced transcutaneous immunization via dissolving microneedle array loaded with liposome encapsulated antigen and adjuvant." **International Journal of Pharmaceutics** 447, 1 – 2: 22 – 30.

Han, I., Kim, M., and Kim, J. (2004). "Enhanced transfollicular delivery of adriamycin with a liposome and iontophoresis." **Experimental Dermatology** 13, 2: 86 - 92.

Harivardhan Reddy, L., et al. (2005). "Influence of administration route on tumor uptake and biodistribution of etoposide loaded solid lipid nanoparticles in Dalton's lymphoma tumor bearing mice." **Journal of Controlled Release** 105, 3: 185 - 198.

Hasanovic, A., et al. (2011). "Modification of the conformational skin structure by treatment with liposomal formulations and its correlation to the penetration depth of aciclovir." **European Journal of Pharmaceutics and Biopharmaceutics** 79, 1: 76 - 81.

Hashida, M. and Yamashita, F. (2000). "Terpenes as penetration enhancers." **Percutaneous penetration enhancers**, United states, CRC Press LLC: 309 – 320

Helgason, T., et al. (2009). "Effect of surfactant surface coverage on formation of solid lipid nanoparticles (SLN)." **Journal of Colloid and Interface Science** 334, 1: 75 - 81.

Herwadkar, A., et al. (2012). "Low frequency sonophoresis mediated transdermal and intradermal delivery of ketoprofen." **International Journal of Pharmaceutics** 423, 2: 289 – 296.

Heurtault, B., et al. (2003). "Physico-chemical stability of colloidal lipid particles." **Biomaterials** 24, 23: 4283 - 4300.

Hofland, H. E., et al. (1995). "Interactions between liposomes and human stratum corneum in vitro: freeze fracture electron microscopical visualization and small angle X-ray scattering studies." **British Journal of Dermatology** 132, 6: 853 - 866.

Honeywell-Nguyen, P. L. and Bouwstra, J. A. (2005). "Vesicles as a tool for transdermal and dermal delivery." **Drug Discovery Today: Technologies** 2, 1: 67 - 74.

Honeywell-Nguyen, P. L., Arenja, S., and Bouwstra, J. A.. (2003). "Skin penetration and mechanisms of action in the delivery of the D2-agonist rotigotine from surfactant-based elastic vesicle formulations." **Pharmaceutical Research** 20, 10: 1619 - 1625.

Honeywell-Nguyen, P. L., et al. (2002). "The in vivo and in vitro interactions of elastic and rigid vesicles with human skin." **Biochimica et Biophysica Acta** 1573, 2: 130 - 140.

Hong, M., et al. (2009). "Efficient tumor targeting of hydroxycamptothecin loaded PEGylated niosomes modified with transferrin." **Journal of Controlled Release** 133, 2: 96 - 102.

Hoogstraate, A. J., et al. (1991). "Kinetics, ultrastructural aspects and molecular modelling of transdermal peptide flux enhancement by N-alkylazacycloheptanones." **International Journal of Pharmaceutics** 76, 1–2: 37 - 47.

Horwitz, E., et al. (1999). "A clinical evaluation of a novel liposomal carrier for acyclovir in the topical treatment of recurrent herpes labialis." **Oral Surgery, Oral Medicine, Oral Pathology, Oral Radiology, and Endodontology** 87, 6: 700 – 705.

Ibrahim, S.A., and Li, S.K. (2010). "Chemical enhancer solubility in human stratum corneum lipids and enhancer mechanism of action on stratum corneum lipid domain." **International Journal of Pharmaceutics** 383, 1 – 2: 89 – 98.

Immordino, M.L., Dosio, F., and Cattel, L. (2006). "Stealth liposomes: review of the basic science, rationale, and clinical applications, existing and potential." **International Journal of Nanomedicines** 1, 3: 297 – 315.

Ita, K. (2015). "Recent progress in transdermal sonophoresis." **Pharmaceutical Development and Technology** (Published online) 1 - 9.

Jain, A. K., Thomas, N. S., and Panchagnula, R. (2002). "Transdermal drug delivery of imipramine hydrochloride.: I. Effect of terpenes." **Journal of Controlled Release** 79, 1 – 3: 93 - 101.

Jain, S., et al. (2003). "Transfersomes--a novel vesicular carrier for enhanced transdermal delivery: development, characterization, and performance

evaluation." **Drug Development and Industrial Pharmacy** 29(9): 1013 - 1026.

Jain, S., et al. (2004). "Ethosomes : A Novel Vesicular Carrier For Enhanced Transdermal Delivery Of An AntiHIV Agent." **Indian Journal of Pharmaceutical Sciences** 66, 1: 72 - 81.

Jain, S., Tiwary, A., and Jain, N. (2008). "PEGylated elastic liposomal formulation for lymphatic targeting of zidovudin." **Current Drug Delivery** 5: 275 – 281.

Johnson, M. E., et al. (1996). "Synergistic effects of chemical enhancers and therapeutic ultrasound on transdermal drug delivery." **Journal of Pharmaceutical Sciences** 85, 7: 670 - 679.

Junyaprasert, V. B., et al. (2012). "Physicochemical properties and skin permeation of Span 60/Tween 60 niosomes of ellagic acid." **International Journal of Pharmaceutics** 423, 2: 303 - 311.

Kakadia, P. G. and Conway, B. R. (2014). "Solid Lipid Nanoparticles: A Potential Approach for Dermal Drug Delivery." **American Journal of Pharmacological Sciences**. 2, 5A: 1 - 7.

Kalluri, H., and Banga, A.K. (2011). "Transdermal Delivery of Proteins." **AAPS PharmSciTech** 12: 431 – 441.

Kang, L., et al. (2000). "Physicochemical studies of lidocaine-menthol binary systems for enhanced membrane transport." **International journal of pharmaceutics** 206, 1-2: 35 - 42.

Karande, P., and Mitragotri, S. (2009). "Enhancement of transdermal drug delivery via synergistic action of chemicals." **Biochimica et Biophysica Acta (BBA) - Biomembranes** 1788, 11: 2362 – 2373.

Kato, A., Ishibashi, Y., and Miyake, Y. (1987). "Effect of egg yolk lecithin on transdermal delivery of bunazosin hydrochloride." **Journal of Pharmacy and Pharmacology** 39, 5: 399 - 400.

Kaushik, D. and Michniak-Kohn, B. (2010). "Percutaneous Penetration Modifiers and Formulation Effects: Thermal and Spectral Analyses." **AAPS PharmSciTech** 11, 3: 1068 - 1083.

Keith, A. D. and Snipes, W. (1982). Phospholipids as moisturizing agents. principles of cosmetics for the dermatologist. Frost. P. and Horovitz, S.N. (eds), The C.V. Mosby Company: 59 - 69.

Kenworthy, A. K., Simon, S. A., and McIntosh, T. J. (1995). "Structure and phase behavior of lipid suspensions containing phospholipids with covalently attached poly(ethylene glycol)." **Biophysical Journal** 68, 5: 1903 - 1920.

Kim, M. K., et al. (1997). "Targeted and sustained delivery of hydrocortisone to normal and stratum corneum-removed skin without enhanced skin absorption using a liposome gel." **Journal of Controlled Release** 46, 3: 243 - 251.

Kirjavainen, M., et al. (1996). "Interaction of liposomes with human skin in vitro — The influence of lipid composition and structure." **Biochimica et Biophysica Acta (BBA) - Lipids and Lipid Metabolism** 1304, 3: 179 - 189.

Kirjavainen, M., et al. (1999). "Phospholipids affect stratum corneum lipid bilayer fluidity and drug partitioning into the bilayers." **Journal of Controlled Release** 58, 2: 207 – 214.

Knorr, F., et al. (2009). "Follicular transport route – Research progress and future perspectives." **European Journal of Pharmaceutics and Biopharmaceutics** 71, 2: 173 - 180.

Knudsen, N.Ø., et al. (2012). "Calcipotriol delivery into the skin with PEGylated liposomes." **European Journal of Pharmaceutics and Biopharmaceutics** 81, 3: 532 – 539.

Krasovitskia, B., et al. (2011). "Intramembrane cavitation as a unifying mechanism for ultrasound-induced bioeffects." **Proceedings of the National Academy of Sciences** 108: 3258 – 3263.

Lademann, J., et al. (2008). "Hair follicles--an efficient storage and penetration pathway for topically applied substances." **Summary of recent results obtained at the Center of Experimental and Applied Cutaneous Physiology**, Charité -Universitätsmedizin Berlin, Germany.Skin Pharmacology and Physiology 21, 3: 150 – 155.

Lasch, J., et al. (1992). "How deep do intact liposomes penetrate into human skin?" **Journal of Controlled Release** 18, 1: 55 - 58.

Lasic, D. D. (1988). "The mechanism of vesicle formation." **Biochemical Journal** 256, 1: 1 - 11.

Lauterbach, A. and Müller-Goymann, C. C. (2015). "Applications and limitations of lipid nanoparticles in dermal and transdermal drug delivery via the follicular route." **European Journal of Pharmaceutics and Biopharmaceutics** 97: 152 - 163.

Lee, S. E., et al. (2010). "Penetration pathways induced by low-frequency sonophoresis with physical and chemical enhancers: iron oxide nanoparticles versus lanthanum nitrates." **Journal of Investigative Dermatology** 130, 4: 1063 – 1072.

Lee, S.C., et al. (2005). "The effect of cholesterol in the liposome bilayer on the stabilization of incorporated Retinol." **Journal of Liposome Research** 15, 3 - 4: 157 - 166.

Liu, T., et al. (2007). "Structure behaviors of hemoglobin in PEG 6000/Tween 80/Span 80/H2O niosome system." **Colloids and Surfaces A** 293, 1–3: 255 - 261.

Lodzki, M., et al. (2003). "Cannabidiol-transdermal delivery and anti-inflammatory effect in a murine model." **Journal of Controlled Release** 93, 3: 377 - 387.Godin, B. and Touitou, E. (2005). "Erythromycin ethosomal systems: physicochemical characterization and enhanced antibacterial activity." **Current Drug Delivery** 2, 3: 269 - 275.

Loizidou, E.Z., et al. (2015). "Structural characterisation and transdermal delivery studies on sugar microneedles: Experimental and finite element modelling analyses." **European Journal of Pharmaceutics and Biopharmaceutics** 89: 224 – 231.

Lombry, C., et al. (2000). "Transdermal delivery of macromolecules using skin electroporation." **Pharmaceutical Research** 17, 1: 32 - 37.

Lopez, R., et al. (2011). "Enhancing the transdermal delivery of rigid nanoparticles using the simultaneous application of ultrasound and sodium lauryl sulfate." **Biomaterials** 32, 3: 933 – 941.

Lu, W.C., et al. (2014). "Skin permeation of d-limonene-based nanoemulsions as a transdermal carrier prepared by ultrasonic emulsification." **Ultrasonics Sonochemistry** 21, 2: 826 – 832.

Madan, J., et al. (2013). "Poly (ethylene)-glycol conjugated solid lipid nanoparticles of noscapine improve biological half-life, brain delivery and efficacy in glioblastoma cells." **Nanomedicine: Nanotechnology, Biology and Medicine** 9, 4: 492 - 503.

Maheshwari, R. G. S., et al. (2012). "Ethosomes and ultradeformable liposomes for transdermal delivery of clotrimazole: A comparative assessment." **Saudi Pharmaceutical Journal** 20, 2: 161 - 170.

Maitani, Y., et al. (2012). "Hydration of surfactant-modified and PEGylated cationic cholesterol-based liposomes and corresponding lipoplexes by monitoring a fluorescent probe and the dielectric relaxation time." **International Journal of Pharmaceutics** 427: 372 - 378.

Mali, N., et al. (2013). "Niosomes as a vesicular carrier for topical administration of minoxidil: formulation and in vitro assessment." **Drug Delivery and Translational Research** 3, 6: 587 - 592.

Manconi, M., et al. (2006). "Niosomes as carriers for tretinoin. III. A study into the in vitro cutaneous delivery of vesicle-incorporated tretinoin." **International Journal of Pharmaceutics** 311, 1 - 2: 11 - 19.

Manconi, M., et al. (2011). "Ex vivo skin delivery of diclofenac by transcutol containing liposomes and suggested mechanism of vesicle-skin interaction." **European Journal of Pharmaceutics and Biopharmaceutics** 78, 1: 27 - 35.

Mandawgade, D.S., and Patravale, V.B. (2008). "Development of SLNs from natural lipids: application to topical delivery of tretinoin." **International Journal of Pharmaceutics** 363: 132 – 138.

Manosroi, A., et al. (2012). "Transfollicular enhancement of gel containing cationic niosomes loaded with unsaturated fatty acids in rice (Oryza sativa) bran semi-purified fraction." **European Journal of Pharmaceutics and Biopharmaceutics** 81, 2: 303 - 313.

Marczak, A. (2009). "Fluorescence anisotropy of membrane fluidity probes in human erythrocytes incubated with anthracyclines and glutaraldehyde." **Bioelectrochemistry** 74, 2: 236 - 239.

Megrab, N. A., et al. (1995). "Oestradiol permeation across human skin, silastic and snake skin membranes: The effects of ethanol/water co-solvent systems." **International Journal of Pharmaceutics** 116, 1: 101 - 112.

Mehnert, W., and Mader, K. (2001). "Solid lipid nanoparticles production, characterization and applications." **Advanced Drug Delivery Reviews** 47: 165 – 196.

Mei, Z., et al. (2003). "Solid lipid nanoparticle and microemulsion for topical delivery of triptolide." **European Journal of Pharmaceutics and Biopharmaceutics** 56: 189 – 196.

Meidan, V. M., et al. (1998). "Phonophoresis of hydrocortisone with enhancers: an acoustically defined model." **International Journal of Pharmaceutics** 170, 2: 157 - 168.

Mendelsohn, R., et al. (2003). "Infrared microspectroscopic imaging maps the spatial distribution of exogenous molecules in skin." **Journal of Biomedical Optics** 8, 2: 185 - 190.

Menon, G.K., Lee, S.H., and Robert, M.S. (1998). "Ultrastructural effects of some solvents and vehicles on the stratum corneum and other skin components: Evidence for an extended mosaic partitioning model of the skin barrier." **Dermal absorption and toxicity assessment**, Roberts, M.S. and Walters, K.A. (Eds). New York: Marcel Dekker; p.727.

Merino, G., et al. (2003). "Frequency and thermal effects on the enhancement of transdermal transport by sonophoresis." **Journal of Controlled Release** 88, 1: 85 - 94.

Mezei, M. and Gulasekharam, V. (1980). "Liposomes--a selective drug delivery system for the topical route of administration. Lotion dosage form." **Life Sciences** 26, 18: 1473 - 1477.

Michinori, S., et al. (1997). "Effects of absorption enhancers on the transport of model compounds in Caco-2 cell monolayers: Assessment by confocal laser

scanning microscopy." **Journal of Pharmaceutical Sciences** 86, 7: 779 – 785.

Mitragotri, S., Blankschtein, D., and Langer, R. (1996). "Transdermal drug delivery using low-frequency sonophoresis." **Pharmaceutical Research** 13, 3: 411 – 420.

Moghassemi, S. and Hadjizadeh, A. (2014). "Nano-niosomes as nanoscale drug delivery systems: An illustrated review." **Journal of Controlled Release** 185: 22 - 36.

Morimoto, Y., et al. (2005). "Elucidation of the transport pathway in hairless rat skin enhanced by low-frequency sonophoresis based on the solute–water transport relationship and confocal microscopy." **Journal of Controlled Release** 103, 3: 587 – 597.

Mura, P., et al. (2007). "Development, characterization and in vivo evaluation of benzocaine-loaded liposomes." **European Journal of Pharmaceutics and Biopharmaceutics** 67, 1: 86 - 95.

Mura, S., et al. (2009). "Penetration enhancer-containing vesicles (PEVs) as carriers for cutaneous delivery of minoxidil." **International Journal of Pharmaceutics** 380, 1–2: 72 - 79.

Mutalik, S., et al. (2009). "A combined approach of chemical enhancers and sonophoresis for the transdermal delivery of tizanidine hydrochloride." **Drug Delivery** 16, 2: 82 – 91.

Muzzalupo, R., and Tavano, L. (2015). "Niosomal drug delivery for transdermal targeting: recent advances." **Research and Reports in Transdermal Drug Delivery** 2015, 4: 23 — 33.

Narishetty, S. T. K. and Panchagnula, R. (2005). "Effect of l-menthol and 1,8-cineole on phase behavior and molecular organization of SC lipids and skin permeation of zidovudine." **Journal of Controlled Release** 102, 1: 59 - 70.

Obata, Y., et al. (2010). "Infrared spectroscopic study of lipid interaction in stratum corneum treated with transdermal absorption enhancers." **International journal of pharmaceutics** 389, 1 – 2: 18 - 23.

Ogura, M., et al. (2008). "Low-frequency sonophoresis: Current status and future prospects." **Advanced Drug Delivery Reviews** 60, 10: 1218 - 1223.

Oh, Y. K., et al. (2006). "Skin permeation of retinol in Tween 20-based deformable liposomes: in-vitro evaluation in human skin and keratinocyte models." **Journal of Pharmacy and Pharmacology** 58: 161 - 166.

Okore, V. C., et al. (2011). "Formulation and Evaluation of Niosomes." **Indian Journal of Pharmaceutical Sciences** 73, 3: 323 - 328.

Ongpipattanakul, B., et al. (1991). "Evidence that oleic acid exists in a separate phase within stratum corneum lipids." **Pharmaceutical Research** 8, 3: 350 - 354.

Panchagnula, R., et al. (2001). "Transdermal delivery of naloxone: effect of water, propylene glycol, ethanol and their binary combinations on permeation through rat skin." **International Journal of Pharmaceutics** 219, 1-2: 95 - 105.

Paolino, D., et al. (2005). "Ethosomes for skin delivery of ammonium glycyrrhizinate: in vitro percutaneous permeation through human skin and in vivo anti-inflammatory activity on human volunteers. **Journal of Controlled Release** 106: 99 - 110.

Park, J. H., et al. (2008). "The effect of heat on skin permeability." **International Journal of Pharmaceutics** 359, 1-2: 94 - 103.

Patzelt, A. and Lademann, J. (2013). "Drug delivery to hair follicles." **Expert Opinion on Drug Delivery** 10, 6: 787 - 797.

Paudel, K. S., et al. (2010). "Challenges and opportunities in dermal/transdermal delivery." **Therapeutic delivery** 1, 1: 109 - 131.

Petchsangsai, M., Opanasopit, P., and Ngawhirunpat, T. (2014). "The Combination of Microneedles with Electroporation and Sonophoresis to Enhance Hydrophilic Macromolecule Skin Penetration." **Biological and Pharmaceutical Bulletin** 37, 8: 1373 – 1382.

Pierre, M. B. R. and Costa, I.S.M. (2011). "Liposomal systems as drug delivery vehicles for dermal and transdermal applications." **Archives of Dermatological Research** 303: 607 - 621.

Pierre, M. B., et al. (2001). "Stratum corneum lipids liposomes for the topical delivery of 5-aminolevulinic acid in photodynamic therapy of skin cancer: preparation and in vitro permeation study." **BMC Dermatology** 1: 1 -5.

Pierre, M., and Santos Miranda Costa, I. (2011). "Liposomal systems as drug delivery vehicles for dermal and transdermal applications." **Archives of Dermatological Research** 303, 9: 607 – 621.

Pilgram, G. S. K., et al. (2001). "The influence of two azones and sebaceous lipids on the lateral organization of lipids isolated from human stratum corneum." **Biochimica et Biophysica Acta (BBA) – Biomembranes** 1511, 2: 244 - 254.

Polat, B. E., et al. (2011). "Ultrasound-mediated transdermal drug delivery: Mechanisms, scope, and emerging trends." **Journal of Controlled Release** 152, 3: 330 - 348.

Polat, B.E., et al. (2012). "A physical mechanism to explain the delivery of chemical penetration enhancers into skin during transdermal sonophoresis — Insight into the observed synergism." **Journal of Controlled Release** 158, 2: 250 – 260.

Porter, C. J. (1997). "Drug delivery to the lymphatic system." **Critical Reviews™ in Therapeutic Drug Carrier Systems** 14, 4: 333 - 393.

Potts, R. O. and Francoeur, M. L. (1991). "The influence of stratum corneum morphology on water permeability." **Journal of Investigative Dermatology** 96, 4: 495 - 499.

Prausnitz, M. R. and Langer, R. (2008). "Transdermal drug delivery." **Nature Biotechnology** 26, 11: 1261 - 1268.

Prausnitz, M.R., and Langer, R. (2009). "Transdermal drug delivery." **Nature Biotechnology** 26, 1: 1261 – 1268.

Qandil, A., et al. (2008). "Synthesis of piperazinylalkyl ester prodrugs of ketorolac and their in vitro evaluation for transdermal delivery." **Drug Development and Industrial** 34, 10: 1054 - 1063.

Quinn, P. J. and Wolf, C. (2009). "Thermotropic and structural evaluation of the interaction of natural sphingomyelins with cholesterol." **Biochimica et Biophysica Acta (BBA) - Biomembranes** 1788, 9: 1877 - 1889.

Rawat, S., et al. (2008). "Transdermal Delivery by Iontophoresis." **Indian Journal of Pharmaceutical Sciences** 70, 1: 5 - 10.

Rich, K. T., et al. (2014). "Relations between acoustic cavitation and skin resistance during intermediate- and high-frequency sonophoresis." **Journal of Controlled Release** 194: 266 - 277.

Riesz, P. and Kondo, T. (1992). "Free radical formation induced by ultrasound and its biological implications." **Free Radical Biology & Medicine** 13, 3: 247 - 270.

Roberts, M. S., et al. (2002). Skin transport. **Dermatological and transdermal formulations.** Walters, K.A. New York, NY, Marcel Dekker, Inc. 1: 89 - 196.

Romero, E. L. and Morilla, M. J. (2013). "Highly deformable and highly fluid vesicles as potential drug delivery systems: theoretical and practical considerations." **International Journal of Pharmaceutics** 8: 3171 - 3186.

Ruozi, B., et al. (2011). "AFM, ESEM, TEM, and CLSM in liposomal characterization: a comparative study." **International Journal of Nanomedicine** 6: 557 - 563.

Santoyo, S. and Ygartua, P. (2000). "Effect of skin pretreatment with fatty acids on percutaneous absorption and skin retention of piroxicam after its topical application." **European Journal of Pharmaceutics and Biopharmaceutics** 50, 2: 245 - 250.

Sarheed, O., and Abdul Rasool, B.K. (2011). "Development of an Optimised Application Protocol For Sonophoretic Transdermal Delivery of a Model Hydrophilic Drug." **The Open Biomedical Engineering Journal** 5: 14 – 24.

Sarheed, O., and Frum, Y. (2012). "Use of the skin sandwich technique to probe the role of the hair follicles in sonophoresis." **International Journal of Pharmaceutics** 423: 179 – 183.

Schaller, M. and Korting, H.C. (1996). "Interaction of liposomes with human skin: the role of the stratum corneum." **Advanced Drug Delivery Reviews** 18, 3: 303 - 309.

Schneider, M., et al. (2009). "Nanoparticles and their interactions with the dermal barrier." **Dermatoendocrinol** 1: 197 - 206.

Schreier, H. and Bouwstra, J. (1994). "Liposomes and niosomes as topical drug carriers: dermal and transdermal drug delivery." **Journal of Controlled Release** 30, 1: 1 - 15.

Shah, D. K., et al. (2008). "Alteration of skin hydration and its barrier function by vehicle and permeation enhancers: a study using TGA, FTIR, TEWL and drug permeation as markers." **Methods and Findings in Experimental and Clinical Pharmacology** 30, 7: 499 - 512.

Shahiwala, A. and Misra, A. (2002). "Studies in topical application of niosomally entrapped Nimesulide." **Journal of Pharmacy & Pharmaceutical Sciences** 5, 3: 220 - 225.

Shi, B., Fang, C., and Pei, Y. (2005). "Stealth PEG-PHDCA Niosomes: Effects of ChainLength of PEG and Particle Size on NiosomesSurface Properties, In Vitro Drug Release,Phagocytic Uptake, In Vivo Pharmacokineticsand Antitumor Activity." **Journal of Pharmaceutical Sciences** 95: 1873 - 1887.

Siddiqui, A., et al. (2014). "Modeling the effect of sonication parameters on size and dispersion temperature of solid lipid nanoparticles (SLNs) by response surface methodology (RSM)." **Pharmaceutical Development and Technology** 19, 3: 342 - 346.

Sinico, C., et al. (2005). "Liposomes as carriers for dermal delivery of tretinoin: in vitro evaluation of drug permeation and vesicle–skin interaction." **Journal of Controlled Release** 103, 1: 123 – 136.

Smijs, T. G. and Bouwstra, J.A. (2010). "Focus on skin as a possible port of entry for solid nanoparticles and the toxicological impact." **Journal of Biomedical Nanotechnology** 6, 5: 469 - 484.

Smith, N. B. (2007). "Perspectives on transdermal ultrasound mediated drug delivery." **Journal of International Journal of Nanomedicine** 2, 4: 585 - 594.

Stott, P. W., et al. (1998). "Transdermal delivery from eutectic systems: enhanced permeation of a model drug, ibuprofen." **Journal of Controlled Release** 50, 1-3: 297 - 308.

Stott, P. W., et al. (2001). "Mechanistic study into the enhanced transdermal permeation of a model beta-blocker, propranolol, by fatty acids: a melting point depression effect." **International Journal of Pharmaceutics.** 219(1-2): 161-176.

Stracke, F., et al. (2006). "Multiphoton microscopy for the investigation of dermal penetration of nanoparticle-borne drugs." **Journal of Investigative Dermatology** 126, 10: 2224 - 2233.

Subongkot, T. and Ngawhirunpat, T. (2015). "Effect of liposomal fluidity on skin permeation of sodium fluorescein entrapped in liposomes." **International Journal of Nanomedicine** 10: 4581 - 4592.

Subongkot, T., et al. (2012). "Ultradeformable liposomes with terpenes for delivery of hydrophilic compound." **Journal of Liposome Research** 22, 3: 254 – 262.

Subongkot, T., et al. (2013). "Visualization of ultradeformable liposomes penetration pathways and their skin interaction by confocal laser scanning microscopy." **International Journal of Pharmaceutics** 441, 1 – 2: 151 – 61.

Swartz, M. A. (2001). "The physiology of the lymphatic system." **Advanced Drug Delivery Reviews** 50, 1-2: 3 - 20.

Szuba, A. and Rockson, S. G. (1997). "Lymphedema: anatomy, physiology and pathogenesis." **Vascular Medicine** 2, 4: 321 - 326.

Tang, H., et al. (2002). "An investigation of the role of cavitation in low-frequency ultrasound-mediated transdermal drug transport." **Pharmaceutical Research** 19, 8: 1160 - 1169.

Tang, H., et al. (2013). "CW/pulsed NIR irradiation of gold nanorods: Effect on transdermal protein delivery mediated by photothermal ablation." **Journal of Controlled Release** 171, 2: 178 - 183.

Tanojo, H., et al. (1999). "Thermal Analysis Studies on Human Skin and Skin Barrier Modulation by Fatty Acids and Propylene Glycol." **Journal of Thermal Analysis and Calorimetry** 57, 1: 313 - 322.

ter Haar, G. (2007). "Therapeutic applications of ultrasound." **Progress in Biophysics and Molecular Biology** 93, 1-3: 111 - 129.

Terahara, T., et al. (2002). "Porous resins as a cavitation enhancer for low-frequency sonophoresis." **Journal of Pharmaceutical Sciences** 91, 3: 753 - 759.

Tezel, A., et al. (2003). "Description of transdermal transport of hydrophilic solutes during low-frequency sonophoresis based on a modified porous pathway model." **Journal of Pharmaceutical Sciences** 92, 2: 381 - 393.

Thomas, J., et al. (2009). "Soft alkyl ether prodrugs of a model phenolic drug: the effect of incorporation of ethyleneoxy groups on transdermal delivery." **Molecules** 14, 10: 4231.

Tiwari, S. B., et al. (2004). "Influence of ultrasound on the percutaneous absorption of ketorolac tromethamine *in vitro* across rat skin." **Drug Delivery** 11, 1: 47 - 51..

Tokudome, Y., and Sugibayashi, K. (2004). "Mechanism of the synergic effects of calcium chloride and electroporation on the in vitro enhanced skin permeation of drugs." **Journal of Controlled Release** 95, 2: 267 – 274.

Touitou, E., et al. (2000). "Ethosomes — novel vesicular carriers for enhanced delivery: characterization and skin penetration properties." **Journal of Controlled Release** 65, 3: 403 – 418.

Tupker, R. A., et al. (1990). "The transient and cumulative effect of sodium lauryl sulphate on the epidermal barrier assessed by transepidermal water loss: inter-individual variation." **Acta Dermato Venereologica** 70, 1: 1 - 5.

Ueda, H., et al. (2009). "Acoustic cavitation as an enhancing mechanism of low-frequency sonophoresis for transdermal drug delivery." **Biological and Pharmaceutical Bulletin** 32, 5: 916 - 920.

Uner, M., and Yener, G. (2007). "Importance of solid lipid nanoparticles (SLNs) in various administration routes and future perspectives." **International Journal of Nanomedicines** 2, 3: 289 - 300.

Valenta, C. and Janisch, M. (2003). "Permeation of cyproterone acetate through pig skin from different vehicles with phospholipids." **International Journal of Pharmaceutics.** 258(1–2): 133-139.

Vemuri, S. and Rhodes, C.T. (1995). "Preparation and characterization of liposomes as therapeutic delivery systems: a review." **Pharmaceutica Acta Helvetiae** 70, 2: 95 - 111.

Verma, D. D. (2002). Invasomes-novel topical carriers for enhanced topical delivery: characterization and skin penetration properties. Germany, Marburg/Lahn. Ph.D. Thesis.

Verma, D. D., et al. (2003). "Liposomes increase skin penetration of entrapped and non-entrapped hydrophilic substances into human skin: a skin penetration and confocal laser scanning microscopy study." **European Journal of Pharmaceutics and Biopharmaceutics** 55, 3: 271 - 277.

Verma, D. D., et al. (2003). "Particle size of liposomes influences dermal delivery of substances into skin." **International Journal of Pharmaceutics** 258, 1 – 2: 141 - 151.

Vora, B., Khopade, A. J., and Jain, N. K. (1998). "Proniosome based transdermal delivery of levonorgestrel for effective contraception." **Journal of Controlled Release** 54, 2: 149 - 165.

Vyas, S.P., Singh, R., and Asati, R.K. (1995). "Liposomally encapsulated diclofenac for sonophoresis induced systemic delivery." **Journal of Microencapsulation** 12, 2: 149 – 154.

Walters, K.A. (2002). "Dermatological and Transdermal Formulation." **The structure and Function of Skin**, Walters, K.A. and Robert, M.S.(Eds). New York: Marcel Dakker.

Wan, D. C., et al. (2014). "Moisturizing Different Racial Skin Types." **The Journal of Clinical and Aesthetic Dermatology** 7, 6: 25 - 32.

Wang, Y. and Chen, L. (2011). "Quantum dots, lighting up the research and development of nanomedicine." **Nanomedicine** 7, 4: 385 - 402.

Watanabe, S., et al. (2009). "Enhanced transdermal drug penetration by the simultaneous application of iontophoresis and sonophoresis." **Journal of Drug Delivery Science and Technology** 19(3): 185-189.

Williams, A. C. (2003). “Transdermal and topical drug delivery”. **Theory to clinical Practice**. London, Pharmaceutical Press.

Williams, A. C. and Barry, B. W. (2004). “Penetration enhancers.” **Advanced Drug Delivery Reviews** 56, 5: 603 - 618.

Wissing, S. A. and Muller, R. H. (2003). "Cosmetic applications for solid lipid nanoparticles (SLN)." **International Journal of Pharmaceutics** 254, 1: 65 - 68.

Wolloch, L. and Kost, J. (2010). “The importance of microjet vs shock wave formation in sonophoresis.” **Journal of Controlled Release** 148, 2: 204 - 211.

Wong, T.-W., et al. (2006). “Painless electroporation with a new needle-free microelectrode array to enhance transdermal drug delivery.” **Journal of Controlled Release** 110, 3: 557 - 565.

Wosicka-Frąckowiak, H., et al. (2015). “Roxithromycin-loaded lipid nanoparticles for follicular targeting.” **International Journal of Pharmaceutics** 495, 2: 807 - 815.

Yadav, V., et al. (2012). “Transdermal drug delivery: A technical writeup.” **Journal of Pharmaceutical and Scientific Innovation** 1, 1: 5 - 12.

Yamane, M. A., et al. (1995). “Terpene penetration enhancers in propylene glycol/water co-solvent systems: effectiveness and mechanism of action. **Journal of Pharmacy and Pharmacology** 47, 12a: 978 - 989.

Yatvin, M. B. and Lelkesm, P.I. (1982). “Clinical prospects for liposomes.” **Medical Physics** 9, 2: 149 - 175.

Yokomizo, Y. and Sagitani, H. (1996). "The effects of phospholipids on the percutaneous penetration of indomethacin through the dorsal skin of guinea pig in vitro. 2. The effects of the hydrophobic group in phospholipids and a comparison with general enhancers." **Journal of Controlled Release** 42(1): 37-46.

Yong, C. S., et al. (2004). “Preparation of ibuprofen-loaded liquid suppository using eutectic mixture system with menthol.” **European Journal of Pharmaceutical Sciences** 23, 4-5: 347 - 353.

Zellmer, S., Pfeil, W., and Lasch, J. (1995). "Interaction of phosphatidylcholine liposomes with the human stratum corneum." **Biophysica Acta (BBA) – Biophysics** 1237, 2: 176 - 182.

APPENDIX

APPENDIX A

Standard curve for the *in vitro* skin penetration study

1. Determination of the amount of NaFl

Standard : NaFl

Method : Fluorescence spectrophotometry

Detector : The excitation wavelength at 485 nm

The emission wavelength at 535 nm

Concentration (ng/mL) : 0, 0.5, 1, 2, 5, 10, 20, 25, 30, 35, 40

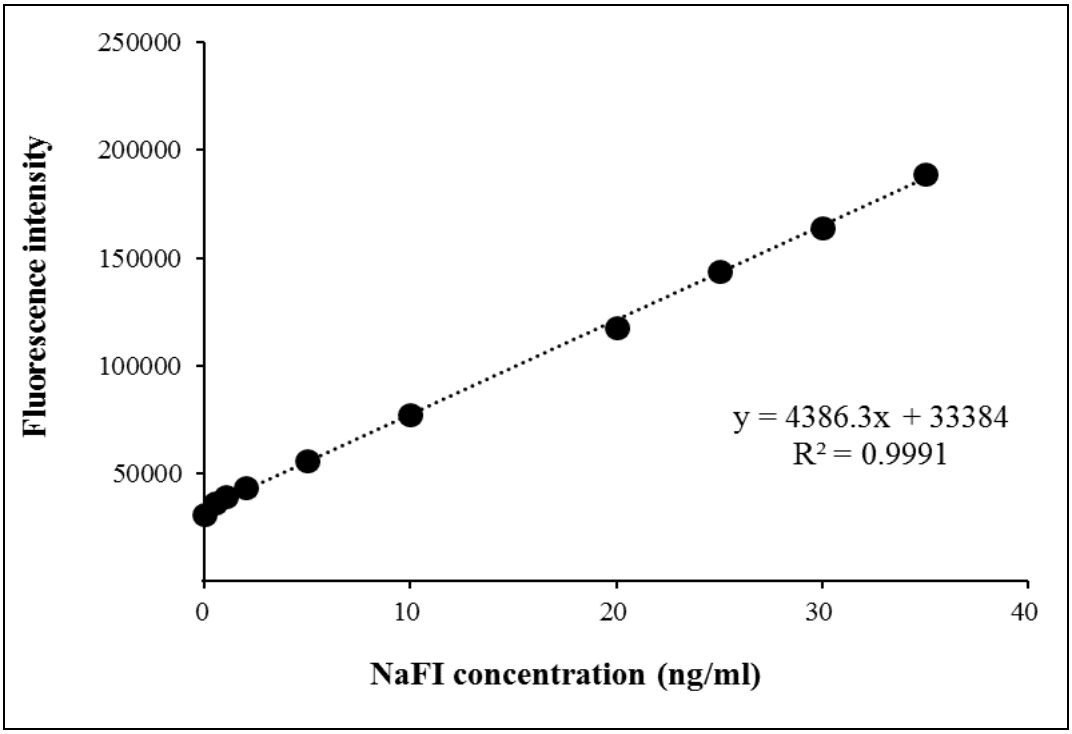

Figure A1 Standard curve of NaFl for the *in vitro* skin penetration study

APPENDIX B

Table B1 Fluorescence anisotropy value of DPH added to the liposome formulations at the temperature of 25 and 32 °C. Results denote the mean ± S.D. (N = 3). *indicates significant difference from PL ($p < 0.05$).

Formulations	**Temperature (°C)**	
	25	**32**
CL	0.1272 ± 0.0016	0.1229 ± 0.0015
PL	0.1322 ± 0.0037	0.1280 ± 0.0018
PL-TW	0.1401 ± 0.0018	0.1343 ± 0.0011
PL-LI0.1%	0.1351 ± 0.0044	0.1277 ± 0.0058
PL-LI1%	0.1194 ± 0.0006	0.1148 ± 0.0014
PL-LI2%	0.1200 ± 0.0020	0.1149 ± 0.0048

Table B2 Cumulative NaFl permeated at various time of *in vitro* NaFl solution without and with SN penetration. Each value represents the mean ± S.D. (n=3)

Time (h)	**Cumulative NaFI permeated (μg/cm^2)**	
	NaFI solution without SN	**NaFI solution with SN**
1	0.0047 ± 0.00	0.1671 ± 0.04
2	0.0092 ± 0.00	0.4004 ± 0.13
4	0.0230 ± 0.00	0.8064 ± 0.25
6	0.0394 ± 0.01	1.3297 ± 0.47
8	0.0469 ± 0.01	1.7264 ± 0.78
24	0.1382 ± 0.04	7.0879 ± 2.72

Table B3 Cumulative NaFl permeated at various time of *in vitro* CL without and with SN penetration. Each value represents the mean ± S.D. (n=3)

Time (h)	**Cumulative NaFI permeated (µg/cm^2)**				
	CL	**PL1**	**PL2**	**PL3**	**PL4**
Without SN					
1	0.0227 ± 0.00	0.0306 ± 0.03	0.0265 ± 0.03	0.0379 ± 0.04	0.0114 ± 0.00
2	0.0395 ± 0.02	0.0726 ± 0.08	0.1091 ± 0.10	0.0959 ± 0.12	0.0767 ± 0.06
4	0.0801 ± 0.04	0.1457 ± 0.15	0.2765 ± 0.24	0.1853 ± 0.22	0.0731 ± 0.03
6	0.1605 ± 0.09	0.2404 ± 0.23	0.4166 ± 0.28	0.3092 ± 0.33	0.1828 ± 0.10
8	0.1972 ± 0.11	0.3346 ± 0.32	0.5470 ± 0.38	0.4840 ± 0.37	0.2049 ± 0.03
24	0.5927 ± 0.21	0.7955 ± 0.73	1.5191 ± 1.22	1.4640 ± 1.01	0.5881 ± 0.08
With SN					
1	0.1500 ± 0.18	0.0281 ± 0.01	0.0342 ± 0.02	0.0100 ± 0.00	0.0241 ± 0.01
2	0.2013 ± 0.17	0.0679 ± 0.04	0.0616 ± 0.03	0.0179 ± 0.01	0.0343 ± 0.01
4	0.2756 ± 0.14	0.1557 ± 0.12	0.1425 ± 0.07	0.0372 ± 0.02	0.0646 ± 0.02
6	0.3737 ± 0.12	0.2337 ± 0.18	0.2239 ± 0.12	0.0554 ± 0.03	0.0915 ± 0.03
8	0.4683 ± 0.10	0.3008 ± 0.23	0.3046 ± 0.17	0.0750 ± 0.04	0.1241 ± 0.03
24	1.0725 ± 0.06	0.9328 ± 0.64	1.0136 ± 0.41	0.2457 ± 0.09	0.4532 ± 0.04

Table B4 Cumulative NaFl permeated at various time of niosome formulations without and with SN. Each value represents the mean ± S.D. (n=3)

Time (h)	**Cumulative NaFI permeated (µg/cm^2)**				
	NI	**NIP1**	**NIP2**	**NIP3**	**NIP4**
Without SN					
1	0.0770 ± 0.04	0.0522 ± 0.07	0.0217 ± 0.01	0.1114 ± 0.16	0.0123 ± 0.00
2	0.1709 ± 0.12	0.0583 ± 0.08	0.0395 ± 0.01	0.1210 ± 0.15	0.0272 ± 0.01
4	0.3001 ± 0.28	0.0694 ± 0.09	0.0848 ± 0.03	0.1586 ± 0.17	0.0659 ± 0.03
6	0.4455 ± 0.38	0.0810 ± 0.09	0.1407 ± 0.05	0.1723 ± 0.15	0.1034 ± 0.04
8	0.7834 ± 0.32	0.0948 ± 0.10	0.2202 ± 0.09	0.2089 ± 0.17	0.1601 ± 0.11
24	2.8131 ± 1.56	0.2922 ± 0.26	0.9406 ± 0.23	0.5120 ± 0.32	0.7376 ± 0.17
With SN					
1	0.0594 ± 0.05	0.0639 ± 0.07	0.0071 ± 0.00	0.0048 ± 0.00	0.0047 ± 0.00

2	0.1067 ± 0.10	0.0996± 0.08	0.0121 ± 0.00	0.0105 ± 0.00	0.0065 ± 0.00
4	0.2362 ± 0.21	0.1656± 0.11	0.0232 ±0.00	0.0233 ± 0.01	0.0122 ± 0.01
6	0.3809 ± 0.32	0.2486± 0.15	0.0385 ±0.01	0.0403 ± 0.01	0.0227 ± 0.02
8	0.5002 ± 0.29	0.3243± 0.17	0.0549 ±0.02	0.0548 ± 0.02	0.0262 ± 0.02
24	1.5430 ± 0.14	1.0021 ± 0.60	0.2479 ± 0.13	0.2684 ± 0.08	0.0985 ± 0.04

Table B5 Cumulative NaFl permeated at various time of SLN formulations without and with SN. Each value represents the mean ± S.D. (n=3)

Time (h)	**Cumulative NaFI permeated (µg/cm^2)**				
	SLN	**SLNP1**	**SLNP2**	**SLNP3**	**SLNP4**
Without SN					
1	0.1158 ± 0.04	0.0411 ± 0.04	0.0168 ± 0.01	0.0328 ± 0.03	0.0093 ± 0.01
2	0.3088 ± 0.05	0.0806 ± 0.09	0.0299 ± 0.02	0.0685 ± 0.07	0.0116 ± 0.01
4	0.7135 ± 0.06	0.1901 ± 0.22	0.0599 ± 0.03	0.1537 ± 0.17	0.0139 ± 0.01
6	1.0786 ± 0.14	0.3208 ± 0.30	0.0983 ± 0.04	0.2354 ± 0.25	0.0190 ± 0.01
8	1.5392 ± 0.35	0.4875 ± 0.36	0.1581 ± 0.06	0.3296 ± 0.35	0.0263 ± 0.00
24	4.5554 ± 1.38	1.5869 ± 0.83	1.3495 ± 0.97	1.0423 ± 0.86	0.1012 ± 0.03
With SN					
1	0.0210 ± 0.01	0.1262 ± 0.14	0.0129 ± 0.00	0.0657 ± 0.02	0.0254 ± 0.01
2	0.0423 ± 0.02	0.1769 ± 0.14	0.0190 ± 0.01	0.1233 ± 0.02	0.0466 ± 0.03
4	0.0926 ± 0.05	0.2648 ± 0.17	0.0319 ± 0.01	0.2391 ± 0.04	0.0963 ± 0.08
6	0.1432 ± 0.08	0.4036 ± 0.19	0.0488 ± 0.02	0.3757 ± 0.07	0.1439 ± 0.11
8	0.2327 ± 0.16	0.5370 ± 0.22	0.0702 ± 0.01	0.5439 ± 0.09	0.3227 ± 0.33
24	0.7180 ± 0.42	1.4236 ± 0.21	0.2742 ± 0.06	1.3778 ± 0.32	0.6339 ± 0.43

Table B6 Cumulative NaFl permeated at various time of *in vitro* PL-TW penetration. Each value represents the mean ± S.D. (n=3).

Time (h)	**Cumulative NaFI permeated (µg/cm^2)**
1	0.0360 ± 0.00
2	0.1013 ± 0.02
4	0.3562 ± 0.16
6	0.6258 ± 0.42
8	0.8247 ± 0.62

24	3.1475 ± 3.18

Table B7 Cumulative NaFl permeated at various time of d-limonene-containing lipid nanocarriers (PL-LI, NIP-LI, and SLNP-LI) with and without SN. Each value represents the mean ± S.D. (n=3)

Time (h)	**Cumulative NaFI permeated (μg/cm^2)**		
	PL-LI	**NIP-LI**	**SLNP-LI**
Without SN			
1	0.3070 ± 0.13	0.1625 ± 0.09	0.0557 ± 0.06
2	0.6487 ± 0.23	0.2966 ± 0.17	0.0717 ± 0.06
4	1.8116 ± 0.53	0.6343 ± 0.20	0.1182 ± 0.09
6	2.7419 ± 0.87	0.9408 ± 0.30	0.1679 ± 0.12
8	4.0541 ± 1.11	1.1935 ± 0.36	0.2114 ± 0.13
24	12.5711 ± 2.68	4.1949 ± 2.13	0.8061 ± 0.28
With SN			
1	0.1413 ± 0.06	0.0846 ± 0.00	0.0566 ± 0.02
2	0.3208 ± 0.16	0.2238 ± 0.06	0.1300 ± 0.06
4	0.7254 ± 0.38	0.4830 ± 0.11	0.3401 ± 0.19
6	1.1380 ± 0.64	0.7553 ± 0.25	0.5471 ± 0.28
8	1.4682 ± 0.73	1.0184 ± 0.37	0.7753 ± 0.42
24	4.5614 ± 2.45	3.5009 ± 1.49	2.3306 ± 1.11

Table B8 The amount of NaFI-remaining stratum corneum (SC), epidermis and dermis (ED), and receiver compartment from NaFI solution with and without SN after 8 h *in vitro* skin permeation. Each value represents the mean ± S.D. (n=3). * indicates significant difference from NaFI solution ($p < 0.05$).

Formulations	**Amount of NaFI (µg)**		
	SC	**ED**	**Receiver compartment**
NaFI solution	1.8899 ± 0.52	1.1945 ± 0.42	0.0920 ± 0.02
NaFI solution with SN	1.3843 ± 0.24	2.6310 ± 1.84	3.3838 ± 1.53*

Table B9 The amount of NaFI-remaining stratum corneum (SC), epidermis and dermis (ED), and receiver compartment from liposome formulations (CL, PL, and PL-LI) with and without SN after 8 h *in vitro* skin permeation. Each value represents the mean ± S.D. (n=3). * indicates significant difference from NaFI solution ($p < 0.05$).

Formulations	**Amount of NaFI (µg)**		
	SC	**ED**	**Receiver compartment**
Without SN			
CL	3.2380 ± 0.45	1.4586 ± 0.16	0.4595 ± 0.25
PL2	3.2179 ± 0.39	1.9005 ± 0.60	1.0721 ± 0.75
PL-LI	2.3576 ± 0.16*	6.4763 ± 2.12*	9.7552 ± 2.67*
With SN			
CL with SN	2.2359 ± 0.23*	0.6911 ± 0.08	0.9178 ± 0.20
PL2 with SN	2.3714 ± 0.12*	1.1467 ± 0.15	0.5970 ± 0.34
PL-LI with SN	1.1754 ± 0.26*	1.7550 ± 0.77	2.8776 ± 1.43

Table B10 The amount of NaFI-remaining stratum corneum (SC), epidermis and dermis (ED), and receiver compartment from niosome formulation (NI, NIP, and NIP-LI) with and without SN after 8 h *in vitro* skin permeation. Each value represents the mean ± S.D. (n=3). * indicates significant difference from NaFI solution ($p < 0.05$).

Formulations	**Amount of NaFI (µg)**		
	SC	**ED**	**Receiver compartment**
Without SN			
NI	3.6831 ± 0.18	1.1081 ± 0.09	1.2292 ± 0.95
NIP2	3.2522 ± 0.68	0.7927 ± 0.02	0.8258 ± 0.67
NIP-LI	2.7900 ± 0.65	0.6897 ± 0.09	2.3393 ± 0.71
With SN			
NI with SN	1.4389 ± 0.18*	0.5340 ± 0.09	1.8792 ± 0.95
NIP2 with SN	1.4570 ± 0.68*	0.6956 ± 0.02	0.1076 ± 0.67
NIP-LI with SN	1.4621 ± 0.65*	0.8096 ± 0.09	1.9961 ± 0.71

Table B11 The amount of NaFI-remaining stratum corneum (SC), epidermis and dermis (ED), and receiver compartment from solid lipid nanoparticle formulations (SLN, SLNP, and SLNP-LI) with and without SN after 8 h *in vitro* skin permeation. Each value represents the mean ± S.D. (n=3). * indicates significant difference from NaFI solution ($p < 0.05$).

Formulations	**Amount of NaFI (µg)**		
	SC	**ED**	**Receiver compartment**
Without SN			
SLN	2.2198 ± 0.43	0.7949 ± 0.25	3.0169 ± 0.68
SLNP2	2.8553 ± 0.62	0.3385 ± 0.12	0.3098 ± 0.11*
SLNP-LI	2.9921± 1.13	0.6889 ± 0.13	0.4143 ± 0.26*
With SN			

SLN with SN	1.3740 ± 0.07	0.9143 ± 0.09	1.0567 ± 0.83*
SLNP2 with SN	1.2901 ± 0.33	0.5821 ± 0.35	0.1375 ± 0.02*
SLNP-LI with SN	1.7343 ± 0.17	0.9631 ± 0.09	1.5197 ± 0.82

Table B12 The cumulative amount and time profiles and flux of NaFI-loaded PL-LI permeated through blocked hair follicles skin with SN and without SN. Each value represents the mean ± S.D. (n=3). *indicates significantly different from open hair follicles ($p < 0.05$).

Time (h)	**Cumulative NaFI permeated (μg/cm^2)**	
	PL-LI without SN	**PL-LI with SN**
1	0.0067 ± 0.00	0.0058 ± 0.01
2	0.0105 ± 0.00	0.0105 ± 0.01
4	0.0160 ± 0.01	0.0240 ± 0.02
6	0.0244 ± 0.01	0.0377 ± 0.03
8	0.0303 ± 0.01	0.0503 ± 0.04
24	0.1031 ± 0.02	0.3253 ± 0.16
Flux (μg.cm^{-2}.h^{-1})	0.0042 ± 0.00*	0.0139 ± 0.01*

APPENDIX C

Table C1 Fluorescence intensity at different skin penetration depth of NaFl at follicular region and nonfollicular region of NaFI solution. Each value represents the mean ± S.D. (n=512).

Skin depth (μm)	**Follicular region**	**Nonfollicular region**
	NaFI	**NaFI**
0	834.99 ± 254.61	745.29 ± 101.84
5	981.19 ± 335.65	905.77 ± 135.63
10	1158.68 ± 405.94	1043.95 ± 166.84
15	1227.94 ± 389.61	1111.27 ± 206.74
20	1216.16 ± 372.97	1069.57 ± 226.92
25	1169.89 ± 325.02	1003.54 ± 226.48
30	1141.60 ± 317.21	919.68 ± 216.78
35	1111.78 ± 362.83	837.90 ± 205.72
40	1056.11 ± 407.70	754.61 ± 176.12
45	973.34 ± 387.94	684.07 ± 158.07
50	878.85 ± 352.35	627.13 ± 134.82
55	802.30 ± 305.77	579.73 ± 119.45
60	742.86 ± 271.64	544.55 ± 112.13
65	678.49 ± 223.21	514.07 ± 100.72
70	636.72 ± 193.99	486.44 ± 88.06
75	582.91 ± 159.25	463.36 ± 80.24
80	554.45 ± 145.69	439.74 ± 73.06
85	520.75 ± 124.79	426.61 ± 60.96
90	501.38 ± 112.66	416.48 ± 56.79
95	479.13 ± 97.87	403.57 ± 54.40
100	459.16 ± 91.38	-
105	443.03 ± 82.30	-
110	431.30 ± 70.31	-
115	416.61 ± 64.45	-
120	406.44 ± 58.90	-
125	397.44 ± 54.55	-
130	391.09 ± 50.55	-

Table C2 Fluorescence intensity at different skin penetration depth of NaFl and Rh-PE at follicular region and nonfollicular region of CL. Each value represents the mean ± S.D. (n=512).

Skin depth (μm)	Follicular region		Nonfollicular region	
	NaFI	RhPE	NaFI	Rh-PE
0	398.17 ± 10.61	214.75 ± 9.47	374.25 ± 12.71	185.04 ± 13.17
5	401.73 ± 11.78	213.66 ± 10.78	385.90 ± 13.76	192.18 ± 17.53
10	407.06 ± 13.23	215.16 ± 11.71	402.55 ± 16.05	203.04 ± 25.86
15	417.08 ± 14.53	215.83 ± 12.70	432.32 ± 19.58	228.38 ± 44.80
20	428.68 ± 16.97	220.30 ± 16.48	485.84 ± 29.13	269.03 ± 96.20
25	452.03 ± 20.76	226.89 ± 25.04	550.71 ± 38.62	294.49 ± 129.15
30	491.19 ± 29.51	240.04 ± 42.38	617.83 ± 46.58	300.12 ± 113.34
35	543.83 ± 46.01	262.37 ± 82.34	648.28 ± 51.32	284.49 ± 78.39
40	601.59 ± 60.86	276.18 ± 112.99	637.00 ± 54.73	257.19 ± 52.84
45	633.01 ± 70.35	277.88 ± 97.41	610.97 ± 55.88	230.75 ± 40.25
50	633.00 ± 73.44	268.72 ± 73.87	575.31 ± 52.74	213.93 ± 31.05
55	618.54 ± 68.59	254.29 ± 56.90	547.08 ± 50.06	201.45 ± 23.63
60	593.68 ± 64.10	237.94 ± 42.17	513.86 ± 46.23	193.54 ± 19.15
65	560.17 ± 57.98	224.30 ± 29.65	489.11 ± 40.72	187.05 ± 15.96
70	529.87 ± 49.70	217.09 ± 25.22	465.51 ± 35.74	182.09 ± 13.15
75	504.12 ± 44.12	209.37 ± 18.54	443.77 ± 33.32	178.28 ± 12.06
80	481.13 ± 39.46	203.70 ± 14.95	424.97 ± 27.52	175.44 ± 10.69
85	460.34 ± 32.72	199.64 ± 12.74	410.91 ± 25.47	173.82 ± 10.07
90	443.76 ± 27.83	197.10 ± 12.46	398.83 ± 23.57	171.91 ± 9.59
95	429.84 ± 23.17	193.34 ± 10.26	386.98 ± 20.67	169.49 ± 9.37
100	417.59 ± 20.43	192.58 ± 9.63	380.24 ± 17.93	167.98 ± 8.54
105	407.80 ± 19.61	190.32 ± 8.94	371.08 ± 15.91	168.52 ± 8.21
110	399.45 ± 17.39	188.60 ± 8.41	365.58 ± 14.95	167.22 ± 7.99
115	392.29 ± 16.14	187.81 ± 8.37	360.38 ± 14.44	166.05 ± 7.68
120	386.24 ± 14.48	185.72 ± 7.47	355.58 ± 13.50	165.43 ± 7.09
125	379.14 ± 13.61	183.90 ± 6.94	350.43 ± 12.40	164.09 ± 6.95
130	373.31 ± 12.14	183.62 ± 7.07	-	-
135	369.80 ± 12.08	182.87 ± 7.27	-	-
140	366.13 ± 11.42	182.31 ± 7.30	-	-
145	363.58 ± 11.53	181.18 ± 6.89	-	-
150	360.88 ± 10.55	180.71 ± 6.49	-	-
155	356.76 ± 10.08	179.24 ± 6.83	-	-
160	355.07 ± 9.76	178.72 ± 6.12	-	-
165	352.70 ± 9.32	178.56 ± 6.92	-	-
170	350.39 ± 9.06	176.62 ± 6.44	-	-
175	348.08 ± 9.19	176.25 ± 6.40	-	-

Table C3 Fluorescence intensity at different skin penetration depth of NaFl and Rh-PE at follicular region and nonfollicular region of PL. Each value represents the mean ± S.D. (n=512).

Skin depth (μm)	**Follicular region**		**Nonfollicular region**	
	NaFI	**RhPE**	**NaFI**	**Rh-PE**
0	413.42 ± 40.54	200.56 ± 48.90	362.83 ± 30.40	185.25 ± 46.79
5	438.61 ± 50.40	201.76 ± 45.74	369.28 ± 33.85	185.84 ± 44.69
10	470.75 ± 52.33	214.20 ± 61.06	380.09 ± 35.00	191.19 ± 51.15
15	533.70 ± 64.45	230.68 ± 72.53	388.24 ± 37.59	195.89 ± 59.27
20	620.35 ± 87.16	246.30 ± 81.30	406.10 ± 41.99	203.96 ± 56.30
25	716.10 ± 104.51	253.89 ± 87.52	435.94 ± 46.96	216.77 ± 72.25
30	729.27 ± 135.27	249.46 ± 93.96	475.13 ± 59.29	243.45 ± 89.42
35	715.02 ± 143.90	237.64 ± 98.59	547.59 ± 70.74	287.51 ± 139.30
40	660.66 ± 140.79	215.63 ± 60.34	636.99 ± 87.74	316.41 ± 162.11
45	616.89 ± 126.58	209.43 ± 58.51	693.40 ± 100.34	337.89 ± 182.08
50	566.42 ± 115.08	202.56 ± 50.82	681.05 ± 106.49	313.56 ± 140.43
55	520.64 ± 100.88	202.54 ± 50.16	633.67 ± 110.32	287.08 ± 124.60
60	496.04 ± 84.86	197.80 ± 42.75	587.55 ± 97.53	247.37 ± 94.38
65	467.92 ± 78.70	192.11 ± 39.19	530.34 ± 88.65	233.18 ± 88.02
70	442.17 ± 66.82	192.14 ± 40.82	500.23 ± 71.53	216.62 ± 72.83
75	426.37 ± 61.71	188.28 ± 30.93	461.79 ± 67.15	206.69 ± 67.27
80	410.14 ± 54.10	188.51 ± 30.96	437.41 ± 56.74	196.22 ± 54.37
85	403.87 ± 49.86	189.68 ± 36.51	423.88 ± 50.25	194.17 ± 60.45
90	388.35 ± 40.99	186.68 ± 31.64	407.43 ± 43.47	186.87 ± 49.04
95	381.24 ± 36.46	188.50 ± 38.26	392.00 ± 40.88	187.90 ± 49.58
100	378.30 ± 35.50	186.13 ± 30.21	382.66 ± 37.87	181.96 ± 43.01
105	369.99 ± 31.67	185.69 ± 30.14	375.37 ± 36.77	184.46 ± 46.44
110	365.39 ± 27.99	185.76 ± 31.81	370.62 ± 33.75	183.90 ± 51.47
115	361.14 ± 27.51	188.19 ± 35.79	363.31 ± 33.14	180.59 ± 43.64
120	361.14 ± 27.51	188.19 ± 35.79	359.39 ± 31.96	175.36 ± 33.31
125	355.10 ± 24.86	184.00 ± 31.41	-	-
130	351.84 ± 22.68	183.49 ± 27.88	-	-
135	349.76 ± 21.96	181.83 ± 25.23	-	-

Table C4 Fluorescence intensity at different skin penetration depth of NaFl and Rh-PE at follicular region and nonfollicular region of PL-LI. Each value represents the mean ± S.D. (n=512).

Skin depth (μm)	Follicular region		Nonfollicular region	
	NaFI	RhPE	NaFI	Rh-PE
0	387.06 ± 19.63	147.66 ± 61.02	416.49 ± 26.11	203.98 ± 105.55
5	394.55 ± 20.68	147.66 ± 59.27	445.10 ± 28.95	227.05 ± 131.70
10	416.30 ± 22.71	157.97 ± 71.74	480.24 ± 36.11	253.04 ± 148.56
15	440.88 ± 27.37	163.16 ± 84.36	535.29 ± 44.19	319.65 ± 188.39
20	467.49 ± 31.06	166.86 ± 76.63	623.35 ± 62.65	415.02 ± 242.42
25	509.54 ± 35.38	184.10 ± 99.13	771.16 ± 87.74	539.12 ± 295.72
30	565.15 ± 44.00	189.95 ± 95.91	1117.27 ± 161.89	770.11 ± 424.99
35	662.67 ± 53.15	248.70 ± 147.48	1631.96 ± 328.00	864.03 ± 449.25
40	848.75 ± 75.47	337.17 ± 209.09	1861.09 ± 489.27	952.09 ± 517.50
45	1286.98 ± 132.13	409.07 ± 244.96	1749.22 ± 537.35	944.60 ± 485.57
50	1883.86 ± 193.50	430.09 ± 277.37	1554.24 ± 521.08	871.78 ± 467.69
55	2201.23 ± 272.89	488.78 ± 327.73	1320.42 ± 452.41	699.05 ± 371.92
60	2246.42 ± 336.84	464.51 ± 317.02	1109.77 ± 376.42	569.41 ± 286.99
65	2141.94 ± 329.29	434.33 ± 287.97	950.24 ± 302.57	533.72 ± 266.04
70	2009.26 ± 317.65	375.53 ± 259.24	809.31 ± 231.43	414.25 ± 221.36
75	1828.26 ± 280.06	338.91 ± 241.89	705.04 ± 180.63	355.13 ± 190.68
80	1656.16 ± 256.68	336.38 ± 238.36	625.46 ± 137.30	315.46 ± 171.95
85	1491.96 ± 231.93	301.48 ± 203.46	570.72 ± 110.93	263.10 ± 162.07
90	1306.49 ± 204.60	260.29 ± 166.36	514.62 ± 89.12	253.19 ± 158.07
95	1155.24 ± 186.50	249.88 ± 142.57	487.57 ± 74.64	225.72 ± 132.46
100	1020.29 ± 164.43	230.48 ± 143.83	457.54 ± 58.58	212.49 ± 113.21
105	885.69 ± 143.12	220.09 ± 141.68	438.96 ± 50.80	194.62 ± 104.40
110	779.80 ± 133.29	199.72 ± 108.65	417.99 ± 43.78	185.23 ± 103.35
115	703.87 ± 118.53	195.51 ± 100.82	401.23 ± 38.08	181.58 ± 98.83
120	636.99 ± 105.75	177.05 ± 88.60	391.25 ± 34.23	172.64 ± 82.80
125	583.15 ± 88.61	168.15 ± 85.50	382.56 ± 31.97	173.00 ± 90.26
130	545.61 ± 74.63	156.27 ± 72.00	374.98 ± 27.93	158.57 ± 72.42
135	517.09 ± 67.73	156.09 ± 72.27	367.01 ± 25.89	151.10 ± 67.56
140	491.50 ± 59.10	147.89 ± 70.74	362.57 ± 23.81	153.31 ± 72.33
145	469.76 ± 51.09	143.41 ± 63.11	354.98 ± 22.07	151.10 ± 70.38
150	449.67 ± 43.05	144.79 ± 60.92	-	-
155	431.24 ± 37.93	150.23 ± 70.57	-	-
160	418.57 ± 33.88	139.65 ± 53.56	-	-
165	431.24 ± 37.93	150.23 ± 70.57	-	-
170	392.81 ± 28.04	131.91 ± 42.59	-	-
175	387.35 ± 26.32	131.15 ± 42.62	-	-
180	380.60 ± 25.33	131.06 ± 40.40	-	-

Table C5 Fluorescence intensity at different skin penetration depth of NaFl and Rh-PE at follicular region and nonfollicular region of PL-LI with SN. Each value represents the mean ± S.D. (n = 512).

Skin depth (μm)	**Follicular region**		**Nonfollicular region**	
	NaFI	**RhPE**	**NaFI**	**Rh-PE**
0	380.14 ± 24.18	211.08 ± 49.24	435.23 ± 26.60	276.03 ± 101.84
5	428.54 ± 24.66	245.76 ± 73.49	515.41 ± 32.89	349.61 ± 160.96
10	494.43 ± 35.93	311.43 ± 128.42	615.77 ± 41.31	404.68 ± 172.91
15	601.27 ± 47.49	391.32 ± 224.49	670.88 ± 45.43	448.67 ± 190.54
20	671.62 ± 55.53	450.39 ± 263.38	685.22 ± 45.45	456.13 ± 205.37
25	713.47 ± 60.61	486.37 ± 260.48	669.94 ± 42.58	462.89 ± 221.62
30	714.12 ± 65.81	458.27 ± 209.12	639.57 ± 46.53	447.75 ± 212.45
35	698.87 ± 71.53	438.01 ± 171.85	604.47 ± 51.50	411.10 ± 178.19
40	658.90 ± 73.74	412.58 ± 160.60	566.01 ± 52.80	384.71 ± 143.17
45	624.03 ± 66.03	379.81 ± 150.34	533.92 ± 50.08	334.75 ± 104.89
50	587.98 ± 59.72	341.31 ± 118.72	496.96 ± 44.63	297.98 ± 87.54
55	552.80 ± 51.96	305.06 ± 89.76	468.30 ± 39.66	260.65 ± 67.08
60	510.66 ± 43.83	266.58 ± 66.10	439.93 ± 35.78	222.34 ± 53.54
65	483.83 ± 40.64	240.46 ± 59.83	421.21 ± 31.30	222.34 ± 53.54
70	466.37 ± 35.84	228.68 ± 55.64	394.33 ± 28.77	210.75 ± 48.34
75	442.30 ± 31.34	210.86 ± 47.18	387.25 ± 25.93	197.07 ± 40.68
80	418.15 ± 26.70	197.16 ± 42.42	372.95 ± 23.87	186.98 ± 38.61
85	403.99 ± 24.07	192.15 ± 39.57	362.36 ± 21.41	177.03 ± 33.72
90	385.04 ± 20.41	182.86 ± 34.77	-	-
95	375.54 ± 19.19	176.58 ± 31.42	-	-

APPENDIX D

Table D1 The ratio of the amide I /amide II intensity from FTIR spectra of the stratum corneum treated with different formulations with and without SN.

Formulations treated stratum corneum	**Intensity**		**Ratio**
	amide I (~1652.3 cm^{-1})	**amide II (~1541.8 cm^{-1})**	
NaFI solution	1.794	0.606	2.96
NaFI solution with SN	1.698	0.806	2.11
CL	1.475	0.668	2.21
CL with SN	0.819	0.431	1.90
PL	1.201	0.519	2.31
PL with SN	1.301	0.543	2.40
PL-LI	2.704	0.964	2.80
PL-LI with SN	1.714	0.753	2.28
NI	1.794	0.606	2.96
NI with SN	1.252	0.583	2.15
NIP	1.684	0.623	2.70
NIP with SN	1.401	0.600	2.34
NIP-LI	1.841	0.769	2.70
NIP-LI with SN	1.305	0.554	2.34
SLN	1.361	0.537	2.53
SLN with SN	1.546	0.648	2.39
SLNP	1.132	0.572	1.98
SLNP with SN	1.272	0.532	2.39
SLNP-LI	1.644	0.613	2.68
SLNP-LI with SN	1.168	0.500	2.34

Table D2 Alterations on the CH_2 asymmetric and symmetric stretching absorbance shifts on the acyl chains of untreated stratum corneum. The temperature was in the range of 20 °C to 100 °C. Each value represents the mean ± S. D. (n = 3).

Temperature (°C)	**CH_2 symmetric stretching**	**CH_2 asymmetric stretching**
20	2848.83 ± 0.00	2916.65 ± 0.28
25	2849.15 ± 0.28	2916.65 ± 0.00
30	2849.15 ± 0.28	2916.81 ± 0.00
35	2849.31 ± 0.00	2916.97 ± 0.28
40	2849.63 ± 0.28	2917.45 ± 0.28
45	2849.95 ± 0.28	2917.93 ± 0.74
50	2850.27 ± 0.48	2918.74 ± 1.28
55	2850.60 ± 0.56	2919.38 ± 1.11
60	2851.08 ± 0.56	2920.18 ± 0.84
65	2851.30 ± 0.84	2920.83 ± 1.11
70	2851.72 ± 0.84	2921.47 ± 1.00
75	2851.88 ± 0.74	2922.27 ± 0.74
80	2852.36 ± 0.74	2922.75 ± 0.56
85	2852.69 ± 0.48	2922.91 ± 0.28
90	2852.85 ± 0.28	2923.07 ± 0.00
95	2853.01 ± 0.28	2923.23 ± 0.28
100	2853.17 ± 0.00	2923.40 ± 0.56

Table D3 Alterations on the CH_2 asymmetric and symmetric stretching absorbance shifts on the acyl chains of stratum corneum lipids treated with SN. The temperature was in the range of 20 °C to 100 °C. Each value represents the mean ± S. D. (n = 3).

Temperature (°C)	**CH_2 symmetric stretching**	**CH_2 asymmetric stretching**
20	2848.83 ± 0.00	2916.65 ± 0.28
25	2848.99 ± 0.28	2916.81 ± 0.00
30	2849.31 ± 0.00	2917.13 ± 0.28
35	2849.47 ± 0.28	2917.13 ± 0.28
40	2849.63 ± 0.28	2917.45 ± 0.28
45	2849.95 ± 0.28	2917.77 ± 0.00
50	2850.27 ± 0.00	2918.09 ± 0.28
55	2850.27 ± 0.00	2918.57 ± 0.28
60	2850.76 ± 0.00	2918.90 ± 0.28
65	2851.08 ± 0.28	2919.54 ± 0.56
70	2851.72 ± 0.28	2920.02 ± 0.56
75	2852.20 ± 0.48	2920.50 ± 0.56
80	2852.36 ± 0.56	2921.15 ± 0.48
85	2852.69 ± 0.83	2921.79 ± 0.28
90	2853.01 ± 0.28	2922.11 ± 0.00
95	2853.33 ± 0.56	2922.43 ± 0.28
100	2853.49 ± 0.28	2922.91 ± 0.28

Table D4 Alterations on the CH_2 asymmetric and symmetric stretching absorbance shifts on the acyl chains of stratum corneum lipids treated with CL. The temperature was in the range of 20 °C to 100 °C. Each value represents the mean ± S. D. (n = 3).

Temperature (°C)	**CH_2 symmetric stretching**	**CH_2 asymmetric stretching**
20	2849.47 ± 0.28	2917.29 ± 0.00
25	2849.47 ± 0.28	2917.29 ± 0.00
30	2849.63 ± 0.28	2917.77 ± 0.00
35	2850.27 ± 0.48	2918.25 ± 0.84
40	2850.92 ± 0.56	2919.86 ± 2.01
45	2851.56 ± 0.74	2921.79 ± 1.00
50	2852.20 ± 0.48	2922.43 ± 0.74
55	2852.52 ± 0.28	2922.59 ± 0.48
60	2853.01 ± 0.28	2922.75 ± 0.28
65	2853.17 ± 0.00	2923.40 ± 0.28
70	2853.65 ± 0.00	2923.72 ± 0.28
75	2853.81 ± 0.28	2924.04 ± 0.00
80	2854.13 ± 0.00	2924.20 ± 0.28
85	2854.13 ± 0.00	2924.52 ± 0.48
90	2854.13 ± 0.00	2924.68 ± 0.28
95	2854.13 ± 0.00	2925.00 ± 0.48
100	2854.29 ± 0.28	2925.16 ± 0.28

Table D5 Alterations on the CH_2 asymmetric and symmetric stretching absorbance shifts on the acyl chains of stratum corneum lipids treated with PL. The temperature was in the range of 20 °C to 100 °C. Each value represents the mean ± S. D. (n = 3).

Temperature (°C)	**CH_2 symmetric stretching**	**CH_2 asymmetric stretching**
20	2849.47 ± 0.28	2917.29 ± 0.00
25	2849.47 ± 0.28	2917.29 ± 0.00
30	2849.63 ± 0.28	2917.77 ± 0.00
35	2850.27 ± 0.48	2918.25 ± 0.84
40	2850.92 ± 0.56	2919.86 ± 2.01
45	2851.56 ± 0.74	2921.79 ± 1.00
50	2852.20 ± 0.48	2922.43 ± 0.74
55	2852.52 ± 0.28	2922.59 ± 0.48
60	2853.01 ± 0.28	2922.75 ± 0.28
65	2853.17 ± 0.00	2923.40 ± 0.28
70	2853.65 ± 0.00	2923.72 ± 0.28
75	2853.81 ± 0.28	2924.04 ± 0.00
80	2854.13 ± 0.00	2924.20 ± 0.28
85	2854.13 ± 0.00	2924.52 ± 0.48
90	2854.13 ± 0.00	2924.68 ± 0.28
95	2854.13 ± 0.00	2925.00 ± 0.48
100	2854.29 ± 0.28	2925.16 ± 0.28

Table D6 Alterations on the CH_2 asymmetric and symmetric stretching absorbance shifts on the acyl chains of stratum corneum lipids treated with PL-LI 1%. The temperature was in the range of 20 °C to 100 °C. Each value represents the mean ± S. D. (n = 3).

Temperature (°C)	**CH_2 symmetric stretching**	**CH_2 asymmetric stretching**
20	2849.15 ± 0.56	2917.45 ± 1.11
25	2849.47 ± 0.28	2917.61 ± 1.00
30	2849.95 ± 0.74	2918.25 ± 0.84
35	2850.43 ± 1.00	2920.02 ± 2.17
40	2851.56 ± 1.55	2920.34 ± 2.28
45	2852.04 ± 1.55	2920.66 ± 2.21
50	2852.52 ± 1.95	2922.11 ± 2.93
55	2852.52 ± 1.95	2922.59 ± 3.34
60	2853.01 ± 1.95	2923.07 ± 2.93
65	2853.17 ± 2.10	2923.07 ± 2.93
70	2853.49 ± 1.55	2923.72 ± 1.95
75	2853.97 ± 1.21	2924.04 ± 2.21
80	2853.97 ± 1.21	2924.36 ± 1.55
85	2854.13 ± 1.28	2924.68 ± 1.47
90	2854.45 ± 0.74	2924.84 ± 1.21
95	2854.77 ± 0.56	2925.00 ± 0.96
100	2854.77 ± 0.56	2925.16 ± 1.00

Table D7 Alterations on the CH_2 asymmetric and symmetric stretching absorbance shifts on the acyl chains of stratum corneum lipids treated with PL-LI 2%. The temperature was in the range of 20 °C to 100 °C. Each value represents the mean ± S. D. (n = 3).

Temperature (°C)	**CH_2 symmetric stretching**	**CH_2 asymmetric stretching**
20	2849.15 ± 0.28	2917.29 ± 0.48
25	2849.31 ± 0.48	2917.93 ± 0.74
30	2850.27 ± 0.00	2918.90 ± 0.28
35	2850.76 ± 0.00	2920.18 ± 0.84
40	2851.72 ± 0.48	2921.63 ± 0.96
45	2852.52 ± 0.28	2922.27 ± 1.21
50	2853.01 ± 0.28	2923.23 ± 0.74
55	2853.33 ± 0.28	2923.56 ± 0.48
60	2853.65 ± 0.00	2923.88 ± 0.56
65	2853.65 ± 0.00	2924.20 ± 0.74
70	2853.97 ± 0.28	2924.36 ± 0.28
75	2853.97 ± 0.28	2924.36 ± 0.28
80	2854.29 ± 0.28	2924.68 ± 0.28
85	2854.29 ± 0.28	2924.68 ± 0.28
90	2854.29 ± 0.28	2924.84 ± 0.28
95	2854.61 ± 0.00	2925.00 ± 0.48
100	2854.77 ± 0.28	2925.16 ± 0.28

BIOGRAPHY

Name	Worranan Rangsimawong, Ms.
Date of birth	November 09, 1989
Place of birth	Bangkok, Thailand
Nationality/Religion	Thai/Buddhism
E-mail address	rangsimawong.w@gmail.com

Education

2012 - 2017	Doctor of Philosophy, Ph.D. in Pharmaceutical Technology, Silpakorn University, Thailand
2007 - 2011	Bachelor of Pharmacy (1st Class Honours) in Pharmaceutical Technology, Ubon Ratchathani University, Thailand

Schoolarship

2012 – 2017	Thailand Research Funds through the Golden Jubilee Ph.D Program (Grant No. PHD/0091/2554)

Presentations

Oral

1. **Worranan Rangsimawong**, Praneet Opanasopit, Theerasak Rojanarata, Tanasait Ngawhirunpat. “Effect of PEGylating liposomes for transdermal drug delivery system” The 3rd Current Drug Development International conference, 1-3 May 2014, Pavilion Queen's Bay, Krabi, Thailand.
2. **Worranan Rangsimawong**, Yasuko Obata, Praneet Opanasopit, Kozo Takayama, Tanasait Ngawhirunpat. “Penetration enhancing effect of PEGylated liposomes on the intercellular lipid organization of stratum corneum" The 4th International Conference on Advanced Pharmaceutical Research “Innovation in Pharmaceutical Research and Development: Progress and Key achievements” 21-22 Feb 2017, Miracle Grand Convention Hotel, Thailand.

Poster:

1. **Worranan Rangsimawong**, Praneet Opanasopit, Theerasak Rojanarata, Tanasait Ngawhirunpat. “Influence of particle size of Ultradeformable

liposomes in dermal delivery of hydrophilic" The 15th Asian Chemical Congress 2013, 19-23 August 2013, Resorts World Sentosa, Singapore.

2. **Worranan Rangsimawong**, Praneet Opanasopit, Theerasak Rojanarata, Tanasait Ngawhirunpat. "Effect of particle size of ultradefomable liposomes on dermal delivery of hydrophilic compound" The 30th Annual Research Conference in Pharmaceutical Sciences, 10 January 2014, Faculty of Pharmaceutical Sciences, Chulalongkron University, Thailand.
3. **Worranan Rangsimawong**, Praneet Opanasopit, Theerasak Rojanarata, Tanasait Ngawhirunpat. "Effect of Various Nonionic Surfactants Incorporated in Liposomes on Dermal Delivery of Hydrophilic Compound" The 3rd International Conference and Exhibition on Pharmaceutical - Nutraceutical and Cosmeceutical Technology 2014, 1-2 December 2014, The Queen Sirikit National Convention Center (QSNCC), Bangkok, Thailand.
4. **Worranan Rangsimawong**, Praneet Opanasopit, Theerasak Rojanarata, Tanasait Ngawhirunpat. "Effect of terpene-containing liposomes on the skin deposition of a hydrophilic compound" The JSPS-NRCT Follow-Up Seminar 2015 and 31st International Annual Meeting in Pharmaceutical Sciences (JSPS-NRCT 2015 and 31st IAMPS), 22-23 January 2015, Faculty of Pharmaceutical Sciences, Chulalongkorn University, Bangkok, Thailand.
5. **Worranan Rangsimawong**, Praneet Opanasopit, Theerasak Rojanarata, Tanasait Ngawhirunpat. "Effect of Sonophoresis Combined with Penetration Enhancer in Coupling Medium on Transdermal Delivery of Hydrophilic Compound" The 7th Annual Northeast Pharmacy Research Conference of 2015 "Challenges and Opportunities of Pharmacy Profession in Post-Millennium Development Agenda", 7-8 March 2015, Faculty of Pharmaceutical Sciences, Khonkaen University, Khonkaen, Thailand.
6. **Worranan Rangsimawong**, Yasuko Obata, Praneet Opanasopit, Theerasak Rojanarata, Tanasait Ngawhirunpat, Kozo Takayama. "Effect of d-limonene-containing liposomes on the skin permeation of a hydrophilic compound" The 136th Annual of the Pharmaceutical Society of Japan, 26-29 March 2016, Pacifico Yokohama, Japan.

7. **Worranan Rangsimawong**, Yasuko Obata, Praneet Opanasopit, Theerasak Rojanarata, Tanasait Ngawhirunpat, Kozo Takayama. “Effect of (+)-limonene-containing PEGylated liposomes on the skin penetration of galantamine” The 31st annual meeting of the acadamy of pharmaceutical science and technology, Japan (APSTJ), 19-21 May 2016, Nagaragawa Convention Centre, Gifu, Japan.
8. **Worranan Rangsimawong**, Praneet Opanasopit, Theerasak Rojanarata, Tanasait Ngawhirunpat. “Effect of using a combination of sonophoresis and PEGylated liposomes with limonene on the skin deposition of hydrophilic compound” The 26th Federation of Asian Pharmaceutical Assocciations Congress “Integrating Asian Pharmacy Wisdom for Better Global Health”, 9-13 Nov 2016, BITEC Bangna, Bangkok, Thailand.
9. **Worranan Rangsimawong**, Praneet Opanasopit, Theerasak Rojanarata, Tanasait Ngawhirunpat. “Combination effect of sonophoresis and d-limonene on the skin penetration of hydrophilic compound loaded niosomes and solid lipid nanoparticles” Seoul International Conference on Engineering and Applied Science (SICEAS), 7-9 Feb 2017, Marriott Seoul Times Square, Seoul, South Korea.
10. **Worranan Rangsimawong**, Praneet Opanasopit, Theerasak Rojanarata, Tanasait Ngawhirunpat. “Combination effect of sonophoresis and terpene-containing liposomes on skin penetration of hydrophilic compound” The JSPS-NRCT Follow-Up Seminar 2017 and 33rd International Annual Meeting in Pharmaceutical Sciences (IJPS-NRCT 2017 and IAMPS 33), 2-3 March 2017, The Berkeley Hotel Pratunam, Thailand.
11. **Worranan Rangsimawong**, Yasuko Obata, Praneet Opanasopit, Kozo Takayama, Tanasait Ngawhirunpat. “Investigation of skin penetration enhancing mechanism of limonene -containing liposomes entrapped hydrophilic compound” 9th Annual Conference of Northeastern Pharmacy Research 2017: Innovative Pharmaceutical Products and Services in Thailand 4.0, 11-12 March 2017, Faculty of Pharmaceutical Sciences, Ubon Ratchathani University, Thailand.

Scientific publications

1. **Worranan Rangsimawong,** Praneet Opanasopit, Theerasak Rojanarata, Tanasait Ngawhirunpat. Terpene-containing PEGylated liposomes as transdermal carriers of a hydrophilic compound. Biological and Pharmaceutical Bulletin. 2014; 37(12), 1936-43.
2. **Worranan Rangsimawong**, Praneet Opanasopit, Theerasak Rojanarata, Tanasait Ngawhirunpat. Effect of Various Nonionic Surfactants Incorporated in Liposomes on Dermal Delivery of Hydrophilic Compound. Advanced Materials Research. 2015; 1060, 12-16.
3. **Worranan Rangsimawong**, Praneet Opanasopit, Theerasak Rojanarata, Tanasait Ngawhirunpat. Mechanistic study of decreased skin penetration using a combination of sonophoresis with sodium fluorescein-loaded PEGylated liposomes with D-limonene. International Journal of Nanomedicine. 2015; 10, 7413-7423.
4. **Worranan Rangsimawong**, Praneet Opanasopit, Theerasak Rojanarata, Sureewan Duangjit, Tanasait Ngawhirunpat. Skin Transport of Hydrophilic Compound-Loaded PEGylated Lipid Nanocarriers: Comparative Study of Liposomes, Niosomes, and Solid Lipid Nanoparticles. Biological and Pharmaceutical Bulletin. 2016; 39, 1–9.
5. **Worranan Rangsimawong**, Praneet Opanasopit, Theerasak Rojanarata, Suwannee Panomsuk, Tanasait Ngawhirunpat. Influence of sonophoresis on transdermal drug delivery of hydrophilic compound-loaded lipid nanocarriers. Pharmaceutical Development and Technology. 2016 Aug 30:1-9. [Epub ahead of print].

Academic articles

1. **Worranan Rangsimawong** and Tanasait Ngawhirunpat. Nanoemulsions in transdermal drug delivery system, Thai Bulletin of Pharmaceutical Sciences (TBPS), 2014: 9 46-61.
2. **Worranan Rangsimawong** and Tanasait Ngawhirunpat. Characterization of liposomes for transdermal drug delivery system, Thai Bulletin of Pharmaceutical Sciences (TBPS), 2015; 10 (1), 61-74.

3. **Worranan Rangsimawong** and Tanasait Ngawhirunpat. Techniques for Follicular Penetration Studies, Isan Journal of Pharmaceutical Sciences (IJPS), 2015, 11 (2), 31-44.

Award

1. Good poster presentation awards. **Worranan Rangsimawong**, Praneet Opanasopit, Theerasak Rojanarata, Tanasait Ngawhirunpat. “Effect of Sonophoresis Combined with Penetration Enhancer in Coupling Medium on Transdermal Delivery of Hydrophilic Compound” The 7th Annual Northeast Pharmacy Research Conference of 2015 “Challenges and Opportunities of Pharmacy Profession in Post-Millennium Development Agenda”, 7-8 March 2015, Faculty of Pharmaceutical Sciences, Khonkaen University, Khonkaen, Thailand.
2. Outstanding Award in Oral Presentation. **Worranan Rangsimawong**, Yasuko Obata, Praneet Opanasopit, Kozo Takayama, Tanasait Ngawhirunpat. “Penetration enhancing effect of PEGylated liposomes on the intercellular lipid organization of stratum corneum" The 4th International Conference on Advanced Pharmaceutical Research “Innovation in Pharmaceutical Research and Development: Progress and Key achievements” 21-22 Feb 2017, Miracle Grand Convention Hotel, Thailand.
3. Outstanding Poster Presentation Award. **Worranan Rangsimawong**, Praneet Opanasopit, Theerasak Rojanarata, Tanasait Ngawhirunpat. “Combination effect of sonophoresis and terpene-containing liposomes on skin penetration of hydrophilic compound” The JSPS-NRCT Follow-Up Seminar 2017 and 33rd International Annual Meeting in Pharmaceutical Sciences (IJPS-NRCT 2017 and IAMPS 33), 2-3 March 2017, The Berkeley Hotel Pratunam, Thailand.
4. Good poster presentation awards. **Worranan Rangsimawong**, Yasuko Obata, Praneet Opanasopit, Kozo Takayama, Tanasait Ngawhirunpat. “Investigation of skin penetration enhancing mechanism of limonene -containing liposomes entrapped hydrophilic compound” 9th Annual Conference of Northeastern Pharmacy Research 2017: Innovative Pharmaceutical Products and Services in Thailand 4.0, 11-12 March 2017, Faculty of Pharmaceutical Sciences, Ubon Ratchathani University, Thailand.

TECHNICAL BACKGROUND:

- Liposomes, Niosomes, and Solid lipid nanoparticles preparation using sonication method
- Characterization of liposomes: DLS, TEM, AFM, Fluorescence anisotropy.
- Enhanced transdermal drug delivery techniques: Sonophoresis
- *In vitro* skin permeation and deposition.
- Skin characterization by FTIR and DSC
- Skin imaging by confocal microscopy (Whole and cryo-section skin) and SEM.